

The ASD-associated CNV 16p11.2:
Functional study of the candidate gene *QPRT*

Dissertation
zur Erlangung des Doktorgrades
der Naturwissenschaften

vorgelegt beim Fachbereich 15
der Johann Wolfgang Goethe-Universität
in Frankfurt am Main

von
Denise Haslinger
aus Braunau am Inn, Österreich

Frankfurt 2018

D 30

vom Fachbereich 15 der

Johann Wolfgang Goethe-Universität als Dissertation angenommen.

Dekan: Prof. Dr. Sven Klimpel

1. Gutachterin: Prof. Dr. Amparo Acker-Palmer

2. Gutachterin: Prof. Dr. Christine M. Freitag

Datum der Disputation:

Index

Index	I
List of figures	IV
List of tables	IV
List of abbreviations used in this study	V
List of genes discussed in this study	VII
Vorwort	XI
Ehrenwörtliche Erklärung	XIII
Zusammenfassung	XV
1 Abstract	1
2 Introduction	3
2.1 <i>Autism spectrum disorder (ASD)</i>	3
2.1.1 Phenotype and diagnostics	3
2.1.2 Epidemiology	4
2.1.3 Aetiology and heritability	5
2.1.4 Molecular genetic findings	6
2.2 <i>Neurobiology and current animal or cell models of ASD</i>	16
2.2.1 Neuropathology	17
2.2.2 Neuroanatomy	17
2.2.3 Genetic basis of altered neurobiology	17
2.2.4 Current animal and cell models	18
2.3 <i>ASD-associated region 16p11.2</i>	23
2.3.1 Penetrance and phenotype of 16p11.2 CNVs	23
2.3.2 Functional studies of the whole CNV or single genes located in 16p11.2	24
2.4 <i>Summary and aims</i>	33
3 Material and methods	35
3.1 <i>Genetic methods</i>	35
3.1.1 DNA extraction	35
3.1.2 Real-time PCR	35
3.2 <i>RNA methods</i>	36
3.2.1 RNA extraction	36
3.2.2 Real-time RT-PCR	36
3.2.3 Whole transcriptome analyses	37
3.3 <i>Protein methods</i>	38

3.3.1	Protein extraction, gel electrophoresis and Western blot	38
3.4	<i>Cell culture methods</i>	40
3.4.1	Cell lines and growth conditions	40
3.4.2	Cell culture assays	43
3.5	<i>Statistics</i>	47
3.5.1	Group differences	47
3.5.2	Correlations	47
3.5.3	Targeted mRNA expression	47
3.5.4	Transcriptome analyses.....	48
3.5.5	Gene list enrichment test in gene networks of brain development	49
4	Results	51
4.1	<i>Characterization of the SH-SY5Y cell model</i>	51
4.1.1	Confirmation and evaluation of neuronal differentiation.....	51
4.1.2	Identification of genes implicated in neuronal differentiation	54
4.1.3	Co-expression network analysis	54
4.2	<i>QPRT as candidate gene for functional validation</i>	55
4.2.1	QPRT is differentially regulated during neuronal differentiation.....	55
4.2.2	QPRT correlates with neuronal morphology during neuronal differentiation	56
4.2.3	Validation of 16p11.2 CNVs.....	57
4.2.4	Validation of QPRT expression in 16p11.2 deletion carrier	58
4.3	<i>Functional validation of QPRT in SH-SY5Y</i>	59
4.3.1	siRNA mediated knock down (KD) of QPRT.....	59
4.3.2	Chemical inhibition of QPRT.....	61
4.3.3	CRISPR/Cas9 mediated knock out (KO) of QPRT	61
5	Discussion	73
5.1	<i>Suitability of the SH-SY5Y neuroblastoma model</i>	73
5.2	<i>Selection of the candidate gene QPRT located in the ASD-associated CNV region Chr16p11.2</i>	74
5.3	<i>The functional impact of QPRT</i>	75
5.3.1	Reduction of QPRT induced subtle morphological changes of differentiated SH-SY5Y cells while a complete loss was lethal	75
5.3.2	Neuronal cell death of SH-SY5Y induced by QPRT loss was independent of QUIN	76
5.3.3	Overlap of ASD and epilepsy: Genes differentially regulated upon KO of QPRT in SH-SY5Y converged on synaptic functions with a suggested impact on E/I balance.....	77
5.3.4	Neuronal cell death of SH-SY5Y induced by QPRT loss: Suggested mechanisms	83
5.3.5	Translation to human brain development: Expression patterns induced by QPRT-KO impacted on neuron-specific markers, developmental processes and brain regions previously associated with ASD	84
5.4	<i>Limitations of the study</i>	86
5.5	<i>Outlook</i>	87
6	Conclusions	88

7	Appendix.....	91
7.1	<i>Supplementary tables</i>	91
7.1.1	List of antibodies used in this study	91
7.1.2	List of real-time PCR primers used in this study.....	91
7.1.3	List of real-time RT-PCR primers used in this study.....	92
7.1.4	sgRNAs and sequencing primers for CRISPR/Cas9	93
7.2	<i>Supplementary methods.....</i>	93
7.2.1	ImageJ macros for Sholl analysis	93
7.2.2	Metabolite analysis	94
8	References	97
9	Ein riesiges Danke	111
10	Curriculum vitae.....	115
11	List of publications	118

List of figures

Figure 1 Contribution of rare and common variation to disease susceptibility in ASD.	10
Figure 2 Validation of neuronal differentiation.....	51
Figure 3 Validation of microarray data.....	52
Figure 4 Expression of neuronal markers.....	53
Figure 5 Evaluation of neuronal differentiation.....	53
Figure 6 Differentially regulated genes during SH-SY5Y neuronal differentiation.....	54
Figure 7 Regulation of WGCNA modules and risk gene enrichment analysis.....	55
Figure 8 Expression of 16p11.2 genes.....	56
Figure 9 Correlation of <i>QPRT</i> expression with morphological parameters.....	57
Figure 10 16p11.2 deletion.....	58
Figure 11 Validation of 16p11.2 deletion.....	58
Figure 12 <i>QPRT</i> expression in LCLs of a 16p11.2 deletion carrier and control cell lines.....	59
Figure 13 Morphological alterations upon reduction of <i>QPRT</i>	60
Figure 14 Chemical inhibition of <i>QPRT</i>	61
Figure 15 Sequencing of <i>QPRT-KO</i> cell lines.....	62
Figure 16 <i>QPRT</i> expression in generated KO and control cell lines.....	63
Figure 17 Viability of <i>QPRT-KO</i> cell lines.	63
Figure 18 Application of QUIN to proliferating and differentiating SH-SY5Y wild type cells.....	64
Figure 19 Rescue experiments of <i>QPRT-KO</i> induced cell death.....	65
Figure 20 Metabolite analysis of <i>QPRT-KO</i> cells.....	65
Figure 21 Heatmap of genes differentially expressed in <i>QPRT-KO</i> cells.....	66
Figure 22 GO-term enrichment for differentially expressed genes upon KO of <i>QPRT</i>	68
Figure 23 Regulation of the darkgrey gene set.	70
Figure 24 Translation of <i>QPRT-KO</i> induced gene expression profile to human development.....	71

List of tables

Table 1 Studies of the chromosomal region 16p11.2 (whole CNV and single genes).....	30
Table 2 Differentially expressed genes upon <i>QPRT-KO</i> with $ \log_2FC > 2.5$	69

List of abbreviations used in this study

Abbreviation	Description
3HAA	3-hydroxyanthranilic acid
3HK	3-hydroxykynurenine
A1	primary auditory
A1C	primary auditory (A1) cortex
AA	anthranilic acid
ACMS	alpha-amino-beta-carboxy-muconate-epsilon-semialdehyde
ADHD	attention deficit hyperactivity disorder
ADI-R	autism diagnostic interview-revised
ADOS	autism observation schedule
AGP	autism genome project
AKT	serine-threonine kinase
AMY	amygdala
ANOVA	analysis of variance
APS	ammonium persulfate
ASD	autism spectrum disorders
ASS	Autismus-Spektrum-Störungen
BDNF	brain derived neurotrophic factor
BP	bipolar disorder
cAMP	cyclic adenosine monophosphate
CAT-3	cationic amino acid transporter
CBC	cerebellar cortex
CDD	childhood disintegrative disorders
cDNA	complementary DNA
CGH	comparative genomic hybridization
Chr	chromosome (p: short arm; q: long arm)
CI	confidence interval
CNV	copy number variation
CoNTEXT	classification of neuroanatomical and temporal expression via transcriptomics
CRISPR	clustered regularly interspaced short palindromic repeats
DD	developmental delay
del268T	QPRT NM_014298 del268T; Ex2.1
DEX	differential expression
DFC	dorsolateral prefrontal cortex
DMEM	Dulbecco's modified Eagle medium
DNA	deoxyribonucleic acid
DSM	diagnostic and statistical manual of mental disorders
DTW	dynamic time warping
EDTA	ethylenediaminetetraacetic acid
E/I	excitation/inhibition
eCtrl	empty control vector
EEG	electroencephalography
ERK/MAPK	extracellular signaling related kinase
FCS	fetal calf serum
FC	fold change
FDR	false discovery rate
fMRI	functional magnetic resonance imaging
FMRP	fragile X mental retardation protein
GC/MS	gas chromatography-mass spectrometry
GEO	gene expression omnibus
GO	gene ontology
GWAS	genome wide association study
GWAS-NR	genome wide association study - noise reduction
HIP	hippocampus
HT	heterozygous
ICA	independent component analysis
ICD	international classification of diseases
ID	intellectual disability

IgG	immunoglobulin G
IL-4	interleukin 4
IL-5	interleukin 5
ins395A	QPRT NM_014298 ins395A; Ex2.2
IPC	posterior inferior parietal cortex
iPSC	induced pluripotent stem cell
IQ	intelligence quotient
ITC	inferior temporal cortex
KA	kynurenic acid
KD	knock down
KO	knock out
KYN	kynurenine
LCL	lymphoblastoid cell line
LD	linkage disequilibrium
L-NAME	N(G)-nitro-L-arginine methyl ester
LOD	logarithm of the odds
LOF	loss of function
MACE	massive analysis of cDNA ends
MAF	minor allele frequency
MEG	magnetoencephalography
MFC	medial prefrontal cortex
MLS	maximum LOD score
MRI	magnetic resonance imaging
mRNA	messenger RNA
mTOR	mechanistic target of rapamycin
NA	not analyzed
NAD	nicotinamide adenine dinucleotide
NGS	next generation sequencing
NLGN	neuroligins
NMDA-R	N-methyl-D-aspartate receptor
NO	nitric oxide
NPC	neuronal progenitor cell
OFC	orbitofrontal cortex
p	p-value
PA	phthalic acid
PARP	poly (ADP-ribose) polymerase
PBS	phosphate buffered saline
PBST	phosphate buffered saline supplemented with Tween-20
PDD-NOS	pervasive developmental disorder - not otherwise specified
PDZ	PSD95-Dlg1-zo-1
PGC	psychiatric genomics consortium
PI	propidium iodide
PI3K	phosphoinositide 3-kinase
PIC	picolinic acid
PSD	postsynaptic density
PZM	postzygotic mosaic mutations
QC	quality control
QTL	quantitative trait locus
QUIN	quinolinic acid
RA	retinoic acid
RIN	RNA integrity number
RNA	ribonucleic acid
RT-PCR	reverse transcriptase polymerase chain reaction
SDS	sodium dodecyl sulfate
SFARI	simons foundation autism research initiative
sgRNA	single guide RNA
shRNA	small hairpin RNA
siCtrl	non-targeting siRNA control
siQ1-siQ3	QPRT targeting siRNA1-3
siRNA	small interfering RNA
SNP	single nucleotide polymorphism

SNV	single nucleotide variant
SSC	simons simplex collection
S-SCAM	synaptic scaffolding molecule
STR	striatum
SZ	schizophrenia
TDT	transmission disequilibrium test
TrkB	tyrosine kinase beta
TRP	tryptophan
UCSC	university of california santa cruz
UHPLC	ultra-high-performance liquid chromatography
UPL	universal probe library
V1	primary visual
V1C	primary visual (V1) cortex
VFC	ventrolateral prefrontal cortex
VPA	valproic acid
WES	whole exome sequencing
WGCNA	weighted gene co-expression network analysis
WGS	whole genome sequencing
WT	wild type

List of genes discussed in this study

Gene ID	Gene description
ABAT	4-aminobutyrate aminotransferase
ACHE	acetylcholinesterase
ACMSD	alpha-amino-beta-carboxy-muconate-epsilon-semialdehyde
ACTB	actin beta
ADORA2A	adenosine A2a receptor
ALDOA	aldolase, fructose-bisphosphate A
APP	amyloid beta precursor protein
ARHGAP20	Rho GTPase activating protein 20
ASPHD1	aspartate beta-hydroxylase domain containing 1
ASTN2	astrotactin 2
ATP2B2	ATPase plasma membrane Ca ²⁺ transporting 2
BOLA2	boIA family member 2
BRINP1	BMP/retinoic acid inducible neural specific 1
C16orf53	PAXIP1 associated glutamate rich protein 1 (PAGR1)
C16orf54	chromosome 16 open reading frame 54
C16orf92	chromosome 16 open reading frame 92
CACNA1C	calcium voltage-gated channel subunit alpha 1 C
CACNB2	calcium voltage-gated channel auxiliary subunit beta 2
CASK	calcium/calmodulin dependent serine protein kinase
CCK	cholecystokinin
CDH13	cadherin 13
CDIPT	CDP-diacylglycerol-inositol 3-phosphatidyltransferase
CDK1	cyclin dependent kinase 1
CELF4	CUGBP Elav-like family member 4
CHAT	choline O-acetyltransferase
CHD2	chromodomain helicase DNA binding protein 2
CHRNA7	cholinergic receptor nicotinic alpha 7 subunit
C-Myc	MYC proto-oncogene, BHLH transcription factor
CNTNAP2	contactin associated protein like 2
CORO1A	coronin 1A
COX17	cytochrome c oxidase copper chaperone
COX17P1	COX17, cytochrome c oxidase copper chaperone pseudogene 1
CSF3R	colony stimulating factor 3 receptor
CTNNB1	catenin beta 1
CUEDC2	CUE domain containing 2
CUX2	cut like homeobox 2
DAT1	= SLC6A3/dopamine transporter 1
DHCR7	7-dehydrocholesterol reductase
DOC2A	double C2 domain alpha

<i>DOCK8</i>	<i>dedicator of cytokinesis 8</i>
<i>DRD2</i>	<i>dopamine receptor D2</i>
<i>DRD4</i>	<i>dopamine receptor D4</i>
<i>EN1</i>	<i>engrailed homeobox 1</i>
<i>ERK1</i>	<i>= MAPK3/ mitogen-activated protein kinase 3</i>
<i>ERK2</i>	<i>= MAPK1/ mitogen-activated protein kinase 1</i>
<i>EXT1</i>	<i>exostosin glycosyltransferase 1</i>
<i>FAM57B</i>	<i>family with sequence similarity 57 member B</i>
<i>FGF1</i>	<i>fibroblast growth factor 1</i>
<i>FMR1</i>	<i>fragile X mental retardation 1</i>
<i>FOXP1</i>	<i>forkhead box P1</i>
<i>FOXP2</i>	<i>forkhead box P2</i>
<i>GABRB3</i>	<i>gamma-aminobutyric acid type A receptor beta3 subunit</i>
<i>GAD1</i>	<i>glutamate decarboxylase 1</i>
<i>GAD2</i>	<i>glutamate decarboxylase 2</i>
<i>GALNT14</i>	<i>polypeptide N-acetylgalactosaminyltransferase 14</i>
<i>GAPDH</i>	<i>glyceraldehyde-3-phosphate dehydrogenase</i>
<i>GDPD3</i>	<i>glycerophosphodiester phosphodiesterase domain containing 3</i>
<i>GLUL</i>	<i>glutamate-ammonia ligase</i>
<i>GPHN</i>	<i>gephyrin</i>
<i>GRIA2</i>	<i>glutamate ionotropic receptor AMPA type subunit 2</i>
<i>GRIK2</i>	<i>glutamate ionotropic receptor kainate type subunit 2</i>
<i>GRIN1</i>	<i>glutamate ionotropic receptor NMDA type subunit 1</i>
<i>GRM1</i>	<i>glutamate metabotropic receptor 1</i>
<i>GRM4</i>	<i>glutamate metabotropic receptor 4</i>
<i>GUCA1A</i>	<i>guanylate cyclase activator 1A</i>
<i>GUSB</i>	<i>glucuronidase beta</i>
<i>HDAC4</i>	<i>histone deacetylase 4</i>
<i>HIRIP3</i>	<i>HIRA interacting protein 3</i>
<i>HNRNPU</i>	<i>heterogeneous nuclear ribonucleoprotein U</i>
<i>IGF1</i>	<i>insulin like growth factor 1</i>
<i>INO80E</i>	<i>INO80 complex subunit E</i>
<i>KANK1</i>	<i>KN motif and ankyrin repeat domains 1</i>
<i>KCND2</i>	<i>potassium voltage-gated channel subfamily D member 2</i>
<i>KCND3</i>	<i>potassium voltage-gated channel subfamily D member 3</i>
<i>KCNQ3</i>	<i>potassium voltage-gated channel subfamily Q member 3</i>
<i>KCTD13</i>	<i>potassium channel tetramerization domain containing 13</i>
<i>KDM5B</i>	<i>lysine demethylase 5B</i>
<i>KIF22</i>	<i>kinesin family member 22</i>
<i>KLF16</i>	<i>Kruppel like factor 16</i>
<i>Klf4</i>	<i>Kruppel like factor 4</i>
<i>KMT2E</i>	<i>lysine methyltransferase 2E</i>
<i>LIN7B</i>	<i>Lin-7 homolog B, crumbs cell polarity complex component</i>
<i>LINC01760</i>	<i>long intergenic non-protein coding RNA 1760</i>
<i>MACROD2</i>	<i>MACRO domain containing 2</i>
<i>MAP2K2</i>	<i>= MEK2/ mitogen-activated protein kinase kinase 2</i>
<i>MAPK1</i>	<i>= ERK2/mitogen-activated protein kinase 1</i>
<i>MAPK3</i>	<i>= ERK1/mitogen-activated protein kinase 3</i>
<i>MAPT</i>	<i>microtubule associated protein tau</i>
<i>MAZ</i>	<i>MYC associated zinc finger protein</i>
<i>MECP2</i>	<i>methyl-CpG binding protein 2</i>
<i>MED13</i>	<i>mediator complex subunit 13</i>
<i>MEK2</i>	<i>= MAP2K2/mitogen-activated protein kinase kinase 2</i>
<i>MSANTD2</i>	<i>Myb/SANT DNA binding domain containing 2</i>
<i>mTOR</i>	<i>mechanistic target of rapamycin kinase</i>
<i>MVP</i>	<i>major vault protein</i>
<i>NDN</i>	<i>necdin, MAGE family member</i>
<i>NELL1</i>	<i>neural EGFL like 1</i>
<i>NGF</i>	<i>nerve growth factor</i>
<i>NLGN2</i>	<i>neuroligin 2</i>
<i>NLGN3</i>	<i>neuroligin 3</i>
<i>NLGN4</i>	<i>neuroligin 4, X-linked</i>
<i>NMNAT2</i>	<i>nicotinamide nucleotide adenylyltransferase 2</i>
<i>NOS1</i>	<i>nitric oxide synthase 1</i>
<i>NOS2</i>	<i>nitric oxide synthase 2</i>
<i>NRXN1</i>	<i>neurexin 1</i>

NT3	<i>neurotrophin 3</i>
NTRK2	<i>neurotrophic receptor tyrosine kinase 2</i>
OCT3/OCT4	<i>POU class 5 homeobox 1</i>
PAX5	<i>paired box 5</i>
PCCB	<i>propionyl-CoA carboxylase beta subunit</i>
PHB	<i>prohibitin</i>
PHF3	<i>PHD finger protein 3</i>
PITX3	<i>paired like homeodomain 3</i>
PQLR2F	<i>RNA polymerase II subunit F</i>
PPP4C	<i>protein phosphatase 4 catalytic subunit</i>
PRRT2	<i>proline rich transmembrane protein 2</i>
PSMD7	<i>proteasome 26S subunit, non-ATPase 7</i>
PTEN	<i>phosphatase and tensin homolog</i>
PTPN5	<i>= STEP61/protein tyrosine phosphatase, non-receptor type 5</i>
PUM2	<i>pumilio RNA binding family member 2</i>
QPRT	<i>quinolinate phosphoribosyltransferase</i>
RhoA	<i>ras homolog family member A</i>
RIMS1	<i>regulating synaptic membrane exocytosis 1</i>
ROBO2	<i>roundabout guidance receptor 2</i>
SCN2A	<i>sodium voltage-gated channel alpha subunit 2</i>
SDC2	<i>syndecan 2</i>
SEMA5A	<i>semaphorin 5A</i>
SEZ6L2	<i>seizure related 6 homolog like 2</i>
SHANK1	<i>SH3 and multiple ankyrin repeat domains 1</i>
SHANK2	<i>SH3 and multiple ankyrin repeat domains 2</i>
SHANK3	<i>SH3 and multiple ankyrin repeat domains 3</i>
SLC17A7	<i>solute carrier family 17 member 7</i>
SLC17A8	<i>solute carrier family 17 member 8</i>
SLC18A3	<i>solute carrier family 18 member A3</i>
SLC1A6	<i>solute carrier family 1 member 6</i>
SLC32A1	<i>solute carrier family 32 member 1</i>
SLC5A7	<i>solute carrier family 5 member 7</i>
SLC6A1	<i>solute carrier family 6 member 1</i>
SLC6A2	<i>solute carrier family 6 member 2</i>
SLC6A3	<i>= DAT1/dopamine transporter 1</i>
SLC6A4	<i>solute carrier family 6 member 4</i>
SLC7A3	<i>solute carrier family 7 member 3</i>
SMARCA4	<i>SWI/SNF related, matrix associated, actin dependent regulator of chromatin, subfamily a, member 4</i>
SNCA	<i>synuclein alpha</i>
SNTG2	<i>syntrophin gamma 2</i>
SOX2	<i>SRY-box 2</i>
SPN	<i>sialophorin</i>
SRRM4	<i>serine/arginine repetitive matrix 4</i>
STAT1	<i>signal transducer and activator of transcription 1</i>
STEP61	<i>= PTPN5/protein tyrosine phosphatase, non-receptor type 5</i>
SULT1A3	<i>sulfotransferase family 1A member 3</i>
SULT1A4	<i>sulfotransferase family 1A member 4</i>
SYNGAP1	<i>synaptic Ras GTPase activating protein 1</i>
TAOK2	<i>TAO kinase 2</i>
TBX6	<i>T-box 6</i>
TGF- β	<i>= TGFB1/transforming growth factor beta 1</i>
TH	<i>tyrosine hydroxylase</i>
TMEM219	<i>transmembrane protein 219</i>
TPH1	<i>tryptophan hydroxylase 1</i>
TPH2	<i>tryptophan hydroxylase 2</i>
TSC1	<i>TSC complex subunit 1</i>
TSC2	<i>TSC complex subunit 2</i>
UBE3A	<i>ubiquitin protein ligase E3A</i>
USP15	<i>ubiquitin specific peptidase 15</i>
VSTM2A	<i>V-set and transmembrane domain containing 2A</i>
YPEL3	<i>yippee like 3</i>

Vorwort

Der Hauptteil dieser Arbeit (funktionelle Analyse des Kandidatengens) wurde eigenständig von Denise Haslinger erarbeitet und verfasst. Die kompletten funktionellen Analysen mit Ausnahme der Metaboliten-Analyse wurden von Denise Haslinger durchgeführt. Die Metaboliten-Analyse wurde durchgeführt von Prof. Gilles J. Guillemin und Dr. Chai K. Lim (Macquarie Universität, Australien).

Diese Arbeit wurde bei *Molecular Autism* als Haslinger et al. eingereicht. Zum Zeitpunkt der Abgabe dieser Dissertation befindet sich das überarbeitete Manuskript zur zweiten Runde im Review-Prozess. Das eingereichte Manuskript ist im Appendix angehängt.

Die Charakterisierung des SH-SY5Y Zellmodels erfolgte durch Denise Haslinger. Das Manuskript wurde zusammen mit Dr. Andreas G. Chiocchetti erarbeitet und publiziert als Chiocchetti, Haslinger et al., 2016 in *Translational Psychiatry*. Denise Haslinger hat hierbei die gesamten zellbiologischen Experimente etabliert, optimiert und durchgeführt. Bioinformatische und statistische Analysen wurden mit Unterstützung von Dr. Andreas G. Chiocchetti sowie Afsheen Yousaf durchgeführt

Zusätzlich zu den beiden oben genannten Publikationen sind in dieser Zeit noch 3 weitere Arbeiten entstanden, für welche Denise Haslinger essenzielle Beiträge geleistet hat (siehe Publikationsliste in Abschnitt 11).

Diese Dissertation wurde gefördert durch Stiftungsmittel der Goethe-Universität verliehen an Denise Haslinger für das Thema „Regulation von Autismus-Kandidatengenen während der neuronalen Differenzierung“ und an Dr. Andreas G. Chiocchetti zur „Validierung von Genkopie-Polymorphismen bei Patienten mit Autismus-Spektrum-Störungen“. Außerdem wurden Teile des Projekts finanziert über den Preis der Dr. Paul und Cilli-Weill-Stiftung verliehen an und gespendet von Dr. Andreas G. Chiocchetti.

Ehrenwörtliche Erklärung

Hiermit erkläre ich, Denise Haslinger, geboren am 12.12.1987, dass ich die im Fachbereich Biowissenschaften an der Johann Wolfgang Goethe-Universität in Frankfurt am Main eingereichte Dissertation mit dem Titel „The ASD-associated CNV 16p11.2: Functional study of the candidate gene *QPRT*.“ in der Klinik für Psychiatrie, Psychosomatik und Psychotherapie des Kindes- und Jugendalters unter Betreuung und Anleitung von Prof. Dr. Christine M. Freitag und Prof. Dr. Amparo Acker-Palmer mit wesentlicher Unterstützung und Anleitung durch Dr. Andreas G. Chiochetti ohne sonstige Hilfe selbst durchgeführt und bei der Abfassung der Arbeit keine anderen als die in der Dissertation angeführten Hilfsmittel benutzt habe.

Ich habe bisher an keiner in- oder ausländischen Universität ein Gesuch um Zulassung zur Promotion eingereicht. Die vorliegende Arbeit wurde bisher nicht als Dissertation eingereicht.

Ort, Datum

Denise Haslinger

Zusammenfassung

Hintergrund:

Autismus-Spektrum-Störungen (ASS) umfassen eine Reihe von genetisch komplexen Störungen mit hoher Erbllichkeit. Als zugrundeliegender Pathomechanismus von ASS werden unter anderem Veränderungen der neuronalen Entwicklung diskutiert. ASS ist definiert durch Einschränkungen in der sozialen Interaktion und Kommunikation sowie durch repetitives und stereotypes Verhalten. Genkopiepolymorphismen (englisch „copy number variations“/CNVs), also Deletionen oder Duplikationen einer chromosomalen Region, wurden wiederholt in Probanden mit ASS identifiziert. Dabei gelten Deletionen im Allgemeinen als verheerender, da sich die Reduktion der Gen-Dosis meist stärker auf den Phänotypen auswirkt als eine Hochregulierung (Chang et al., 2015). Die in ASS mit am häufigsten von CNVs betroffene Region liegt auf Chromosom 16p11.2 und umspannt mit einer Größe von ~600kb insgesamt 29 Gene (Woodbury-Smith and Scherer, 2018). Einige dieser Gene wurden bereits funktionell charakterisiert. Zum Beispiel konnte das Gen *KCTD13* in einer Zebrafischstudie als verantwortliches Gen für Veränderungen der Kopfgröße identifiziert werden; ein Phänotyp welcher auch bei humanen Trägern eines 16p11.2 CNVs beobachtet wurde (Golzio et al., 2012; Steinman et al., 2016). Während Träger einer 16p11.2 Deletion sowie das Zebrafisch-Modell mit reduzierter *KCTD13*-Gendosis häufig eine Makrozephalie entwickeln, wird in Duplikationsträgern bzw. Zebrafischen mit hochreguliertem *KCTD13* von einer Mikrozephalie berichtet. Dennoch können die bisherigen Einzelgenstudien nicht alle Aspekte erklären, die durch CNVs der Region 16p11.2 hervorgerufen werden. Ziel dieser Studie war es daher, ein weiteres neuronal assoziiertes Kandidatengen dieser Region zu identifizieren und im Anschluss funktionell im Kontext der neuronalen Differenzierung zu charakterisieren.

Methoden:

Zunächst wurde die SH-SY5Y Neuroblastomzelllinie auf ihre Eigenschaften als Modell für die neuronale *in-vitro* Differenzierung untersucht. Während der 11-tägigen Differenzierung mittels Retinsäure (RA) und dem Zytokin „brain derived neurotrophic factor“ (BDNF) wurden die Zellen mittels Microarray auf Transkriptomebene und mittels Sholl-Analyse (Ristanović et al., 2006) auf morphologischer Ebene

charakterisiert. Drei komplementäre statistische Methoden wurden verwendet, um differenziell regulierte Gene zu identifizieren (Chiocchetti et al., 2016). Mittels „weighted gene co-expression network analysis“ (WGCNA) wurden Gene zu ko-regulierten Modulen zusammengefasst. Zusätzlich wurden auf RNA- (Real-time reverse Transkriptase/RT-PCR) und Protein-Ebene (Western Blot) Marker der Zellteilung bzw. der neuronalen Differenzierung analysiert. Die Expression der 16p11.2 Gene wurde in Hinblick auf die Expressionshöhe sowie deren Veränderung über die Zeit miteinander verglichen. Mittels real-time PCR wurde eine vermutliche *de novo* Deletion der Region 16p11.2 in der DNA eines Probanden mit ASS untersucht und gegen die DNA seiner gesunden Eltern verglichen. Als erster Schritt der funktionellen Validierung wurde über real-time RT-PCR die Gendosis-abhängige Expression von *QPRT* in lymphoblastoiden Zelllinien (englisch „lymphoblastoid cell lines“/LCLs) des Deletions-Trägers sowie dessen Eltern analysiert. In SH-SY5Y Zellen wurde die Expression des Kandidatengens *QPRT* auf Korrelation mit neuromorphologischen Parametern getestet. Die Funktion von *QPRT* wurde in SH-SY5Y auf drei Ebenen gehemmt: (i) mittels knock down (KD) durch siRNA, (ii) durch chemische Inhibition mit Phthalsäure und (iii) über gezielten knock out (KO) durch CRISPR/Cas9 gesteuerte Geneditierung. Die Morphologie von differenzierenden KD-Zellen wurde mittels Sholl-Analyse untersucht und gegen Kontrollzellen verglichen. Zellen mit chemischer Inhibition oder KO des Kandidatengens wurden über Viabilitäts-Assays charakterisiert. Stimulationen durch Quinolinsäure (QUIN), dem Substrat von *QPRT*, wurden in Wildtyp-Zellen durchgeführt und über Viabilitäts-Assays gemessen, um die durch den KO bedingte vermutete Anreicherung von QUIN zu imitieren. In KO-Zellen wurde zudem versucht die Exzitotoxizität von QUIN durch Antagonisten und Inhibitoren der QUIN-Zielstrukturen zu hemmen, um so den KO-Effekt zu kompensieren. Zusätzlich wurden in den KO-Zellen die Metaboliten des *QPRT*-assoziierten Tryptophanstoffwechsels mittels Gaschromatographie/Massenspektrometrie sowie Ultrahochleistungsflüssigkeitschromatographie untersucht. Zudem wurde eine Transkriptom-Analyse mittels „next generation RNA-sequencing“ über „massive analysis of cDNA ends“ (MACE) durchgeführt. MACE-Daten wurden erneut mittels WGCNA zu Gruppen ko-regulierter Gene zusammengefasst, welche in Hinblick auf deren Rollen innerhalb biologischer Prozesse analysiert wurden. Gleichmaßen wurden die infolge des *QPRT-KO*

differenziell regulierten Gene auf ein überdurchschnittlich häufiges Vorkommen in definierten biologischen Prozessen („gene ontology“/GO) und in Autismuskandidatengeneten getestet. Schließlich wurden differenziell regulierte Gene auf ihren Zusammenhang mit Gehirn-Regionen und Prozessen des humanen Gehirns basierend auf Kang et al., 2011 untersucht.

Ergebnisse:

Die neuronale Differenzierung des SH-SY5Y Zellmodells wurde auf RNA- und Protein-Ebene durch eine Reduktion des Zellteilungsmarkers CDK1 und eine Hochregulierung des neuronalen Markers MAPT bestätigt. Das hier verwendete Differenzierungsprotokoll führte zu Zellen typisch für eine Entwicklungsstufe, welche Neuronen *in vivo* 16-19 Wochen nach Konzeption erreichen. Obwohl die Kulturen generell aus Mischungen verschiedener Zelltypen bestanden, exprimierten die Zellen überwiegend kortikale Marker. Mittels der Transkriptomdaten ließen sich 20 Module von ko-regulierten Genen identifizieren. Module, die im Laufe der Differenzierung hochreguliert wurden, waren assoziiert mit neuronalen Prozessen wie „synaptic transmission“. Von den 20 identifizierten Modulen enthielten 6 überdurchschnittlich viele ASS-Risikogene. Von allen Genen der 16p11.2 Region zeigte das Gen *Quinolinat-Phosphoribosyltransferase (QPRT)* im Vergleich zu den anderen Genen des Locus eine hohe Expression und die stärkste sowie robusteste Regulierung über den Verlauf der neuronalen Differenzierung *in vitro*. Im Probanden konnte eine *de novo* Deletion von 16p11.2 bestätigt werden. Ebenso war die Expression von *QPRT* in den LCLs vermindert, also Gendosis-abhängig reguliert. In SH-SY5Y Zellen korrelierte die Expression von *QPRT* signifikant mit der Entwicklung der neuritischen Komplexität während der Differenzierung. Auch die *QPRT*-beinhaltende Gruppe ko-regulierter Gene zeigte eine signifikante Korrelation mit diesem morphologischen Parameter. Wir vermuteten daher einen kausalen Zusammenhang zwischen *QPRT* und der Neuromorphologie differenzierender SH-SY5Y Zellen und testeten im weiteren Verlauf der Studie, wie sich eine Reduktion oder die vollständige Abwesenheit von *QPRT* auf die Differenzierung der Zellen auswirkt. Die Reduktion von *QPRT* führte zu einer milden Veränderung der neuronalen Morphologie von differenzierten SH-SY5Y Zellen, indem die maximale Komplexität der Neuriten

in KD-Zellen im Vergleich zu Kontroll-Zellen näher am Soma gemessen wurde. Die chemische Inhibition sowie der KO von *QPRT* führten zum Zelltod bei differenzierenden aber nicht bei proliferierenden Zellen. *QPRT* codiert für ein Enzym, welches am Tryptophan-Stoffwechsel beteiligt ist und dabei Quinolinsäure (QUIN) abbaut. QUIN wirkt exzitotoxisch, indem es an NMDA-Rezeptoren bindet und diese über-aktiviert. Das Fehlen von *QPRT* sollte daher über eine Akkumulation von QUIN zum neuronalen Zelltod führen (Fukuoka et al., 1998; Braidy et al., 2009). Eine Behandlung des SH-SY5Y Wildtyps mit QUIN führte jedoch weder in proliferierenden noch in differenzierenden Zellen zum Zelltod. Auch die Behandlung der KO-Zellen mit Chemikalien, welche den vermutlich durch QUIN hervorgerufenen Phänotypen mildern sollten, zeigte keinen Effekt. Keiner der nachweisbaren Metaboliten des Tryptophan-Stoffwechsels zeigte Unterschiede zwischen KO und Kontrollen. Auf Transkriptom-Ebene waren dagegen Gene vom KO betroffen, welche mit Prozessen der neuronalen Entwicklung, mit synaptischen Strukturen sowie der Regulierung des Zellzyklus im Zusammenhang stehen. Unter den differenziell regulierten Genen waren überdurchschnittlich viele ASS Risikogene wie zum Beispiel *GABRB3*, welches für eine Untereinheit des GABA-Rezeptors codiert. Ko-regulierte Netzwerke dieser Gene standen im Zusammenhang mit der Entwicklung des dorsolateralen präfrontalen Cortex, des Hippocampus und der Amygdala, welche bei ASS funktionell verändert sind.

Diskussion und Conclusio:

Die hier angewendete Differenzierungsmethode führte zu Neuronen mit einer Entwicklungsstufe welche adäquat ist, um frühe Prozesse der kortikalen Entwicklung abzubilden. Komplexe Interaktionen zwischen den Zellen sowie Prozesse nach der 19. Schwangerschaftswoche können jedoch nicht abgebildet werden. Je nach Anforderung ist das Modell somit für funktionelle Studien neuronaler Prozesse geeignet, auch wenn sich nicht alle Aspekte reifer Neuronen analysieren lassen.

Des Weiteren zeigten wir in dieser Studie einen kausalen Zusammenhang zwischen *QPRT* und der neuronalen Differenzierung *in vitro*. Während eine Reduktion von *QPRT* nur einen milden Einfluss auf die neuronale Morphologie zeigte, führten die chemische Inhibition sowie der genetische KO zum Zelltod differenzierender Zellen. Der vermutete Mechanismus über QUIN-Akkumulation konnte in diesem

Zellmodell nicht bestätigt werden. In der hier untersuchten Neuroblastom-Zelllinie SH-SY5Y zeigte der KO von *QPRT* einen Einfluss auf die Regulation von ASS-assoziierten Genen sowie Gen-Netzwerken synaptischer Vorgänge. Interessant ist hierbei, dass besonders ASS-assoziierte Gene, welche in der postsynaptischen Dichte agieren, differenziell reguliert sind. In der Literatur ist zudem eine Interaktion zwischen *QPRT* und *NLGN3* bekannt (Shen et al., 2015). *NLGN3* ist beteiligt an der Synaptogenese sowie an der Interaktion von Gliazellen und Neuronen. Nachgewiesen wurde *NLGN3* sowohl in GABAergen als auch in glutamatergen Postsynapsen (Budreck and Scheiffele, 2007), sodass wir annehmen, dass es bei einer Reduktion von *QPRT* zu einer gestörten Ausbildung, Stabilität oder Funktion der Neuriten bzw. Synapsen kommt. Dies könnte letztendlich zu einem Exzitations-Inhibitions-Ungleichgewicht führen (Rubenstein and Merzenich, 2003) – ein Prozess, der sowohl für die Krankheitsentstehung von ASS als auch für Epilepsie beschrieben wurde (Bozzi et al., 2017). Bei einem kompletten Verlust von *QPRT* könnte diese Instabilität so weit führen, dass verschiedene Apoptose-Mechanismen angeregt werden, wie zum Beispiel durch eine reduzierte oder inhibierte Aufnahme von Wachstumsfaktoren oder durch eine pathologische Veränderung des Zellzyklus (Fricker et al., 2018). Als Limitierung der Studie sei genannt, dass sich im verwendeten Zellmodell keine funktionellen Synapsen abbilden lassen und somit die Identifikation der synaptischen Prozesse als potenzielle Zielmechanismen von *QPRT* in geeigneteren Zellmodellen bestätigt werden muss. Jedoch konnten wir den Zusammenhang zwischen *QPRT* und der neuronalen Entwicklung mittels KD, chemischer Inhibition und KO auf drei verschiedenen Ebenen zeigen.

Aufgrund der Befunde der Literatur und unseren hier präsentierten Ergebnissen vermuten wir eine duale Rolle für *QPRT*: Zum einen kann eine Reduktion von *QPRT* zu den hier gezeigten neuromorphologischen Veränderungen unabhängig von *QUIN* führen, z.B. durch eine Störung des Zellzyklus, und zum anderen kann es zu der in der Literatur beschriebenen Anreicherung von *QUIN* kommen, welche in Folge zum neuronalen Zelltod führen kann. Unsere Ergebnisse heben in Summe die Rolle von *QPRT* in der Krankheitsentstehung von ASS, insbesondere in Trägern einer 16p11.2 Deletion, hervor.

1 Abstract

Autism spectrum disorders (ASD) comprise a set of highly heritable and genetically complex disorders with a heterogeneous phenotype defined by impairments in social interaction and communication as well as repetitive and stereotyped behaviors. Copy number variations (CNVs) were recurrently identified in individuals diagnosed with ASD, with deletions and duplications of Chr16p11.2 being one of the most frequent. Among other processes, altered neuronal development has been discussed as pathomechanism underlying ASD. Here, we aimed at investigating the expression of 16p11.2 genes during neuronal differentiation and functionally characterizing the highest regulated gene of this CNV, namely *quinolinate phosphoribosyltransferase (QPRT)*, an enzyme of the tryptophan catabolism, for its role in SH-SY5Y differentiation.

First, we confirmed at transcriptomic and neuromorphological level that the SH-SY5Y neuroblastoma cell line is suitable to study neuronal differentiation at a basic level *in vitro*. The obtained neuronal cells were most likely of cortical identity and reminiscent of brain tissue developed for 16-19 weeks post-conception. We further observed that of the 29 genes within the 16p11.2 region *QPRT* showed a high expression and the strongest regulation during *in-vitro* neuronal differentiation. We further confirmed the CNV of a potential 16p11.2 deletion carrier and his parents and report a gene dosage dependent change of *QPRT* in lymphoblastoid cell lines (LCLs) generated from the same individuals. In SH-SY5Y cells, *QPRT* expression significantly correlated with neurite maturation. To functionally characterize *QPRT*, its function was inhibited using (i) siRNA-induced knock down (KD), (ii) chemical inhibition, and (iii) complete CRISPR/Cas9-mediated knock out (KO). The siRNA-induced reduction of *QPRT* altered neuronal morphology of differentiated SH-SY5Y cells. Chemical inhibition as well as complete KO were lethal upon induction of neuronal differentiation but did not affect proliferation. Metabolite analysis showed that the *QPRT*-associated tryptophan pathway was not affected by the KO. Additionally, *QPRT-KO* cells underwent whole transcriptome analysis and genes differentially expressed were identified to be linked to neurodevelopmental processes and synaptic structures. Differentially regulated genes were enriched for ASD candidates. Co-regulated gene networks were implicated in the development of the dorsolateral

prefrontal cortex, the hippocampus, and the amygdala, which have been reported to be functionally altered in ASD.

Thus, in this study *QPRT* was causally related to *in-vitro* neuronal differentiation and affected the regulation of genes and gene-networks previously implicated in ASD. Functionally, these genes converge on synaptic processes, alterations of which are suggested to lead to an imbalance of excitation and inhibition which ultimately induces neuronal cell death. Therefore, our data suggest that *QPRT* may play an important role in the pathogenesis of ASD in Chr16p11.2 deletion carriers.

2 Introduction

2.1 Autism spectrum disorder (ASD)

Autism spectrum disorders (ASD) are complex, neuropsychiatric disorders persisting over the whole lifespan and presenting with a variety of symptoms, especially impairing social interaction. Aberrant neuronal development is discussed as major pathomechanism for ASD. The aetiology of ASD has a strong genetic component with heritability estimates of 64-91% (Tick et al., 2016). An example for recurrent genetic alterations observed in ASD are copy number variations (CNVs) of the chromosomal region 16p11.2 (Woodbury-Smith and Scherer, 2018).

2.1.1 Phenotype and diagnostics

The core symptoms of ASD consist of impairments in social interaction and communication, repetitive and stereotyped behavior, and in some cases delayed or absent language development as well as intellectual disability (ID; American Psychiatric Association, 2013). The phenotype of ASD is heterogeneous regarding IQ, comorbid psychiatric disorders, and language as well as motor abilities. This heterogeneity in part may arise from the diverse genetic backgrounds and multiple genetic hits that are discussed to additively lead to a diagnosis of ASD. In most of the cases the “responsible” mutation leading to ASD cannot be identified as the disorder is assumed to be caused by a combination of various, in most cases unknown, mutations that shape the phenotypes (Bourgeron, 2015; also see section 2.1.3).

While “the autisms” were put into different diagnoses in DSM-IV (American Psychiatric Association, 1994) and ICD-10 (WHO, 1992), namely autistic disorder, Asperger syndrome, childhood disintegrative disorder (CDD) and pervasive developmental disorder - not otherwise specified (PDD-NOS), the spectrum of disorders was merged to one diagnosis in DSM-5, i.e. “autism spectrum disorder” (American Psychiatric Association, 2013). Further, DSM-5 categorizes ASD in two behavioral domains, (i) difficulties in social communication and social interaction and (ii) unusually restricted, repetitive behaviors and interests. It could be argued that Asperger syndrome, where individuals often present with a higher IQ, differs from the

other former subtypes of ASD. However, the sensitivity and specificity of the diagnostic tools is too low to discriminate between them accurately.

To date, ASD is diagnosed by behavior observation. It is assumed that ASD is arising during embryonic development but the first symptoms including delayed language development and problems of social interaction usually can be observed around the age of 1-2 years. Trained psychiatrists and clinical psychologists often use the questionnaire ADI-R (Autism Diagnostic Interview – Revised) to obtain a detailed parent/caregiver report on the development of the offspring (Lord et al., 1994; Poustka et al., 1996, Rutter et al., 2003, 2003). In addition, the child's behavior can be assessed in a highly structured way by the ADOS (Autism Diagnosis Observation Schedule). Here, the clinician is directly interacting and playing with the child to observe the child's interaction, communication, and stereotyped, repetitive behavior (Lord et al., 1989; Bölte and Poustka, 2004; Lord et al., 2012).

ASD often presents with comorbidities, e.g. attention deficit hyperactivity disorder (ADHD). Simonoff and colleagues investigated a sample of 112 children with ASD and identified a single comorbidity in 70% of participants and two or more comorbid disorders in 41% (Simonoff et al., 2008). The most common comorbid disorders were social anxiety disorder, ADHD and oppositional defiant disorder. Interestingly, ASD individuals with comorbid ADHD had a second comorbid diagnosis in 84% of the cases (Simonoff et al., 2008). Epilepsy is diagnosed in 6-27% of children with ASD while 5-37% of epileptic children are diagnosed with ASD (Bozzi et al., 2017).

2.1.2 Epidemiology

In 2012, the estimated prevalence for ASD as assessed using DSM-IV among 8-year-old children was set to 1 in 68 or 14.6 in 1,000 in the United States (Christensen et al., 2016). The authors reported a higher estimated evidence for boys (23.6 in 1,000) than for girls (5.3 in 1,000) reflecting the usual male to female ratio of 4 to 1 described in ASD (Woodbury-Smith and Scherer, 2018). A meta-analysis of 36 epidemiological studies resulted in an ASD prevalence of 2.8-94/10,000 with the median of 17/10,000 (Elsabbagh et al., 2012).

Early studies of autistic symptoms in the United States using DSM-III reported a prevalence of 3.26 in 10,000 individuals aged 2-18 years (Burd et al., 1987), indicating an increase of ASD diagnoses during the last decades (Weintraub, 2011; Lai et al., 2014).

It is uncertain to which extent this rise of ASD diagnoses reflects a real increase of ASD cases. One possible reason for more ASD diagnoses is the higher awareness for the disorder. As estimated in Weintraub, 2011, the combination of well-informed parents and well-trained pediatricians can explain 15% of the increase. Another explanation for the increase in ASD diagnoses can arise from their overlap with differential diagnoses including ID or developmental delay (DD). For example, a decrease of ID diagnoses could be observed while ASD diagnoses increased (Polyak et al., 2015). Overall, diagnostic accretion is able to explain 25% of the increase of ASD (Weintraub, 2011).

In general, the symptoms of ASD remain over the whole lifespan. For individuals diagnosed with ASD in childhood long-term studies confirmed the stability of ASD symptoms, especially problems in social interaction, with a tendency of better outcomes for Asperger than for a diagnosis of autistic disorder. In general adults, also those with a professional career, still needed support in their everyday life (Billstedt et al., 2007).

2.1.3 Aetiology and heritability

Although the exact mechanisms are still elusive, ASD is suggested to be caused by genetic alterations probably interacting with environmental factors. A review of environmental risk factors for ASD suggests a possible contribution of e.g. non-causative association, gene-related effects (environmental factors increasing the risk of gene mutations, e.g. vitamin D deficiency) or oxidative stress (Modabbernia et al., 2017). Another well-studied non-genetic risk factor for ASD is valproic acid (VPA), an antiepileptic and mood stabilizing drug with teratogenic action. A population-based study in Denmark analyzed the incidence of children with ASD for mothers with epilepsy (Christensen et al., 2013). While 4.15% of children born to mothers treated with VPA during pregnancy were diagnosed with ASD, the ASD rate was 1.02% for children whose mothers did not take VPA during pregnancy.

Twin studies analyzing the concordance rates of ASD diagnoses between monozygotic (identical) and dizygotic (fraternal) twin pairs have been used to estimate the variance explained by genetic (heritability) and environmental factors. To date, 13 twin studies have been conducted for ASD, 7 of which were included in a recent meta-analysis (Tick et al., 2016). The meta-analysis reports correlations of 0.98 (95% Confidence Interval CI, 0.96-0.99) for monozygotic twins. For dizygotic twins the authors report correlations of 0.53 (95% CI, 0.44-0.60) at an ASD prevalence rate of 5% and 0.67 (95% CI, 0.61-0.72) at a rate of 1%. Modelling genetic as well as shared and non-shared environmental effects, heritability estimates were set to 64-91% in the meta-analysis (Tick et al., 2016), while shared environmental effects only reached significance when the prevalence rate was decreased from 5 to 1% (7-35%). Thus, environmental effects are not able to explain the majority of the variance in ASD (Tick et al., 2016).

2.1.4 Molecular genetic findings

In general, the genetics of ASD is very complex, i.e. polygenic, but there are rare cases of so called syndromal autism. In these monogenic disorders the mutation of a single gene leads to an autistic phenotype (see 2.1.4.1). Cases where the individual mutations impacting on the observed phenotype are unknown are also referred to as “idiopathic” autism. Various types of molecular genetic studies have been and are currently performed to elucidate the underlying contributors, with the earliest ones being conducted in the form of family-based linkage analysis (see 2.1.4.2) to identify genetic regions linked to the disorder. Later approaches of genetic studies including the whole genomic sequence (see 2.1.4.3) are grouped into (i) genome-wide association studies (GWAS) of single nucleotide polymorphisms (SNPs), (ii) genome-wide copy number variation (CNV) studies and (iii) next generation sequencing (NGS) studies mainly analyzing single nucleotide variation (SNVs).

2.1.4.1 Monogenic forms

Monogenic, Mendelian or syndromic forms of ASD include fragile X syndrome where CGG repeats in the promotor of *fragile X mental retardation 1 (FMR1)* lead to silencing of the gene resulting in the syndrome (Sztainberg and Zoghbi, 2016; also see Figure 1). Approximately 43% of individuals diagnosed with fragile X

syndrome are also diagnosed with ASD (La Torre-Ubieta et al., 2016). Another example is the heterozygous loss (CNV or loss of function mutation) of the gene *SH3 and multiple ankyrin repeat domains 3 (SHANK3)* inducing Phelan-McDermid syndrome, where 80% of carriers are also diagnosed with ASD (La Torre-Ubieta et al., 2016). Up to 50% of individuals suffering from tuberous sclerosis, caused by mutations in the genes *TSC1* or *TSC2*, are also diagnosed with ASD (Smalley, 1998). Mutations of the tumor suppressor gene *phosphatase and tensin homolog (PTEN)* are associated with macrocephaly and ASD (Butler et al., 2005; McBride et al., 2010). In a small set of individuals (N=18) diagnosed with ASD and macrocephaly 17% of probands were shown to have mutations in *PTEN* (Butler et al., 2005).

2.1.4.2 Linkage

Linkage analyses were originally conducted in family-based approaches to identify genetic loci that are in linkage disequilibrium with a disease or phenotypic trait. These analyses test if within a given large pedigree the recombination rate between a known genetic marker and an unknown disease locus is below the expectations of Mendelian laws, i.e. they are located close to each other and inherited together. Linkage of two markers is defined by the LOD (logarithm of the odds) score, i.e. the log ratio between the odds of a marker being co-inherited with the disease and the odds of a random co-inheritance. The resulting linkage regions defined by high LOD or maximum LOD scores (MLS) can contain several candidate genes which are then investigated further.

As reviewed in Freitag et al., 2010, the following regions have been found to be linked to ASD in at least two independent studies: 2q21-33, 3q25-27, 3p25, 4q32, 6q14-21, 7q22, 7q31-36, 11p12-13 and 17q11-21 (Freitag et al., 2010). The region 7q22-32 has been confirmed in a meta-analysis while suggestive evidence for linkage to 10p12-q11.1 and 17p11.2-q12 were reported (Freitag et al., 2010). Another region reported by two independent linkage studies (Weiss et al., 2009; Werling et al., 2014) is located in Chr20p13.

A study by Liu and colleagues demonstrated that the selection of informative subphenotypes to define a homogeneous set of ASD families could help in detecting susceptibility loci in ASD (Liu et al., 2008). When analyzing data of a subset of probands with an IQ ≥ 70 they found linkage to Chr15q13.3-q14, a region also

linked to SZ. The authors also investigated ASD families with a delayed onset of first phrases and found linkage to Chr11p15.4-p15.3 (Liu et al., 2008).

2.1.4.3 Genome-wide studies

2.1.4.3.1 Principles of genome-wide study types

In general, these hypothesis-free study types allow identifying new variation as well as comparing the frequencies of known variants across the investigated groups (rare or common). Further, depending on the study design, genome-wide studies enable to identify *de novo* mutations that are suggested to be of higher penetrance than variants inherited from non-affected parents. Different types and study designs are summarized in the following.

2.1.4.3.1.1 Genome-wide association studies (GWAS)

Utilizing array-based technologies GWAS are used to scan the genome for associated SNPs. GWAS can be performed in a case/control or in a family- or trio-based approach. The case/control approach compares the frequencies of SNPs between cases and controls. Trio (parents-offspring) based analyses test the increased inheritance of variants by comparing the genomes of affected children to that of their parents making use of the transmission disequilibrium test (TDT, Spielman et al., 1993). If a locus is in transmission disequilibrium, i.e. transmitted more often to the affected children than assumed by Mendelian laws, this locus is associated with the disease. An advantage of family-based genome-wide studies is their insusceptibility to population stratification (i.e. different populations can have different allele frequencies due to their ancestries) which needs to be accounted for in case-control association studies. For variation at the level of a single nucleotide at a specific site of the genome, we distinguish between SNPs and SNVs. Usually, a SNP is an annotated variation occurring in the general population with a frequency of >1% in contrast to SNVs which are private or very rare (minor allele frequency MAF < 1%) mutations that are not annotated.

2.1.4.3.1.2 Genome-wide CNV studies

Genome-wide CNV studies are also performed using microarray-based technologies such as whole-genome comparative genomic hybridization arrays (Array-CGH) or bead-arrays to identify a reduction or an increase in gene dosage based on the intensity of the probes on the respective array. The minimum size of reliably called CNVs depends on the resolution of the used array, i.e. the distance between the individual probes, as well as on the used detection software(s). In family-based approaches, genome-wide CNV studies enable the differentiation between *de novo* or inherited copy number deletions (loss of one of the two genomic copies) or duplications (gain of one or more copies). *De novo* CNV variation arises spontaneously in the parental germline during meiosis and is an important aspect in elucidating the etiology of ASD, as these variants only occur in the affected children but not in their parents. Also, genome-wide CNV analyses can be conducted in a case/control manner, which allows estimating frequencies of specific CNVs in cases compared to controls.

2.1.4.3.1.3 Next generation sequencing (NGS) studies

A rather new approach to perform genome-wide studies implies NGS which is able to identify indels, SNVs and in some cases also CNVs. There are two common types of NGS: whole genome sequencing (WGS) and whole exome sequencing (WES). The latter is the cheaper and faster approach as it is only sequencing the ~1% coding part of the genome. Although the coding part of the genome contains a majority of the pathogenic mutations it has to be considered that WES is not able to identify mutations in intergenic regulatory sequences which also have been shown to be disease-related. NGS is again a hypothesis-free approach without preselection of specific genetic regions which makes it a powerful tool for the identification of new mutations as well as comparing their frequencies between cases and controls or detecting *de novo* variation in a family-based approach.

2.1.4.3.2 Genetic architecture of ASD: findings from genome-wide studies

Overall, the sum of inherited variants is contributing to the variation of the human genome to a much higher extent than *de novo* variation (see Figure 1; Gaugler et al., 2014) and rare variants are thought to

have a higher effect on the etiology of ASD than common variation (An and Claudianos, 2016). Common variants are defined at a frequency of > 1% and are thought to have a small effect size but increase genetic liability for ASD in combination (Figure 1). Although smaller in effect, common variants may account for ~40% of the genetic risk for ASD (An and Claudianos, 2016). As further reviewed in An and Claudianos, 2016, *de novo* variation in ASD includes large chromosomal variations, CNVs (> 1kb), small insertions/deletions (indels; 2-1,000bp) and SNVs (1 bp).

Looking at the total population of individuals diagnosed with ASD, syndromic forms (monogenic/Mendelian; see section 2.1.4.1) account for 3.40% of the cases (Gaugler et al., 2014). Overall, 6% of ASD individuals harbor known ASD-associated genetic mutations. Regarding variation in ASD liability, 49% can be explained by common inherited variants, 4% by non-additive genetic effects, 3% by rare inherited and 3% by *de novo* genetic effects (Gaugler et al., 2014; La Torre-Ubieta et al., 2016). In addition, the penetrance of the rare genetic events like SNVs is modulated by the individual's genetic risk score (Weiner et al., 2017).

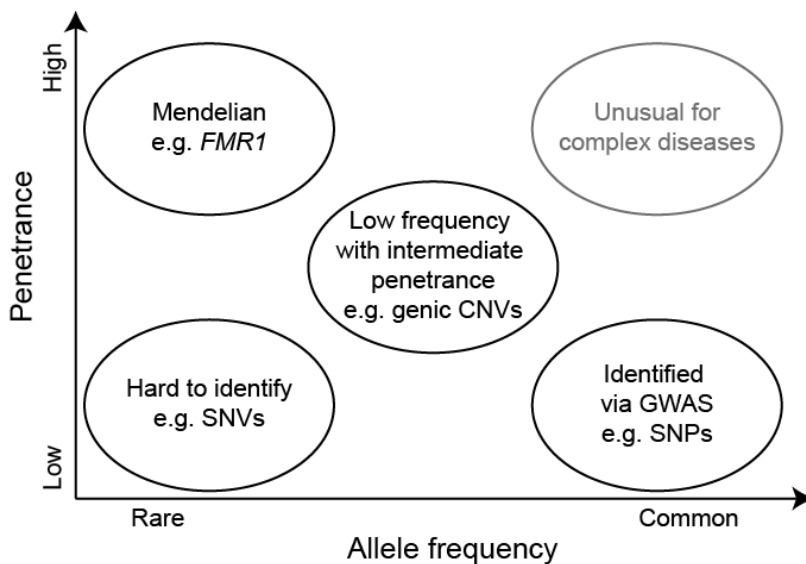


Figure 1 Contribution of rare and common variation to disease susceptibility in ASD.

Rare variants are suggested to have a high penetrance as observed in mendelian diseases where in the case of fragile X syndrome a mutation of the gene *FMR1* is causing the disease. There is also rare variation with a low penetrance, e.g. single nucleotide variants (SNVs). Common variation usually has a lower penetrance, e.g. single nucleotide polymorphisms (SNPs) which can be identified via genome wide association studies (GWAS). Variants with a low frequency and intermediate penetrance occur in the form of e.g. genic copy number variations (CNVs). Common variation with high penetrance is very unlikely in the etiology of complex diseases. Image modified from McCarthy et al., 2008; Manolio et al., 2009.

2.1.4.3.2.1 GWAS

Early GWAS of ASD included findings of chromosomal regions 5p14.1 (Ma et al., 2009; Wang et al., 2009), the gene *semaphorin 5A* (*SEMA5A*) located in Chr5p15 (Weiss et al., 2009), as well as the regions Chr5q21.1 and Chr15q22.1-q22.2 (Salyakina et al., 2010). In 2011, Hussman and colleagues introduced the method of

GWAS-NR. It utilizes a noise reduction method increasing the power to detect true association in GWAS which is especially useful for investigations of complex diseases like ASD (Hussman et al., 2011). In addition to the identified associated SNPs, the multiple flanking SNPs in linkage disequilibrium (LD) are taken into account. Applying their proposed method, they resulted in 860 candidate genes and reported a significant proportion of these genes to be implicated in the regulation of the directional protrusion of axons and dendrites to their appropriate synaptic targets. The most significant finding was a block in LD with ASD spanning the region Chr2p24.1 (Chr2 204444539-20446116; $p = 1.8E-06$) with ASD proximal to the gene *pumilio RNA binding family member 2 (PUM2)*, encoding for a translational repressor during embryonic development and cell differentiation (Hussman et al., 2011).

Additional studies, one including two Chinese cohorts and three European data sets reported genome-wide significant association of variants within the ASD-linked region Chr1p13.2 (Xia et al., 2014) and the SNP rs4141463 in *MACRO domain containing 2 (MACROD2)*; Anney et al., 2010), respectively.

A meta-analysis conducted by the Psychiatric Genetics Consortium (PGC) using GWAS data of ASD patients identified a genome-wide significant locus at 10q24.32 (Anney et al., 2017). This region includes *PITX3*, coding for a transcription factor playing a role in neuronal differentiation, and *CUEDC2*, a gene associated with social skills. Furthermore, the authors replicated findings of loci implicated in schizophrenia (SZ) supporting previous reports of a strong genetic correlation of ASD and SZ.

Another GWAS testing for association with ADI-R questionnaire items identified eight genome-wide significant SNPs. Among the most prominent were SNPs of the gene *potassium voltage-gated channel subfamily D member 2 (KCND2)*, *nitric oxide synthase 2 (NOS2)*, or the *neural EGFL like 1 (NELL1)*; Connolly et al., 2013).

By combining PGC GWAS data of ASD and SZ the authors identified 12 novel loci which may elucidate a common neurodevelopmental phenotype of the disorders, e.g. the previously ASD implicated genes *forkhead box P1 (FOXP1)* or *ATPase plasma membrane Ca²⁺ transporting 2 (ATP2B2)*. Also, they found ASD to be associated with neurodevelopmental genes like *MACROD2*, *HDAC4*, *EXT1* or *ASTN2* (Anney et al., 2017; also see List of genes discussed in this study). Furthermore, a cross-disorder analysis including ASD,

ADHD, schizophrenia, bipolar disorder and major depressive disorder identified genome-wide significant hits in the chromosomal regions 3p21, 10q24, as well as SNPs in *calcium voltage-gated channel subunit alpha1 C (CACNA1C)* and *calcium voltage-gated channel auxiliary subunit beta 2 (CACNB2)*; Smoller et al., 2013).

2.1.4.3.2.2 Genome-wide CNV studies

A study in 2008 reported most of the CNVs found in ASD individuals to be inherited and only 7% to be *de novo* in families having one child with ASD or 2% in families with two or more children diagnosed with ASD (Marshall et al., 2008). This study reported 13 loci with recurrent or overlapping CNVs: 2q14.1, 2q32.1, 6q22.31, 7q36.2, 8q11.23, 9p24.1, 11p12, 13q21.32, 15q11.2-q13.3, 16p12.2, 16p11.2, 22q11.2 and 22q13.31 (Marshall et al., 2008). Having a closer look at the genes located in all the recurrent CNV regions the authors reported the genes to converge on synaptic functions, e.g. the postsynaptic density genes *SH3 and multiple ankyrin repeat domains 3 (SHANK3)*; located at 22q13.3), *neuroligin 4 (NLGN4X)*; at Xp22.31) and *neurexin 1 (NRXN1)*; at 2p16.3; Marshall et al., 2008). Another CNV study focusing on rare variation in ASD reported a higher global burden of genic CNVs in individuals diagnosed with ASD when compared to controls (Pinto et al., 2010). This effect was even clearer when the authors looked at known ASD or ID implicated regions. The study also reported new ASD candidate genes, e.g. *SH3 and multiple ankyrin repeat domains 2 (SHANK2)* located in 11q13.3 or synaptic *Ras GTPase activating protein 1 (SYNGAP1)* located in 6p21.32, as well as an enrichment of CNVs disrupting functional gene sets, e.g. involved in cell proliferation, projection or motility (Pinto et al., 2010).

Levy and colleagues studied rare genomic CNVs in a cohort of N=858 children diagnosed with ASD and N=863 unaffected siblings (Levy et al., 2011). Affected individuals had a higher burden of *de novo* CNV events (75 *de novo* events in 68 probands; 7.9% of all probands) than their non-affected siblings (19 *de novo* events in 17 siblings; 2% of all siblings) and male affected individuals had more *de novo* deletions than duplications (39 to 22, $p=0.04$; Levy et al., 2011). Furthermore, as previously identified by Pinto et al., 2010, the *de novo* CNVs in affected individuals were significantly more often hitting genes when compared to their healthy siblings (61/75 in affected, 9/19 in siblings, $p=0.006$; Levy et al., 2011). This effect became

even stronger when they only considered deletions. While most of the *de novo* events were unique, the authors also reported 16 recurrent events, 10 of which were located in the previously reported genomic region Chr16p11.2 (6 deletions and 4 duplications). As 9 of these CNVs were found in males, the authors assume a gender bias in the penetrance of ASD at 16p11.2 (Levy et al., 2011). The other loci recurrently hit by *de novo* CNVs in this study were 7q11.23, 16p13.2 and the previously reported region 15q11.2. Another study of rare CNVs in ASD confirmed the findings regarding recurrent CNVs of 16p11.2, 7q11.23 and 16p13.2 (Sanders et al., 2011). Furthermore, this study reported additional rare recurrent events at chromosomal regions 1q21.1, 15q13.2-q13.3 and 16q23.3 with a disruption of *cadherin 13* (*CDH13*; Sanders et al., 2011). Another comprehensive study focusing on rare CNVs confirmed an excess of genic CNVs in ASD individuals when compared to controls (Pinto et al., 2014). The identified *de novo* CNVs or loss-of-function single-nucleotide variants were associated with neuronal signaling and development, synapse function and chromatin regulation (Pinto et al., 2014).

In 2015, a study by Sanders and colleagues replicated the findings of increased *de novo* CNVs in affected individuals when compared to controls which in this case was observed for both, deletions and duplications (Sanders et al., 2015). Also, this study confirmed a former observation of the group of a higher burden of *de novo* CNVs in female probands when compared to affected males (ratio: 1.6, 95% CI: 0.9–2.3, $p = 0.04$; Sanders et al., 2015). A review of copy number variation in neurodevelopmental disorders highlights and summarizes the importance of the genomic regions 1q21.1, 3q29, 15q11.2, 15q13.3, 16p11.2, 16p13.1 and 22q11 (Torres et al., 2016). According to the latest estimate, CNVs of the region Chr16p11.2 are among the most recurrent ones with a frequency of 0.8% in ASD (Woodbury-Smith and Scherer, 2018).

A CNV meta-analysis of five different cohorts including individuals with SZ, bipolar disease (BP), ADHD, depression and ASD identified novel associations with duplication of Chr9p24 showing an especially strong association with ASD. The region is harboring the genes *dedicator of cytokinesis 8* (*DOCK8*) and *KN motif and Ankyrin repeat domains 1* (*KANK1*; Glessner et al., 2017). Based on their findings the authors suggest a common genetic component in the pathogenesis of neurodevelopmental disorders.

Regarding overall genetic influences shaping the phenotype of ASD, it was shown that stronger functional insults induced by truncating *de novo* CNVs in combination with truncating SNVs of network genes lead to more severe intellectual, social and behavioral phenotypes (Chang et al., 2015). Specifically investigating CNVs affecting network genes the authors found deletion carriers to have lower IQs (64.8) than duplication carriers (83.9). Affected genes associated with more severe phenotypes, i.e. lower IQ or higher ADI-R scores, showed significantly higher expression in the brain (Chang et al., 2015).

2.1.4.3.2.3 NGS studies

To date, around 50 NGS studies have been performed in ASD research. Most of the NGS studies between 2011 and 2015 are reviewed in Sener et al., 2016. The studies with the highest impact in the field are summarized in the following section:

Sanders et al., 2012 sequenced 238 families of the Simons Simplex Collection (SSC) on whole exome level and identified highly disruptive *de novo* mutations in brain-expressed genes in the affected individuals. Overall, the authors identified 279 *de novo* mutations in coding regions. In one gene, *synuclein alpha* (*SNCA*), they found nonsense *de novo* mutations in two different affected individuals (Sanders et al., 2012). Another big study performed WES on 343 families with one affected child and at least one unaffected sibling (Iossifov et al., 2012). The authors reported twice as many *de novo* gene disrupting mutations in affected individuals when comparing to the unaffected siblings (59 to 28). Many of those mutations were associated with the gene *FMR1* coding for fragile X mental retardation protein (FMRP).

WES studies published in 2014 included the following three studies with the biggest sample sizes: Iossifov et al., 2014, Rubeis et al., 2014 and Dong et al., 2014. Iossifov and associates sequenced ~2,500 simplex families including ~1,900 unaffected siblings (Iossifov et al., 2014). The authors reported *de novo* likely gene-disrupting mutations to be enriched for chromatin modifiers, as well as genes associated with FMRP and genes expressed during embryology. Rubeis et al., 2014 performed WES on ~3,800 individuals diagnosed with ASD as well as ~9,900 ancestry-matched or parental controls. The identified variants converged on the developmental pathways of chromatin remodeling, transcription and splicing as well as synaptic function. In another study, 787 families were whole exome sequenced and report ASD to be

associated with *de novo* indels inducing frameshifts (Dong et al., 2014). Furthermore, the authors identified multiple *de novo* indels in the genes *lysine methyltransferase 2E (KMT2E)*, a chromatin regulator, and *regulating synaptic membrane exocytosis 1 (RIMS1)* regulating the release of synaptic vesicles. Again, this study confirmed the role of synaptic function, chromatin modification and FMRP targets in ASD.

To investigate postzygotic mosaic mutations (PZM) another study exome-sequenced 282 trios (Lim et al., 2017b). PZM develop after fertilization and can lead to distinct cell populations in one individual. They gained interest in the context of ASD as PZM have the potential to give rise to the diverse phenotypes observed in ASD. The authors reported 7.5% of the identified *de novo* mutations to be PZM, 83.3% of which were not described before. The affected genes were enriched for expression in the amygdala, a region reported to be implicated in ASD before (Amaral et al., 2008). Furthermore, the authors reported the genes *kruppel like factor 16 (KLF16)* and *Myb/SANT DNA binding domain containing 2 (MSANTD2)* to show genome wide significant enrichment for PMZs and support previous findings for the ASD candidate genes *sodium voltage-gated channel alpha subunit 2 (SCN2A)*, *heterogeneous nuclear ribonucleoprotein U (HNRNPU)* and *SWI/SNF related, matrix associated, actin dependent regulator of chromatin, subfamily A, member 4 (SMARCA4)*; Lim et al., 2017b).

In another study, WES of 116 trios revealed recurrent *de novo* loss of function mutations in *ubiquitin specific peptidase 15 (USP15)*; Chen et al., 2017). Furthermore, the authors could support evidence for the previously reported genes *FOXP1* (O'Roak et al., 2011) and *lysine demethylase 5B (KDM5B)*; Iossifov et al., 2014). Again, this study reported the identified genes to be involved in FMRP signaling, synaptic formation and transcriptional regulation. In 2017, Yuen and colleagues performed WGS of ~5,200 samples from families with ASD and identified 18 novel ASD candidate genes, e.g. *mediator complex subunit 13 (MED13)* or *PHD finger protein 3 (PHF3)*; C Yuen et al., 2017).

2.1.4.4 Summary on the molecular genetics of ASD

Meta-analysis of ASD twin studies estimated the heritability of the disorder to range between 64-91% (Tick et al., 2016). Early genetic studies identified regions linked to ASD, e.g. the recurrently identified region 7q22-32 (Freitag et al., 2010). Results of SNP-based GWAS include the genome-wide significant locus

10q24.32, harboring the genes *PITX3*, coding for a transcription factor playing a role in neuronal differentiation, and *CUEDC2*, associated with social skills (Anney et al., 2017). CNV studies identified recurrent CNVs in ASD with deletions and duplications of the region Chr16p11.2 being the most recurrent ones with a frequency of 0.8% (Woodbury-Smith and Scherer, 2018). Overall, when compared to healthy controls, CNVs in individuals with ASD are more often *de novo* and spanning genes (Levy et al., 2011). Further, these *de novo* CNVs as well as loss-of-function single-nucleotide variants were associated with neuronal signaling and development, synapse function and chromatin regulation (Pinto et al., 2014). Finally, NGS-GWA studies repeatedly identified genes involved in synaptic function, FMRP signaling, transcription and chromatin remodeling to be associated with ASD. Overall, common variants may account for ~40% of the genetic risk for ASD (An and Claudianos, 2016) while the rare monogenic forms of ASD, e.g. fragile X syndrome, account for 3.4% of ASD cases (Gaugler et al., 2014).

The etiology of ASD is currently estimated to involve 200 to 1,000 potential risk genes (Berg and Geschwind, 2012). There are several databases supplying lists of candidate genes to give an overview of the multitude of reported risk genes, e.g. AutismKB (<http://autismkb.cbi.pku.edu.cn/>) or SFARI gene (<https://gene.sfari.org/>). The latter is organized by the Simons Foundation Autism Research Initiative (SFARI) and uses more stringent criteria than AutismKB. SFARI gene to date reports ~1,000 ASD candidate genes sorted into different categories according to their evidence. Categories are ranged from 1 (most evidence) to 6. Category 1 harbors a small set of genes, including the syndromic candidate *FMR1* (see also 2.1.4.1).

2.2 Neurobiology and current animal or cell models of ASD

To date, the pathomechanisms behind ASD are not fully understood, but there are several reports of an aberrant neuronal development in individuals with ASD. These findings mostly result from studies of *post mortem* brain tissue or from imaging studies of individuals diagnosed with ASD (see 2.2.1 and 2.2.2). As access to *post mortem* brain tissue is limited and the process of neuronal development cannot be assessed *in vivo* in humans it was and is still used to be studied in model organisms or cell lines (see 2.2.4).

2.2.1 Neuropathology

Early studies reported abnormalities in limbic structures, including smaller and more densely packed neurons in the hippocampus and the amygdala (Kemper and Bauman, 1993). Furthermore, dendritic branching was found to be reduced in the hippocampus of individuals with ASD (Raymond et al., 1996). The limbic system is known to be important for emotional processing - a process affected in ASD (Lartseva et al., 2014). Purkinje cells, located in the cerebellum, were found to be smaller and fewer in ASD in several studies (reviewed in Chen et al., 2015). The cerebellum is important for motor control, fitting to findings of a weak motor coordination in ASD patients (Fournier et al., 2010). Furthermore, recent findings also suggest a role of the cerebellum in social and emotional processing, language and cognition (Chen et al., 2015). Reports of studies of the cerebral cortex range from no differences between controls and ASD to an altered cytoarchitecture in ASD. For example, in ASD an aberrant minicolumnar organization was shown to lead to a decreased inter-areal connectivity (Casanova et al., 2006). Furthermore, layers of the prefrontal and temporal cortex were found to be disorganized (Stoner et al., 2014).

2.2.2 Neuroanatomy

The enhancing neuroimaging genetics through meta-analysis (ENIGMA) ASD working group performed a meta-analysis over magnetic resonance imaging (MRI) scans of 1,571 individuals with ASD and 1,651 healthy controls (2-64 years; van Rooij et al., 2018). The authors reported ASD to be associated with smaller subcortical volumes of the pallidum, putamen, amygdala and nucleus accumbens. In addition, individuals with ASD exhibited increased cortical thickness in the frontal cortex and decreased thickness in the temporal cortex. Further analysis of cortical thickness dependent on the age of the subjects revealed strongest alterations in ASD around adolescence while the other subcortical partitions did not show age-related effects (van Rooij et al., 2018).

2.2.3 Genetic basis of altered neurobiology

At genetic level (also see 2.1.4), multiple studies report ASD candidate genes to converge on genes controlling neurogenesis, growth and neuron migration, axon growth or guidance, dendrite arborization as

well as genes regulating synaptogenesis and synaptic function (Krishnan et al., 2016; reviewed in La Torre-Ubieta et al., 2016). As reviewed in Chiocchetti et al., 2014, ASD-associated genetic variants were enriched in glutamatergic pathways, affecting receptor signaling, metabolism and transport. By analyzing ASD risk genes in the context of human brain development, another study identified new ASD risk genes in addition to genes involved in synaptic transmission, as mentioned above (Krishnan et al., 2016). Furthermore, the authors assigned ASD-associated genetic changes to developmental stages and regions of the brain (Krishnan et al., 2016). As also published by other groups before, they found ASD risk genes to affect the development of the fetal prefrontal, temporal and cerebellar cortex (Krishnan et al., 2016).

A further aspect highly discussed in the neuropathology of ASD is the excitatory/inhibitory (E/I) balance (Dickinson et al., 2016). Different genetic causes of ASD are suggested to converge on a dysfunction of excitatory and inhibitory neuronal circuits in various brain regions resulting in a perturbation of the E/I balance (Bozzi et al., 2017). Depending on the underlying genetics, this E/I imbalance is resulting from an interplay of dysfunctions of the GABAergic, glutamatergic, metabolic and immune system as well as the environment and can ultimately lead to cognitive impairment, altered social behavior as well as an increased seizure susceptibility (Bozzi et al., 2017). The recurrent overlap of ASD and epilepsy with an underlying E/I imbalance suggests a common neurobiological basis of the two disorders (Bozzi et al., 2017; also see section 2.1.1).

2.2.4 Current animal and cell models

While there are several examples for animal models, e.g. zebrafish, most researchers will resort to mouse models (see 2.2.4.1) to study the development and phenotypes of ASD. These models are useful for functionally investigating candidate genes or chromosomal regions including rescue experiments to reverse the altered phenotype. This knowledge can then be translated to humans and help in understanding the pathomechanism and finding potential treatments. Further, functional studies of ASD-associated genes or genomic regions are performed in human-derived cellular models (see 2.2.4.2).

2.2.4.1 Mouse models

Numerous mouse models were generated to study ASD at molecular, cellular and behavioral level. Although not to the same level or extent, mice do exhibit several behavioral features of humans which can be measured in well-established tests. Repetitive behavior as seen in individuals diagnosed with ASD can be assessed in mice using the marble-burying test or by monitoring grooming habits. Another important factor in ASD, sociability, is measured in mice using the three-chamber test where the mouse under study can decide to spend time in an empty chamber or a chamber with an unfamiliar mouse (Moy et al., 2004). While a wild type mouse will spend more time in the chamber with the unfamiliar mouse, mouse models for ASD will prefer staying in the empty chamber.

CNTNAP2-KO mice show a decreased number of interneurons and an abnormal neuronal migration. These mice show an impairment of social interaction and communication, repetitive behavior, seizures and hyperactivity. The phenotypes of grooming and hyperactivity could be rescued by administration of risperidone (Peñagarikano et al., 2011). In addition to this *CNTNAP2-KO* mouse there are several mouse models for single genes, e.g. *T-box brain 1 (TBR1)* heterozygous KO (Huang et al., 2014), *FMR1-KO* (Yan et al., 2005b; Bernardet and Crusio, 2006; Lim et al., 2014), *TSC1* heterozygous KO (Tsai et al., 2012) or *PTEN-KO* (Kwon et al., 2006). Several studies in mouse have been performed for the synaptic adhesion molecule families neurexin and neuroligin: *NRXN1A-KO* (Etherton et al., 2009; Grayton et al., 2013), *NLGN3-KO* (Baudouin et al., 2012) and *NLGN4-KO* (Jamain et al., 2008). The main findings of those studies as reviewed in La Torre-Ubieta et al., 2016 include alterations of glutamatergic as well as GABAergic signaling and a reduction of brain volume. The SHANK genes, a family of synaptic scaffolding molecules, have been extensively studied in mice: *SHANK2* exon 7 KO (Schmeisser et al., 2012), *SHANK2* exon 6-7 KO (Won et al., 2012; Lee et al., 2015), *SHANK3B-KO* (Peça et al., 2011), *SHANK3* exons 4-9 KO (Wang et al., 2011), and *SHANK3* heterozygous KO (Bozdagi et al., 2010). These knock outs mainly impact on NMDA-R function (La Torre-Ubieta et al., 2016). The autistic-like phenotype induced by KO of *SHANK2* exon 6-7 could be improved by restoring NMDA-R function (Won et al., 2012). For further reading on mouse models presenting with neuronal phenotypes see La Torre-Ubieta et al., 2016.

Rather than knocking out a single gene, other studies generated mice harboring a deletion or duplication of a bigger chromosomal region, e.g. 15q11-13. Mice with a duplication of this region showed an altered serotonergic signaling and increased spine dynamics and presented with impaired social interaction and communication as well as behavioral inflexibility (Nakatani et al., 2009; Isshiki et al., 2014). The mouse model harboring a hemideletion of the chromosomal region 16p11.2 will be further discussed below (see 2.3.2.1; Grissom et al., 2017).

2.2.4.2 Human-derived *in vitro* cellular models

Regarding the direct investigation in humans, there are limited options of analyzing the brain tissue of ASD individuals *post mortem*. For *in vitro* studies using neuronal cell lines (e.g. SH-SY5Y; see 2.2.4.2.1), patient-specific mutations can be introduced into the cells, e.g. using CRISPR/Cas9, followed by subsequent functional analysis. Also, newer methods, especially the development of induced pluripotent stem cells (iPSCs; see 2.2.4.2.2), allow modeling the disorder in cell lines directly generated from patients' fibroblasts or blood.

2.2.4.2.1 SH-SY5Y

The neuroblastoma cell line SH-SY5Y, also used in our study here, is a well-studied and characterized, commercially available cell line with a relatively cheap and fast neuronal differentiation protocol of two weeks. The cells were originally isolated from a metastatic bone tumor biopsy of a four-year-old girl with neuroblastoma. These cells were subcloned three times, resulting in the SH-SY5Y subclone. The cytogenomic profile of SH-SY5Y was analyzed thoroughly (Yusuf et al., 2013) which makes it easier to focus on the gene under study. The most important findings include a chromosome 7 trisomy and a duplication of chromosome 1q (Yusuf et al., 2013).

Our group has previously performed functional analysis of newly identified *CNTNAP2* promoter variants in SH-SY5Y cells (Chiocchetti et al., 2015). Using electrophoretic mobility shift assays, a method to study DNA-protein binding, we found the promoter variants to result in weaker or stronger binding of nuclear factors, respectively. Furthermore, the effects differed between SH-SY5Y and the embryonic kidney cell line

HEK293T, suggesting a cell type specific expression of nuclear proteins. Luciferase assays were performed to measure transcriptional activation resulting from the different promoter variants. Again, the different variants led to reduced or increased transcriptional activation, respectively. Our results led to the conclusion that *CNTNAP2* promoter variants impact on ASD liability via an alteration of transcription factor binding sites (Chiocchetti et al., 2015). In another study, the ASD candidate gene *forkhead box P2 (FOXP2)* was overexpressed in SH-SY5Y to analyze the effects on gene networks (Oswald et al., 2017). At transcriptional level, the authors report differentially regulated genes to be enriched for ontology terms including e.g. cellular signaling and communication, cellular migration and differentiation as well as terms including the words “neuron” or “axogenesis”. The study emphasized the role of *FOXP2* in nervous system development overlapping with pathways previously reported to be altered in ASD (Oswald et al., 2017). Furthermore, SH-SY5Y cells were modified to harbor an extra copy of Chr15q to study the imprinting effects of the ASD-associated chromosomal region 15q11-13 (Meguro-Horike et al., 2011). The generated SH(15M) cell line was differentiated using phorbol myristate acetate, an activator of protein kinase C. When compared to differentiated wild type SH-SY5Y, mRNA expression of a subset of genes located in 15q11-13 showed a decreased expression (e.g. *NDN*, *GABRB3*, *CHRNA7*) in contrast to the expected increase due to the duplication. The authors could not find methylation differences in the promoters of the respective genes, rather they hypothesize higher order inter- or intra-chromosomal epigenetic alterations to lead to the observed decreased expression at transcriptional level in the 15q duplication syndrome (Meguro-Horike et al., 2011). A follow up study made use of the same cell lines, SH-SY5Y wild type and SH(15M): Via siRNA-mediated knock down of *UBE3A* the authors found *UBE3A*, located in 15q11-13, to impact on genes implicated in gene regulation, DNA binding and brain morphology. Furthermore, the alterations of *UBE3A* levels influenced the methylation levels of up to half of known imprinted genes (Lopez et al., 2017).

Although SH-SY5Y is a feasible, highly cited in vitro model in neuropsychiatric research its suitability and assignability to *in vivo* neuronal differentiation is often questioned. Therefore, in this work here we also analyzed the transcriptome of differentiating SH-SY5Y cells and confirmed their ability to differentiate into

mature neurons (Chiocchetti et al., 2016). Thus, the here applied differentiation method of SH-SY5Y cells allows us to study genes relevant during early cortical development in the context of ASD.

2.2.4.2.2 Human induced pluripotent stem cells (hiPSCs)

iPSCs are patient-specific pluripotent stem cells that can be generated from e.g. fibroblasts taken from a skin punch, from whole blood or from deciduous teeth. The primary cells are cultured and then reprogrammed by introducing the four “Yamanaka factors” Oct3/4, Sox2, c-Myc, and Klf4 (Takahashi and Yamanaka, 2006). After the verification of successful reprogramming, the cells can be differentiated into other cell types, e.g. neurons.

iPSCs have been generated from carriers of the monogenic ASD-associated fragile X syndrome (Muotri, 2016). In different studies, neurons differentiated from these cells showed aberrant differentiation or reduced neuritogenesis (Urbach et al., 2010; Sheridan et al., 2011; Doers et al., 2014; summarized by Muotri, 2016). Another syndromic iPSC model investigated the genomic region 22q13.3 including *SHANK3*, where a deletion leads to Phelan-McDermid syndrome (Shcheglovitov et al., 2013). Neurons generated from these iPSCs exhibited an altered excitatory electrophysiology and a reduction of synapses – effects that could be reversed by an overexpression of *SHANK3* (Shcheglovitov et al., 2013).

Due to the huge amount of probable phenotype-causing candidate genes studying iPSCs generated from non-syndromic ASD is more challenging. Mariani and colleagues generated iPSCs from members of four families with a carrier of ASD with increased head circumference (Mariani et al., 2015). The authors differentiated the generated iPSCs to three-dimensional neural cultures, i.e. organoids, and report alterations of cell proliferation, neuronal differentiation and synaptic assembly in the cells generated from individuals diagnosed with ASD. Furthermore, neurons originating from ASD individuals showed an increase of GABAergic progenitor and neuronal cells resulting from an up-regulation of *FOXP1* (Mariani et al., 2015; La Torre-Ubieta et al., 2016). Another study generated and investigated iPSCs from carriers of 16p11.2 deletions and duplications compared to those generated from controls (Deshpande et al., 2017). This study will be discussed in more detail below (see 2.3.2.2).

Although modeling ASD in human iPS cells is a rather new approach a multitude of studies have been published and to date were summarized in the following reviews: Muotri, 2016, Ben-Reuven and Reiner, 2016, and La Torre-Ubieta et al., 2016.

Despite the huge progress and advantages of using patient-specific neurons generated from iPSCs to investigate mechanisms underlying ASD there are limitations and disadvantages: First of all, the generation of iPSCs and their differentiation is very time consuming and expensive. Establishing iPSC lines from fibroblasts and their characterization usually takes several months, and depending on the differentiation protocol used, it can take two additional months to receive mature neurons that can be used for functional analyses (Xia et al., 2016). On the one hand it is beneficial to use cells that have the same genetic background as the probands; on the other hand, when using cell lines of different individuals, their individual genetic backgrounds can falsify the effect of the gene or genetic variant under study.

2.3 ASD-associated region 16p11.2

2.3.1 Penetrance and phenotype of 16p11.2 CNVs

The ASD-associated chromosomal region 16p11.2 spans ~600kb including 29 genes. As mentioned before, duplications and deletions of 16p11.2 can be identified in 0.8% of ASD cases (Woodbury-Smith and Scherer, 2018) making it one of the most recurrent CNV regions in ASD. While the frequencies of each, 16p11.2 deletion and duplication, is < 0.1% in the general population, it is 0.2% in ASD (Woodbury-Smith and Scherer, 2018). The penetrance of 16p11.2 CNVs was reported to be variable: In a study investigating 85 individuals with a deletion of 16p11.2 and 153 non-carrier familial controls, 93% of deletion carriers had at least one diagnosis of a psychiatric disorder compared to only 21% of the related healthy controls (Hanson et al., 2015). As measured by ADI-R and ADOS, 24% of the carriers were diagnosed with ASD. The deletion carriers not diagnosed with ASD had higher rates of autism-related characteristics, e.g. social and behavioral difficulties measured by the Social Responsiveness Scale (SRS; Hanson et al., 2015). Also, as mentioned before (see section 2.1.4.3), Levy et al., 2011 suggested a higher penetrance of 16p11.2 in males than in females.

Besides their implication in ASD, CNVs of this region are also associated with ID, DD, SZ, congenital anomaly (Torres et al., 2016) and seizures or epilepsy (Shinawi et al., 2010). Notably, the phenotypic outcomes of deletions compared to that of duplications differ in some aspects (see Table 1). While the deletion usually induces macrocephaly, carriers of 16p11.2 duplications present with microcephaly (Steinman et al., 2016). A deletion of this region is associated with a nine times higher likelihood of developing ASD, the duplication is associated with a nine times higher risk of both ASD and SZ (Stein, 2015). Seizures are reported in 40% of carriers of a 16p11.2 deletion and in 30% of duplication carriers suggesting a shared underlying etiology of ASD and epilepsy (Shinawi et al., 2010). Interestingly, deletions of the 16p11.2 locus are also associated with obesity (Maillard et al., 2015) and BP (McCarthy et al., 2009). While DD or ID can occur in some cases of 16p11.2 duplication carriers, they are more common in deletions. The duplication affects expressive and receptive language skills comparably, while in the deletion state expressive language skills are more severely affected (<https://ghr.nlm.nih.gov/condition/16p112-deletion-syndrome>; <https://ghr.nlm.nih.gov/condition/16p112-duplication>).

2.3.2 Functional studies of the whole CNV or single genes located in 16p11.2

2.3.2.1 Animal models for 16p11.2 CNVs

2.3.2.1.1 Zebrafish and mouse models for single genes located in 16p11.2

A study in zebrafish showed that morpholino mediated loss of function (LOF) of 21 out of 22 tested homologous genes of 16p11.2 resulted in measurable phenotypes and that most of the tested genes were required for nervous system development including brain morphology, eye development, axonal density or organization as well as motor response (Table 1; Blaker-Lee et al., 2012). At least two of these genes, *aldolase A*, *fructose-bisphosphate (ALDOA)* and *kinesin family member 22 (KIF22)*, were deletion dosage sensors, i.e. resulting in a phenotype after reducing their expression by 50% using shRNA (Blaker-Lee et al., 2012). Double heterozygous knock outs of the Chr16p11.2 homologs *double C2 domain alpha (DOC2A)* and *family with sequence similarity 57, member Ba (FAM57BA)* induced hyperactivity, increased seizure susceptibility as well as body length and head size in zebrafish (McCammon et al., 2017). Golzio and

colleagues overexpressed each of the 29 human transcripts of the region Chr16p11.2 in zebrafish and report *KCTD13* to be the major driver for the differing head sizes observed in carriers of 16p11.2 CNVs (Golzio et al., 2012). The authors suggest overexpression of *KCTD13* in zebrafish as well as mouse embryos to induce microcephaly via a decreased proliferation of neuronal progenitors accompanied by an increase of apoptosis in the developing brain. A repression of *KCTD13* in contrast led to macrocephaly due to an increase of proliferation with no change of apoptosis (Golzio et al., 2012). In a more recent study, the deletion of *KCTD13* in zebrafish and mice did neither lead to a change in cell proliferation nor could the authors observe a significant effect on zebrafish brain size (Escamilla et al., 2017). Although the authors could not confirm the association of *KCTD13* with head size, they report its deletion to reduce synaptic transmission in mice via an increase of RhoA, a member of the Rho family GTPases which are important for the reorganization of the actin cytoskeleton, regulation of cell shape and motility (Escamilla et al., 2017). In mouse hippocampal slices, the reduction of synaptic transmission could be reversed by inhibiting RhoA (Escamilla et al., 2017).

As a contribution of neuronal polarity in the etiology of ASD has been proposed before (Rasband, 2010), a study aimed at elucidating the role of single genes located in Chr16p11.2 in neuronal polarity in mouse (Li et al., 2013). Using shRNA induced knock down, the authors analyzed the effect of a decreased gene product of 25 16p11.2 genes. They found *DOC2A*, *KIF22* and *T-box 6 (TBX6)* to be required for neuronal polarity in mouse hippocampal cultures in that the knock down cells showed an increased number of multiple axon neurons and a decreased number of single axon neurons (Li et al., 2013; summarized in Table 1). While *DOC2A* knock out mice did not show an apparent phenotype, neurons of hippocampal CA1 slices exhibited altered electrophysiological properties supporting the potential role of *DOC2A* in the release of synaptic vesicles (Sakaguchi et al., 1999).

Down-regulation of 16p11.2 gene *TAO kinase 2 (TAOK2)* in mouse cortical pyramidal neurons was found to impair axonal projections and basal dendrite formation *in vivo* without affecting apical dendrites (Calderon de Anda et al., 2012; also see Table 1). A recent study analyzed behavioral and neuronal parameters in mice harboring a heterozygous or complete knock out of *TAOK2* (Richter et al., 2018). The mice expressed gene-

dosage dependent impairments in cognition, anxiety and social interaction as well as changes of brain size and neural connectivity, deficits in cortical layering, dendrite and synapse formation and reduced excitatory neurotransmission (Richter et al., 2018). Furthermore, via whole exome sequencing the authors identified three *de novo* mutations in *TAOK2*. Functional analyses of these variants in mouse and human cells revealed their implication in protein stability with differing roles in kinase activity, dendrite growth and synapse development. The authors further reported loss of *TAOK2* to result in a reduced activation of RhoA accompanied by an impairment of synapse development. This effect could be rescued by pharmacological activation of RhoA (Richter et al., 2018). A hemizygous deletion of *major vault protein (MVP)*, implicated in the regulation of cellular transport mechanisms, led to impaired strengthening of open-eye responses after monocular deprivation, i.e. reduced ocular dominance plasticity. The authors report a decreased frequency of mEPSCs in pyramidal neurons after extended monocular deprivation suggesting a reduction of functional synapses (Ip et al., 2018). Further, this study identified MVP as a regulator of the homeostatic component of experience-dependent plasticity via the regulation of STAT1 and ERK signaling (Ip et al., 2018).

In this study here, the 16p11.2 gene *quinolinate phosphoribosyltransferase (QPRT)* will be of central interest. To our knowledge, this gene has not been investigated in the context of ASD or the CNV region 16p11.2 before. *QPRT* is coding for an enzyme of the kynurenine pathway, the catabolism of tryptophan resulting in the production of NAD^+ . The role of *QPRT* is to catabolize quinolinic acid (QUIN), a potent neuronal excitotoxin acting as NMDA-R agonist. So far, in a KO mouse model, *QPRT* has only been functionally investigated for its role in Parkinson's disease (Fukuoka et al., 2012; Campbell et al., 2014) and niacin deficiency (Terakata et al., 2012). These *QPRT-KO* mice suffered from neurodegeneration in the striatum suggested to be induced by an accumulation of QUIN (Fukuoka et al., 1998) and further showed a significant increase of urinary QUIN excretion (Terakata et al., 2012; see Table 1). While the KO mice did not show alterations of histological features in the cerebrum, heart, liver, kidney, stomach or spleen, the authors observed that the inner circular layer of the smooth muscle cells of the small intestine was missing in *QPRT-KO* mice (Terakata et al., 2012). Interestingly, elevated QUIN levels were also found in plasma samples of children with ASD (Lim et al., 2015).

2.3.2.1.2 Mouse models for the whole 16p11.2 CNV

Horev and colleagues generated and investigated mouse models for a heterozygous 16p11.2 deletion and duplication (Horev et al., 2011; also see Table 1). The mice showed dosage dependent changes of gene expression, viability, brain architecture and behavior, with the deletion leading to a stronger phenotype than the duplication. Regarding brain architecture, the authors reported the relative volume (percentage of total brain volume) of 8 brain regions to be increased upon deletion of 16p11.2: basal forebrain, superior colliculus, fornix, hypothalamus, mammillothalamic tract, medial septum, midbrain, and periaquaeductal grey (Horev et al., 2011). For mice carrying the 16p11.2 deletion the authors report a postnatal death rate of 50%. By studying the deletion mice described in Horev et al., 2011, another group reported the homologous heterozygous 16p11.2 deletion to lead to an altered cortical cyto-architecture and a reduced brain size – the opposite effect as observed in human deletion carriers (Pucilowska et al., 2015). This was accompanied by a reduction of downstream extracellular signaling related kinase/mitogen activated protein kinase (ERK/MAPK) effectors (Pucilowska et al., 2015). In contrast, mice carrying a microduplication of the region showed increased dendritic arborization of cortical pyramidal neurons (Blizinsky et al., 2016). Via network analysis of protein-protein-interactions the authors identified the gene coding for *MAPK3* as an interesting hub gene (Blizinsky et al., 2016).

Another study performed in mice showed a hemideletion of Chr16p11.2 to induce a male-specific phenotype where male mice only showed a deficit in reward-directed learning and maintaining motivation to work for a sucrose reward accompanied by male-specific overexpression of *dopamine receptor D2* (*DRD2*) and *adenosine receptor 2a* (*ADORA2A*) in the striatum (Grissom et al., 2017). The authors investigated ERK signaling in the striatum and again found differences of protein expression between male and female 16p11.2 hemideletion mice. As discussed by the authors, *ERK1/MAPK3* is coding for an enzyme diminishing synaptic plasticity in the striatum and playing a role in striatal-mediated learning and memory (Mazzucchelli et al., 2002) while *ERK2/MAPK1* enhances striatal synaptic plasticity (Grissom et al., 2017). Grissom and colleagues identified a hyperphosphorylation of ERK1 in male mice after a sucrose reward. Female mice did not only lack this ERK1 hyperphosphorylation but also showed lower baseline levels of

total ERK1 protein. Furthermore, female mice showed an overexpression of ERK2. While levels of mitogen-activated ERK (MEK2), an enzyme phosphorylating ERK1 and ERK2, were not altered upon hemideletion of 16p11.2, again male mice only showed a down-regulation of striatum-enriched protein-tyrosine phosphatase (StEP61), an enzyme dephosphorylating ERK proteins. While it is known that striatal activation in response to rewards differs between males and females, the underlying mechanism is not fully understood (Spreckelmeyer et al., 2009) but could be associated with the sex specific ERK expression and phosphorylation as described in Grissom et al., 2017.

Another study of a 16p11.2 deletion mouse model reports hyperactivity of deletion mice when compared to control mice (Angelakos et al., 2017). Furthermore, when assessing sleep, male mice were found to sleep less and with shorter non-rapid-eye-movement phases, resembling sleep disturbances observed in humans diagnosed with ASD and ADHD (Angelakos et al., 2017). These gender biases revealed in mouse studies, i.e. male mice to be more severely affected by copy number changes of 16p11.2, mirror the findings from studies in individuals diagnosed with ASD: Of 10 identified 16p11.2 CNVs 9 occurred in male ASD individuals (Levy et al., 2011; also mentioned earlier in this chapter).

2.3.2.2 Human-derived cellular models for the whole 16p11.2 CNV

The genes located in Chr16p11.2 showed gene dosage dependent expression in lymphoblastoid cell lines (LCLs) of CNV carriers, leading to differential expression of genes implicated in biological processes such as synaptic function or chromatin modification (Blumenthal et al., 2014).

To elucidate the underlying mechanism of the opposite effects on brain size of Chr16p11.2 deletions and duplications in humans a recent study generated iPSCs from 16p11.2 deletion and duplication carriers as well as from controls (Deshpande et al., 2017). The authors differentiated the generated iPS cells into forebrain neuronal progenitor cells (NPCs) and neurons until 14 weeks post differentiation. They reported no differences of NPC proliferation of the tested cell lines and excluded proliferation as mechanism for a change of total brain size. Neuronal morphology differed according to CNV status – neurons generated from deletion carriers showed an increased soma size and total dendrite length as well as a higher dendritic complexity (Table 1). While neurons generated from duplication carriers showed opposite effects regarding

soma size and total dendrite length (i.e. both decreased) the authors did not observe an effect on the dendritic complexity of these cells. The cells showed alterations in their electrophysiological properties: In general deletion neurons needed higher voltages to fire an action potential, while neurons generated from duplication carriers did not differ from controls in all but one property– they seemed to compensate their reduced somatic size by increasing the outward potassium current in order to stabilize intrinsic excitability (Deshpande et al., 2017). Although deletion and duplication neurons had less synapses they showed higher synaptic strength when compared to control cells and seemed to be able to compensate some but not all of their deficits. Some of the genes located in Chr16p11.2 are encoding proteins interacting with PI3K/AKT and Ras/MAPK, two important cell growth pathways. The alterations of morphology and synapse density are likely to affect neuronal function and formation of networks which in turn could contribute to the neuropathology observed in 16p11.2 deletion and duplication carriers (Deshpande et al., 2017).

Although the chromosomal region 16p11.2 as well as a selection of single genes located in this region have been studied before, not all of the observed phenotypes resulting from deletion or duplication of this region could be fully explained by these findings. Therefore, further studies are needed to elucidate the individual contribution of single genes located in Chr16p11.2.

Table 1 Studies of the chromosomal region 16p11.2 (whole CNV and single genes)

Whole CNV	Deletion, heterozygous	Duplication, heterozygous
Patients	ASD (Woodbury-Smith and Scherer, 2018) BP, DD, ID, obesity, epilepsy (Stein, 2015) macrocephaly (Steinman et al., 2016) expressive language skills are more severely affected (https://ghr.nlm.nih.gov/condition/16p112-deletion-syndrome)	ASD (Woodbury-Smith and Scherer, 2018) schizophrenia, epilepsy (DD, ID) (Stein, 2015) microcephaly (Steinman et al., 2016) expressive and receptive language skills affected comparably (https://ghr.nlm.nih.gov/condition/16p112-duplication)
Human cell lines	↑ soma size ↑ total dendrite length ↑ dendritic complexity ↑ synaptic strength (Deshpande et al., 2017)	↓ soma size ↓ total dendrite length - dendritic complexity ↑ synaptic strength (Deshpande et al., 2017)
Mouse models	strong phenotype, e.g. motor delay, attention deficit, feeding defect 50% postnatal death ↑ relative volume of 8 brain regions (Horev et al., 2011) microcephaly altered cortical cyto-architecture ↓ downstream extracellular signaling related kinase (ERK/MAPK) effectors (Pucilowska et al., 2015) ↓ brain volume ↓ body weight ↑ DRD2 positive striatal medium spiny neurons with synaptic defects hyperactivity, problems in movement control, lack of habituation (Portmann et al., 2014) deficit in reward-directed learning and maintaining motivation to work for sucrose reward in ♂ mice only ♂ striatal ↑ of DRD2 and ADORA2A ♂ ↑ ERK signaling (Grissom et al., 2017) hyperactivity ♂ sleep disturbances (Angelakos et al., 2017)	mild phenotype, e.g. motor delay, attention deficit, feeding defect (Horev et al., 2011) ↑ dendritic arborization of cortical pyramidal neurons; hub gene MAPK3 (Blizinsky et al., 2016)

Table 1 continued

Single gene		Deletion	Duplication
<i>QPRT</i>	Mouse	KO: neurodegeneration in striatum induced by accumulation of QUIN (Fukuoka et al., 1998) ↑ of urinary QUIN excretion (Terakata et al., 2012)	NA
<i>KCTD13</i>	Zebrafish	morpholino LOF: altered brain morphology (Blaker-Lee et al., 2012) morpholino KD: macrocephaly (Golzio et al., 2012) KO and HT KD: - brain size - neurogenesis ↑ RhoA ↓ synaptic transmission (Escamilla et al., 2017)	mRNA overexpression: microcephaly (Golzio et al., 2012)
	Mouse	in utero shRNA KD: ↑ proliferation of neuronal progenitors, suggesting macrocephaly (Golzio et al., 2012) KO and HT KD: - brain size; - neurogenesis ↑ RhoA with ↓ of synaptic transmission inhibition of RhoA restored synaptic transmission (Escamilla et al., 2017)	NA
<i>ALDOA</i>	Zebrafish	morpholino LOF: altered brain morphology (Blaker-Lee et al., 2012) shRNA KD deletion dosage sensor (Blaker-Lee et al., 2012)	NA
<i>KIF22</i>	Zebrafish	morpholino LOF: altered brain morphology (Blaker-Lee et al., 2012) shRNA KD deletion dosage sensor (Blaker-Lee et al., 2012)	NA
	Zebrafish	morpholino LOF: altered brain morphology (Blaker-Lee et al., 2012)	NA
<i>MVP</i>	Mouse	HT del: ↓ of functional synapses (Ip et al., 2018)	NA
	Zebrafish	morpholino LOF: altered brain morphology (Blaker-Lee et al., 2012)	NA
<i>TBX6</i>	Mouse	shRNA KD: neuronal polarity in mouse hippocampal cultures (Li et al., 2013)	NA

Table 1 continued

<i>TAOK2</i>	Zebrafish	morpholino LOF: altered brain morphology (Blaker-Lee et al., 2012)	NA
	Mouse	shRNA KD in mouse cortical pyramidal neurons: ↓ axonal projections and basal dendrite formation (Calderon de Anda et al., 2012) gene-dosage dependent impairments in cognition, anxiety and social interaction changes of brain size and neural connectivity ↓ cortical layering, dendrite and synapse formation ↓ reduced excitatory neurotransmission ↓ RhoA activation pharmacological RhoA activation rescued synapse development (Richter et al., 2018)	NA
<i>DOC2A</i>	Zebrafish	morpholino LOF: altered brain morphology (Blaker-Lee et al., 2012)	NA
	Mouse	sh KD: neuronal polarity in mouse hippocampal cultures (Li et al., 2013) KO in neurons of hippocampal slices: altered electrophysiological properties (Sakaguchi et al., 1999)	NA
<i>DOC2A+</i> <i>FAM57B</i>	Zebrafish	double HT KD: hyperactivity ↑ seizure susceptibility ↑ increased body length ↑ head size (McCammon et al., 2017)	NA
<i>ASPHD1</i>	Zebrafish	morpholino LOF: each single gene altered brain morphology (Blaker-Lee et al., 2012)	NA
<i>BOLA2</i>			
<i>C16orf53</i>			
<i>CDIPT</i>			
<i>CORO1A</i>			
<i>FAM57B</i>			
<i>GDPD3</i>			
<i>HIRIP3</i>			
<i>INO80E</i>			
<i>MAPK3</i>			
<i>MAZ</i>			
<i>PPP4C</i>			
<i>SEZ6L2</i>			
<i>YPEL3</i>			

Abbrev.: ASD: Autism spectrum disorders. BP: Bipolar disorder. DD: Developmental delay. ID: Intellectual disability. KO: Knock out. NA: Not analyzed. QUIN: Quinolinic acid. LOF: Loss of function. KD: Knock down. HT: Heterozygous. shRNA: Small hairpin RNA. For gene descriptions see the List of genes discussed in this study.

2.4 Summary and aims

The etiology of ASD is predominantly genetically determined and altered neuronal development has been suggested as one of the major underlying pathomechanisms. Recent whole genome analyses have shown that in ASD common and rare inherited as well as rare *de novo* variation contributes to ASD risk (Gaugler et al., 2014). For example, *de novo* CNVs, especially deletions, have been recurrently shown to alter genic regions in ASD individuals (Sanders et al., 2015), specifically spanning neurodevelopmental genes (Pinto et al., 2014). One of the most recurrent CNVs in ASD resides within Chr16p11.2 (Woodbury-Smith and Scherer, 2018). The effects of deletions and duplications of this region have previously been studied in zebrafish, mouse and human neuronal cell lines (see section 2.3.2 and Table 1). Taken together, the findings converge on alterations of brain size as well as aberrations of neuronal cell morphology and function including altered ERK signaling (Horev et al., 2011; Pucilowska et al., 2015; Blizinsky et al., 2016; Deshpande et al., 2017; Grissom et al., 2017). While the functional validation of the entire CNV models the genomic status of the patients, investigating gene dosage effects of single genes located in Chr16p11.2 is useful to understand their individual contribution to the complex and diverse pathologies of ASD. Still, only few genes of the Chr16p11.2 region have been investigated for their specific role in human neuronal differentiation. The neuroblastoma cellular model SH-SY5Y is a widely used and feasible model to study neuronal differentiation *in vitro* but its suitability to depict the respective processes sufficiently has been questioned.

Therefore, the aims of this study were:

1. The characterization of the SH-SY5Y cellular model at transcriptomic and morphological level for its qualification as model system for human *in vitro* neuronal differentiation.
2. The investigation of the genes located in the ASD-associated chromosomal region 16p11.2 for their transcriptomic regulation during neuronal differentiation to select a 16p11.2 gene potentially involved in the development of neuromorphology for functional validation.

3. Based on the results from aim 2, testing the hypotheses that the chosen candidate gene, *quinolinate phosphoribosyltransferase (QPRT)* is implicated in neuronal differentiation, and that loss or reduced expression of this gene is resulting in alterations of neuromorphological development.
 - 3.1. Testing if the expression of *QPRT* shows correlation with the development of SH-SY5Y neuronal morphology.
 - 3.2. Comparing *QPRT* expression in lymphoblastoid cell lines of a 16p11.2 deletion carrier and his non-carrier parents to check if *QPRT* is expressed in a gene dosage dependent manner.
 - 3.3. Studying the functional effect of loss of *QPRT in vitro* by inhibiting *QPRT* function in SH-SY5Y cells using (i) siRNA-induced KD, (ii) chemical inhibition, and (iii) complete CRISPR/Cas9-mediated KO with subsequent analyses of cellular viability, neuronal morphology and metabolites.
 - 3.4. Exploring the systems-wide gene interaction network of *QPRT* by analyzing the transcriptomic signature of *QPRT-KO* cells.
 - 3.5. Finally, to understand the role of *QPRT* in neuronal development, testing the genes associated with *QPRT-KO* for enrichment among gene-networks implicated in human brain development (Kang et al., 2011).

3 Material and methods

The here described methods have in part been used and published in Chiocchetti, Haslinger et al., 2016 and Haslinger et al., currently under review at *Molecular Autism*.

3.1 Genetic methods

3.1.1 DNA extraction

DNA of patient blood (S-Monovette EDTA, Sarstedt) or cell lines was extracted using the Masterpure DNA extraction kit (Epicentre) following the manufacturer's protocol. For DNA extraction of saliva (Oragene DNA OG-500, DNA Genotek) we used the PrepIT-L2P kit (DNA Genotek). In all cases, extracted DNA was solved in TE buffer (Epicentre) and concentration was measured using the nanovolume application of a Nanophotometer device (IMPLEN).

3.1.2 Real-time PCR

Here, we performed validation of one *de novo* Chr16p11.2 deletion identified in chip array data (Illumina Human Omni Bead Express Chip, Life and Brain; unpublished data) provided by Dr. Andreas G. Chiocchetti and Dr. Dalila Pinto (Icahn School of Medicine, USA). The cohort used for the chip array is described in Waltes et al., 2014. To assess the relative copy numbers of DNA (CNV validation) we performed real-time PCRs making use of the Universal Probe Library/UPL system (human, probes #1-90, Roche). Primer-probe combinations (see 7.1.2) were designed on genomic DNA sequences in a 2in2out design covering close regions spanning the CNV and 2 sites inside the CNV using the Roche Assay Design Center (<https://qpcr.probefinder.com>). Primers were checked for hairpins (QC cutoff $-2 \leq \Delta G \leq 2$; $T_m < 40^\circ\text{C}$) as well as homo- and heterodimers ($\Delta G \geq -8$) using the IDT Oligo Analyzer tool (<https://eu.idtdna.com/calc/analyzer>). Additionally, DNA primers were tested for specificity using the UCSC in-silico PCR (<https://genome.ucsc.edu/cgi-bin/hgPcr>) and the NCBI nucleotide BLAST tool (<https://blast.ncbi.nlm.nih.gov>). One PCR reaction in a well of a 96 well plate (BioCentrix, Steinbrenner) contained 10ng DNA, 1x ABSolute QPCR Mix, ROX (Thermo Fisher Scientific), 200nM forward primer,

200nM reverse primer (both Sigma Aldrich), 100nM UPL probe (Roche) and nuclease free H₂O (Ambion, Thermo Fisher) ad 20µl. Plates were run using a StepOne Plus device and the corresponding StepOne Plus software with the following protocol: two initial holding steps, 2 min 50°C (enzyme activation) and 10 min 95°C (DNA denaturation) followed by 40 cycles of 15 seconds 95°C and 1 min 60°C. All assays were performed in technical triplicates and analyzed using the StepOne Software v2.3 software and the ExpressionSuite Software (Applied Biosystems). Copy number was estimated using the $2^{-\Delta\Delta Ct}$ method by Livak and Schmittgen, 2001. Two genes, *SNCA* and *CSF3R*, were used as reference genes as they were neither affected by CNVs in our sample nor in the Database of genomic variation (<http://projects.tcag.ca/variation>; 7.1.2). DNA of one 16p11.2 deletion carrier was compared to that of his parent and one unrelated control. As control sample we used DNA of an individual with a low number of significant CNVs.

3.2 RNA methods

3.2.1 RNA extraction

RNA of cell lines was extracted using the GeneJet RNA Purification Kit (Thermo Fisher Scientific) according to the manufacturer's protocol including DNase treatment. Extracted RNA was eluted in nuclease free H₂O (Ambion, Thermo Fisher) and concentrations were measured using the nanovolume application of a Nanophotometer (IMPLEN).

3.2.2 Real-time RT-PCR

To assess relative gene expression, we performed real-time reverse transcription/RT-PCR. RNA was transcribed into cDNA using the RevertAid H Minus First Strand cDNA Synthesis Kit (Thermo Fisher Scientific) kit following the manufacturer's instructions. Generated cDNA was subsequently analyzed using the Universal Probe Library/UPL set (human, probes #1-90, Roche). Specific primer-probe combinations (7.1.3) for genes of interest were designed as described above (3.1.2). One PCR reaction in a well of a 96 well plate (BioCentrix, Steinbrenner) contained 10ng cDNA, 1x Absolute QPCR Mix, ROX (Thermo Fisher Scientific), 200nM forward primer, 200nM reverse primer (both Sigma Aldrich), 100nM UPL probe (Roche)

and nuclease free H₂O (Ambion, Thermo Fisher) ad 20μl. Plates were run and analyzed as described above (3.1.2). The following housekeeping genes (7.1.3) were used for different assays in this study: *GUSB*, *GAPDH*, *POLR2F* and *PSMD7*, selected based on their overall stable expression as reported by literature and based on our own observations. LCLs (see 3.4.1.1) were tested for *QPRT* expression compared to *GUSB*. Microarray data of SH-SY5Y cells (see 3.4.1.2 and 3.2.3.1) were validated for the cell division marker *CDK1*, the axonal marker *MAPT*, as well as selected ASD risk genes (*SHANK3*, *NRXN1*, *CNTNAP2*, *DHCR7*, *GABRB3* and *GRIK2*), glutamatergic (*GRIN1*, *GRIA2*, *GRM1* and *GRM4*) and dopaminergic (*TH* and *DRD4*) markers with the housekeeping genes *GAPDH* and *POL2RF*. To confirm KO of *QPRT* at RNA level in SH-SY5Y cells we analyzed *QPRT* compared to the expression of *GUSB* and *GAPDH*. For the validation of MACE data (see 3.2.3.2 and 3.4.2.4) we assessed expression of a total of 12 genes differentially expressed with a $\log_2FC > 2.5$ between KOs and eCtrl (see Table 2) as well as the genes of interest *QPRT*, *NMNAT2* (only downstream enzyme of *QPRT* differentially regulated upon KO of *QPRT*) and *NLGN3* (interaction partner of *QPRT*; Shen et al., 2015).

3.2.3 Whole transcriptome analyses

3.2.3.1 mRNA microarray raw-data SH-SY5Y

For whole-transcriptome analysis of the wild type SH-SY5Y cell line, whole RNA of three biological replicates of seven time points during neuronal differentiation (0/proliferating to 11 days of differentiation; see 3.4.1.2) was extracted as described in section 3.2.1. Samples passing quality check (RIN > 7) were analyzed on HumanHT-12 v4 Expression BeadChips (Illumina) at Atlas Biolabs. Raw intensity data for each probe were extracted using the GenomeStudio software v2011.1 (Illumina) and mean signal intensities per probe were exported for further analysis. Microarray data are published in Chiocchetti et al., 2016 and can be accessed through the gene expression omnibus repository (GEO) under the accession number GSE69838.

3.2.3.2 Massive analysis of cDNA ends (MACE)

To investigate the overall changes induced by *QPRT-KO* in SH-SY5Y cells (3.4.2.4) we performed a whole transcriptome analysis using MACE. This method in contrast to microarrays allows the detection of low

abundant transcripts and differentiation between alternative 3'UTRs with high accuracy (Zhernakov et al., 2017). RNA was prepared as described in section 3.2.1. RNA integrity number (RIN) was analyzed using the LabChip GX system and only samples with RINs > 9.7 underwent further analysis. MACE analysis including quality control was outsourced to GenXPro. MACE data are available under the GEO accession number GSE113734 and results will be published in Haslinger et al., currently under review at *Molecular Autism*.

3.3 Protein methods

3.3.1 Protein extraction, gel electrophoresis and Western blot

3.3.1.1 Confirmation of neuronal differentiation

For protein extraction for subsequent confirmation of neuronal differentiation, cell pellets of 0/proliferation to 11 days of differentiation were resuspended in 200µl NET2 buffer: 20mM tris pH 7.5, 150mM NaCl (both AppliChem), 0.05% IGEPAL (Sigma Aldrich) supplemented with 1 proteinase inhibitor cocktail tablet for 10ml of total buffer (cOmplete ULTRA Tablets Mini Easypack, Roche). After a 15 min incubation on ice, the cells underwent 5 repetitive freeze (-80°C) and thaw cycles. Cell debris was centrifuged 15 min at 4°C at 17,000g. Protein concentration was measured using the Pierce BCA Protein Assay Kit (Life Technologies) following the manufacturer's protocol. Colorimetric measurements in cuvettes were performed using a Nanophotometer (IMPLEN) at 562nm. Proteins were precipitated with 1x volume 20% TCA (Carl Roth) and washed three times for 10 min with 1ml of 100% EtOH on ice. Proteins were pelleted for 10' at 4°C and 20,000g. Finally, air dried pellets were resuspended in 1x SDS-sample buffer diluted from 4x SDS sample buffer: 0.0627M tris, 1% SDS (both AppliChem), 10% glycerol, 2% 2-mercaptoethanol (both Carl Roth) and 0.1% bromophenol-blue (AppliChem). The solution was denatured for 5 min at 95°C. Samples were electrophoresed on a 12% SDS gel (resolving gel: 12% acrylamide/bis-acrylamide (37.5:1; Serva), 0.375M tris pH8.8, 0.1% SDS (both AppliChem), 0.05% APS, 0.1% TEMED (both Carl Roth); stacking gel: 4% acrylamide/bis-acrylamide (37.5:1; Serva), 0.125M tris pH8.8, 0.1% SDS (both AppliChem), 0.1% APS, 0.2% TEMED (both Carl Roth)) using a Mini-PROTEAN Tetra Cell (Bio-rad) with 1x running buffer (10x running buffer: 250mM tris, 1.92M glycine, 1% SDS (all

AppliChem)). The gels were blotted in a semi dry approach (Trans-Blot Semi-Dry Transfer Cell, Bio-rad) on a PVDF membrane (Immobilon-FL) for 1 hour applying 20V (anode buffer 1: 20%MeOH (Fisher Chemical), 300mM tris (AppliChem); anode buffer 2: 20%ml MeOH (Fisher Chemical), 25mM tris (AppliChem); cathode buffer: 20% MeOH (Fisher Chemical), 40mM Aminohexanoic acid (Sigma Aldrich)). Successful blotting was confirmed using Ponceau S-Solution (AppliChem) with subsequent PBST (1xDPBS (Thermo Fisher), 0.1% Tween-20 (AppliChem)) washes until the Ponceau staining was completely removed. Membranes were blocked for 1 hour with SuperBlock Blocking Buffer (Pierce). Primary antibodies were incubated overnight in blocking buffer. Secondary antibodies were incubated 1 hour at room temperature. Blots were washed in between three times for 5 min in DPBS + 0.05% Tween-20. Protein size and antibody specificity allowed applying CDK1 and MAPT antibodies simultaneously (1:500 in SuperBlock; both rabbit; GeneTex). GAPDH antibody (1:2,500 in SuperBlock; mouse; Santa Cruz) was applied after stripping of blots with 100mM 2-mercaptoethanol (Carl Roth), 2%SDS, 62.5mM tris pH 6.7 (AppliChem) for 30 min at 50°C. Secondary antibodies (2nd goat anti-rabbit poly HRP or 2nd goat anti-mouse poly HRP; 1:5,000 in SuperBlock; Pierce/Thermo Scientific) were visualized using the ECL Prime Western Blot Detection Reagent (GE Healthcare). See section 7.1.1 for a list of all used antibodies.

3.3.1.2 Confirmation of QPRT knock down and knock out

For the subsequent analysis of QPRT dosage, cell pellets of *QPRT-KD* cells (see section 3.4.2.2) and *QPRT-KO* (see section 3.4.2.4) were resuspended in 60-100µl (according to cell pellet size) RIPA buffer: 50mM tris pH8, 150mM NaCl, 1% Triton X-100, 2mM MgCl₂ (all AppliChem), 0.5% Sodium Deoxycholate (Sigma Aldrich) plus freshly added 0.1% SDS (AppliChem), 0.5µl-1µl/ml Universal Nuclease (Pierce) and 1 proteinase inhibitor cocktail tablet for 10ml of total buffer (cComplete ULTRA Tablets Mini Easypack, Roche). After 30 min incubation on ice, suspensions were centrifuged for 15 min at 4°C at 14,000 x g. Concentrations of supernatants, containing total protein, were measured using the Pierce BCA Protein Assay Kit (Life Technologies) following the manufacturer's protocol. Colorimetric measurements in cuvettes were performed using a Nanophotometer (IMPLEN) at 562nm. For RIPA extracts, 50-100µg of total protein lysate were mixed with protein loading dye (60mM tris pH6.8, 1% SDS (both AppliChem), 5% glycerol,

0.01mg/ml bromophenol blue (both Carl Roth)) and samples were adjusted to a final volume of 20µl with water. Protein samples were denatured for 5 min at 95°C. Gel electrophoresis was performed at 100V until all samples entered the stacking gel (5% acrylamide/bis-acrylamide (37.5:1; Serva), 0.1% SDS, 125mM tris pH6.8 (both AppliChem), 0.1% APS, 0.1% TEMED (both Carl Roth)) and migrated into the resolving gel (12% acrylamide/bis-acrylamide (37.5:1; Serva), 0.1% SDS, 250mM tris pH8.8 (both AppliChem), 0.1% APS, 0.04% TEMED (both Carl Roth)). Thereafter, voltage was increased up to 140V. Using a semidry approach, proteins were transferred to a nitrocellulose membrane (GE Healthcare) with 1mA/cm² for 1-2 hours. After Western blotting (blotting buffer 125mM tris, 1.25mM glycine, 0.1% SDS (all AppliChem), 20% methanol (Fisher Chemical)), membranes were incubated in SuperBlock (Pierce) for 1 hour at room temperature. After application of first (anti-QPRT antibody, 1:1,000 in SuperBlock; mouse; Abcam) and secondary antibody (anti-mouse IgG HRP conjugate; 1:5,000 in SuperBlock; Santa Cruz) membranes were washed three times with PBST for 10 min each. Proteins were detected using the ECL Prime Western Blot Detection Reagent and the Amersham Hyperfilm ECL (both GE Healthcare). Prior to application of controls, blots were stripped with 100mM 2-mercaptoethanol (Carl Roth), 2% SDS, 62.5mM tris pH6.7 (both AppliChem) for 30 min at 50°C and again blocked with SuperBlock for 1 h. β-Actin (Sigma Aldrich; mouse, 1:10,000 in SuperBlock) or GAPDH (1:2,500 in SuperBlock; mouse; Santa Cruz) were applied for 1 hour at room temperature. The subsequent steps including secondary antibody and visualization were performed as described above. See section 7.1.1 for a list of all used antibodies.

3.4 Cell culture methods

3.4.1 Cell lines and growth conditions

3.4.1.1 Lymphoblastoid cell lines (LCLs): Transduction and growth conditions

LCLs were established as published in Neitzel, 1986. In short, a 50ml Leucosep™ (Greiner) reaction tube with an inserted polyethylene filter was filled with 15ml of Ficoll (Biocoll) and centrifuged at 1,000 x g for 3 min to establish a density gradient. After 9ml of EDTA-treated blood were mixed with 9ml of HBSS (Life Technologies) the solution was carefully poured onto the filter. To separate the lymphocytes from the

erythrocytes, the Ficoll gradient was centrifuged at 1,000 x g for 10 min with minimal deceleration afterwards. The lymphocytes, now in the foggy layer right above the filter, were transferred into 10ml HBSS (Life Technologies) and washed three times by centrifugation at 1,000 x g for 5 min, 800 x g for 5 min and 700 x g for 5-10 min. The pellet was resuspended in 2-2.5ml of pre-warmed (37°C) culture medium, i.e. RPMI medium supplemented with 20% FCS, 1X GlutaMAX (all Life Technologies) and 1% penicillin/streptomycin (PAA). After transferring this suspension to a 25cm² flask, 10µl of cyclosporine A (Sigma Aldrich; 1mg/ml dissolved in 100% EtOH) were added to inhibit the propagation of the T-lymphocytes. Finally, 500µl of active Epstein-Barr virus (EBV) containing supernatant were added for the generation of lymphoblastoid cell lines. The lymphoblastoid cell lines were cultured as suspension cultures in flasks in an upright position. They were grown at 37°C with 5% CO₂ and 95% humidity. The cells were fed by adding fresh medium at least once a week. The RPMI medium contained phenol red as pH indicator, which changes from red to yellow according to the metabolism of the cells. After the cultures had turned to yellow, they were fed every second day by adding medium. When the cells reached stable growth (observable by cell clumps), they were further grown in standard medium containing 10% FCS instead of 20% FCS.

To investigate gene expression (see 3.2.2) in exponentially growing LCL cultures, 1×10^6 viable cells were inoculated into standard medium. Volume was doubled each time cultures reached a density of 1×10^6 cells/ml until total volume was 40ml. Cells were harvested by centrifugation at 1,000 x g for 5 min and washed with DPBS (Life Technologies) followed by a centrifugation at 1,500 x g for 5 min. Pellets were stored at -80°C until further processing.

For validation of gene dosage at transcription level, RNA was extracted as described above (see 3.2.1). Real-time RT-PCR for *QPRT* and the housekeeper *GUSB* was performed as described in section 3.2.2. For used primers see 7.1.3.

3.4.1.2 SH-SY5Y neuroblastoma cell line: Expansion and differentiation

SH-SY5Y identity was confirmed by DNA fingerprinting using AmpF ℓ STR Profiler and AmpF ℓ STR NGM Select PCR Amplification Kits (Applied Biosystems) according to the manufacturer's protocol (performed by Dr. Thomas Rothämel, Institute of Legal Medicine, Hannover Medical School).

For proliferation, cells were cultured in DMEM supplemented with 10% FCS, 1% sodium pyruvate (all Life Technologies) and 1% penicillin/streptomycin (PAA). As described in Chiocchetti et al., 2016, cells were differentiated using a continuous application of retinoic acid (RA) and brain derived neurotrophic factor (BDNF). Differentiation media consisted of Neurobasal[®]-A medium supplemented with 1x GlutaMAX, 1x B-27 supplement (all Life Technologies), 10 μ M retinoic acid, 2mM cAMP (both Sigma Aldrich), 50ng/ml hBDNF (Immunotools), 1% penicillin/streptomycin (PAA) and 20mM KCl (Sigma Aldrich). Cells were differentiated for 11 days changing the medium every other day. The time points for extraction of mRNA or protein and imaging were set to 24 hours after media changes: 0/undifferentiated, i.e. proliferating cells, 1, 3, 5, 7, 9 and 11 days of *in vitro* differentiation.

For subsequent microarray analysis, SH-SY5Y WT cells were seeded with a density of 5 x 10³ cells/cm² and differentiated for 11 days with harvesting time points as described above.

For MACE analysis, cell lines (three biological replicates of each WT, eCtrl and KO cells; see 3.4.2.4) were seeded with a density of 2 x 10⁴ cells/cm² in proliferation medium. After 3 days, media were changed to differentiation and cells were differentiated for 3 days without media changes.

For subsequent protein extraction (see 3.3.1.1 and 3.3.1.2) cells were seeded with a density of 2 x 10⁴ cells/cm² in T75 flasks.

Growth conditions for proliferating and differentiating cells in cell culture assays are defined in the respective sections below (3.4.2).

3.4.2 Cell culture assays

3.4.2.1 Transfection methods

For morphological analysis of SH-SY5Y wild type (see section 3.4.2.3), 5×10^5 cells were seeded in a well of a 12 well plate and allowed to attach overnight. The following day cells were transfected with $1\mu\text{g}$ of the respective plasmid and $4\mu\text{l}$ of Metafectene Pro (Biontexas) per well of a 12 well plate following the manufacturer's protocol (DNA [μg] : reagent [μl] = 1 : 4).

The same transfection method was used for generation of CRISPR/Cas9 induced knock outs (see 3.4.2.4) in SH-SY5Y cells using pSpCas9(BB)-2A-Puro (PX459) V2.0 (Plasmid #62988; Addgene). Here, we seeded 4.5×10^5 cells in a well of a 6 well plate (5×10^4 cells/ cm^2) and let them attach overnight. The following day cells were transfected with $2\mu\text{g}$ of plasmid DNA plus $8\mu\text{l}$ of Metafectene Pro.

Lipofectamine RNAiMAX Reagent and OptiMEM (both Thermo Fisher Scientific) were used for co-transfecting SH-SY5Y cells with siRNAs (see also 3.4.2.2) and the pcDNA3 mCherry LIC cloning vector (6B) (Plasmid #30125, Addgene). In a 96 well format 1.7×10^5 cells per well were reversely transfected with 120ng of mCherry plasmid DNA and 5nM siRNA using Lipofectamine RNAi Max and OptiMEM (Thermo Fisher). To confirm siRNA knock down at protein level, 5×10^5 WT cells were seeded and reversely transfected in a 6cm dish. Cells were harvested for protein extraction (see 3.3.1.2) after 3 days.

3.4.2.2 Small interfering RNA (siRNA) mediated knockdown

To study the functional effect of a knock down of *QPRT*, we used 3 different siRNAs targeting *QPRT* (Ambion Silencer Select siRNA, Thermo Fisher) and one non-targeting control siRNA, respectively: "siQ1": s23898 (Lot# ASO20MTK), "siQ2": s23899 (Lot# ASO20MTJ) and "siQ3": s23900 (Lot# ASO20MTI); and the Silencer® Select Negative Control 1 (Ambion, Thermo Fisher). Lyophilized pellets were diluted in nuclease-free water (Ambion, Thermo Fisher) and stored at -20°C as $20\mu\text{M}$ stocks. The final concentration for transfection was 5nM . To allow imaging and studying the morphology of single transfected cells only, cells were co-transfected with pcDNA3 mCherry LIC cloning vector (6B) (Plasmid #30125, Addgene; for details on

transfection see section 3.4.2.1). siRNA generated KD targeting the three different sites of *QPRT* was proven on RNA level when compared to the non-targeting control.

3.4.2.3 Morphological analysis

To study morphological development of wild type SH-SY5Y cells during neuronal differentiation we transfected proliferating cells with pmaxGFP (Lonza; see also section 3.4.2.1). One day after transfection, cells were seeded 1:2 in co-cultures with untransfected cells with a density of 1×10^4 cells/cm² to allow imaging of individual transfected cells. Cultures were differentiated for 11 days and imaged every other day using a Motic AE31 fluorescence microscope (Motic).

Images of single cells were analyzed using custom macros in ImageJ (see 7.2.1). In short: All images were equalized, despeckled and background was subtracted using the rolling ball method prior to binarization (Auto threshold "Otsu-dark"). Sholl analysis (Ristanović et al., 2006), a concentric circle method, was performed using the respective ImageJ plugin with manual selection of the cells' center and with fitting polynomial regression of the 5th degree, as suggested by the manual (http://imagej.net/Sholl_Analysis). Following morphological parameters were assessed: average number of intersections (number of intersecting radii divided by the number of intersections analyzed; a measure describing neuritic complexity), maximum intersections (maximum number of intersections for one radius), sum of intersections (sum of all intersections of one cell), the enclosing radius (the outer radius intersecting the cell, describing the longest distance between soma and neurites), the intersecting radii (number of radii intersecting a cell, also distance between soma and neurites) and the maximum intersections radius (the distance from the soma where most neurites are present, i.e. the site of the highest branching density).

To study the effects of siRNA-induced KD of *QPRT* in SH-SY5Y cells we transfected wild type cells as described in sections 3.4.2.1 and 3.4.2.2. The day after transfection, differentiation medium was applied and changed every other day. Cells were imaged after 11 days of differentiation using an ImageXPress Micro XLS (Molecular Devices). Images were analyzed using the MetaXPress software and ImageJ (Sholl analysis) as described above.

3.4.2.4 CRISPR/Cas9 mediated knockout

To study the functional effect of complete knock out of *QPRT* we used CRISPR/Cas9 genome engineering as described elsewhere (Ran et al., 2013). In short, sgRNAs were designed using the tool crispr.mit.edu and cloned into pSpCas9(BB)-2A-Puro (PX459) V2.0 (Plasmid #62988; Addgene). For knockouts, 2 sgRNAs (Sigma Aldrich) targeting different sequences of *QPRT* were used in addition to one non-targeting control (see 7.1.4). Validated plasmids (Sanger-sequencing) were transfected into SH-SY5Y cells (see section 3.4.2.1) followed by puromycin (Sigma Aldrich) selection using 750ng/ml for 7 to 14 days. Single cell clones were isolated using 5µl of Trypsin-EDTA (Thermo Fisher Scientific) and expanded in 96 well plates. Homozygous single cell clones for the 2 constructs were identified by Sanger sequencing and termed as following: del268T (*QPRT*^{-/-} NM_014298; CR1/Ex2.1); ins395A (*QPRT*^{-/-} NM_014298 ins395A; CR3/Ex2.2); eCtrl (empty control vector). Both indels were in silico checked for frameshift-induced premature stop codons.

3.4.2.5 Viability assays

Viability of SH-SY5Y cells was assessed using propidium iodide (PI) viability-assays. PI and Hoechst33342 (both Sigma Aldrich) were pre-diluted in DPBS and used with final concentrations of 1µg/ml and 10µg/ml for the assay, respectively. Cells were incubated for 5 min at 37°C and imaged using the ImageXPress Micro XLS microscope (Molecular Devices). Wells were imaged through the channels for DAPI, assessing cells with Hoechst33342 stained DNA, i.e. the total cell population, and TRITC, assessing cells stained with PI, i.e. dead cells only as PI is not able to cross the membrane of living cells. Acquired images were analyzed using the MetaXPress macro “Cell Scoring” which uses the different fluorescence signals to analyze the percentage of dead cells.

To measure the effect of chemical *QPRT* inhibition we seeded wild type SH-SY5Y cells with a density of 2.5×10^4 cells/cm². After cells have attached overnight, media were changed to either fresh proliferation or differentiation media containing 0 (reference), 5 or 10mM of the *QPRT* inhibitor phthalic acid (PA; Sigma Aldrich; directly diluted in the respective media; (Braidy et al., 2011)) and incubated for 3 days followed by PI assays. Percentage of dead cells after application of 5 and 10mM PA was compared to the 0mM reference for proliferating and differentiating cells, respectively.

To measure the effect of *QPRT-KO* on viability of differentiating SH-SY5Y, KO and eCtrl cells were seeded with a density of 2.5×10^4 cells/cm². The following day, media were changed to differentiation media. PI viability-assays were performed after 3 days.

To test if the observed cell death during differentiation in KO cells is driven by an accumulation of the QPRT substrate quinolinic acid (QUIN; Sigma Aldrich), we exposed WT cells to this neurotoxin. Cells were seeded with a density of 2.5×10^4 cells/cm² and media were changed after 24 hours to either fresh proliferation or differentiation media containing 0 (reference; vehicle H₂O only), 5 or 250µM of QUIN (Braidy et al., 2009) and incubated for 3 days followed by PI viability-assays. Percentage of dead cells after application of 5 and 250µM QUIN was compared to the 0µM reference for proliferating and differentiating cells, respectively.

Finally, we aimed to rescue the effects of a potential *QPRT-KO* driven increase of QUIN by inhibiting downstream pathways. Cells were seeded with a density of 2.5×10^4 cells/cm². After 24 hours, media were changed to differentiation media containing (i) 0 (reference; vehicle H₂O only), 6 and 12µM of the NMDA-R antagonist MK801 (Sigma Aldrich; Petroni et al., 2013), (ii) 0 (reference; vehicle H₂O only), 0.5 and 1mM of nitric oxide synthase 1 (NOS1) inhibitor L-NAME (Sigma Aldrich; Candemir et al., 2016) and (iii) 0 (reference; vehicle H₂O only), 5 and 10mM of NAD⁺ (Sigma Aldrich; Zheng et al., 2013). PI viability-assays were performed after an incubation of 3 days. All rescue experiments were performed with differentiating *QPRT-KO* cell lines compared to the eCtrl.

3.4.2.6 Metabolite analysis

To characterize *QPRT-KO* at the level of the kynurenine pathway, i.e. tryptophan catabolism, cell culture supernatants were analyzed for metabolites by Dr. Edwin Lim and Prof. Gilles J. Guillemin (Macquarie University, Faculty of Medicine and Health Sciences, Australia). They used their established and previously published methods of ultra-high-performance liquid chromatography (UHPLC; for tryptophan, kynurenine, 3-hydroxykynurenine, 3-hydroxyanthranilic acid, anthranilic acid and kynurenic acid) and gas chromatography-mass spectrometry (GC/MS; for picolinic acid and quinolinic acid). Cell lines were seeded with a density of 2×10^4 cells/cm² and grown in proliferation or differentiation media for 3 days as described above. Supernatants of replicates were harvested and stored at -80°C until further proceedings.

UHPLC and GC/MS were performed as described previously by Dr. Lim (Lim et al., 2015; Lim et al., 2017a; see 7.2.2 in the appendix).

3.5 Statistics

If not stated otherwise, statistical analyses were performed using R version 3.2.3.

3.5.1 Group differences

Group differences between mRNA expression foldchange in LCLs of a deletion carrier compared to his non-carrier parents were tested using t-test and considered significant at a p-value < 0.05. Group differences of morphological parameters (siRNA assay) were tested using t-tests with Benjamini-Hochberg correcting for multiple testing (10 tests). FDRs were considered significant below a threshold of $FDR \leq 0.05$. Group differences between treated and untreated samples (e.g. PI-assays) were tested using t-test; uncorrected p-values are reported and considered significant at a p-value < 0.05. All samples were compared to their respective control (e.g. non-targeting siRNA) or reference (e.g. 0mM of inhibitor).

3.5.2 Correlations

Correlation between morphological parameters and gene expression, or eigengene expression, or between real-time RT-PCR and microarray log₂FC data was tested based on the Pearson's correlation coefficient. Reported p-values are FDR corrected for 132 tests (6 morphological parameters, 20 gene modules, 2 gene expressions).

3.5.3 Targeted mRNA expression

Data of real-time RT-PCR experiments were analyzed using the $2^{-\Delta\Delta Ct}$ method (Livak and Schmittgen, 2001). Group differences were tested using t-test. For validation of RNA-Seq data (3.2.3.1 and 3.2.3.2), real-time RT-PCR data and RNA-Seq normalized reads were tested for correlation as described above using Pearson correlation.

3.5.4 Transcriptome analyses

3.5.4.1 Microarray

To validate neuronal differentiation at transcriptomic level (also see 3.2.3.1) CoNteXT analysis has been implemented (Stein et al., 2014; Chiocchetti et al., 2016). This framework is based on human post-mortem brain data and allows estimating the developmental stage and regional identity of transcriptomic signatures.

Biostatistical methods to identify regulated genes during neuronal differentiation were implemented by Dr. Andreas G. Chiocchetti using three complementary biostatistical methods as described in Chiocchetti et al., 2016: (i) differentially expressed genes (DEX), identifies genes by comparing two time points, (ii) dynamic time warp analysis (DTW), identifies genes that are regulated across a temporal trajectory and (iii) parallel independent component analysis (ICA), extracts individual processes and underlying genes. Genes that were significant in all three analyses were defined as robustly regulated. In addition, we performed weighted gene co-expression network analysis (WGCNA) to identify modules of co-regulated genes (Langfelder and Horvath, 2007). The complete analysis has been published in Chiocchetti et al., 2016. To understand which modules are associated with neuromorphological development of neurons we tested for significant Pearson correlations between eigenvalues of individual networks and the respective morphological parameters (see section 3.4.2.3).

3.5.4.2 MACE

Overall, 32,739 transcripts were targeted by MACE analysis (see 3.2.3.2) and defined as the gene universe (Reference gene panel). Differentially expressed genes were identified using the "DESeq2" pipeline (Love et al., 2014) by GenXPro. Only genes not differentially expressed between WT and eCtrl (FDR > 0.1) were further checked for significant differential expression between eCtrl and the KO cell lines (FDR ≤ 0.05 with fold change in the same direction). Up- and down-regulated genes underwent GO term analysis using the "topGO" package in R implementing the *weight01* algorithm. This algorithm accounts for the hierarchical

diacyclic graph structure of the GO-annotation, thus p-values extracted can be considered as corrected for multiple testing (Alexa et al., 2006).

Genes surviving QC (more than 10 reads per gene in at least 6 of the 12 samples) were subjected to weighted gene co-expression network analysis (WGCNA). For WGCNA, the signed adjacency was defined as $a = (0.5 * (1 + \text{cor}))^{\text{stp}}$, where stp is the soft thresholding power chosen to obtain a scale free network. Here, a stp of 32 resulted in a scale free network based on a regression coefficient $R^2 > 0.8$ from a scale free topology modeling approach. Modules (i.e. genes with high topological overlap) were defined using hierarchical clustering (distance=distance of topological overlap, method=average linkage) and the 'cutreeDynamic' algorithm as published, with a minimum module size of $N = 30$ (Langfelder and Horvath, 2007). Modules were clustered (distance=Euclidean, linkage=complete) based on correlation distance between their eigenvalues (eigengene values) and merged below a cluster height=0.1.

3.5.5 Gene list enrichment test in gene networks of brain development

To gain a deeper insight into the brain-specific effects of up- and down-regulated genes from MACE analysis, we implemented part of the gene network analysis integrating brain expression data as developed by Afsheen Yousaf, MSc in our department (Yousaf et al., 2018). This framework uses the Allen Brain Atlas dataset of Kang and colleagues, who have identified 29 co-regulated gene sets using the spatio-temporal transcriptome of the human brain from early embryonal development to late adulthood (Kang et al., 2011). Each module corresponds to specific biological processes involved in brain development and ageing. We tested these modules for enrichment with the sets of genes up- or down-regulated upon *QPRT-KO* in SH-SY5Y cells using Fisher's exact-tests. Expression patterns of the enriched modules were then visualized using heatmaps of the eigenvalues of the respective modules for each human brain region over time.

4 Results

Results presented in section 4.1 are part of the publication Chiocchetti, Haslinger et al., 2016. Results presented in sections 4.2 and 4.3 are currently under review at *Molecular Autism* in the revised manuscript Haslinger et al..

4.1 Characterization of the SH-SY5Y cell model

4.1.1 Confirmation and evaluation of neuronal differentiation

In the first step we evaluated *in-vitro* differentiation of the SH-SY5Y cell model. Cells exposed to differentiation media with a combination of RA and BDNF for 11 days resulted in a stereotypical multipolar neuronal morphology with one or two long axon-like processes and several shorter dendrite-like processes as reported in the original publication (Encinas et al., 2000). Neuronal differentiation was confirmed by known markers for cell cycle (*cyclin dependent kinase 1/CDK1*) and axonal outgrowth (*microtubule associated protein tau/MAPT*), which were down-regulated and up-regulated respectively at protein level (Western blot) as well as mRNA level (real-time RT-PCR in red and microarray data in turquoise; Figure 2).

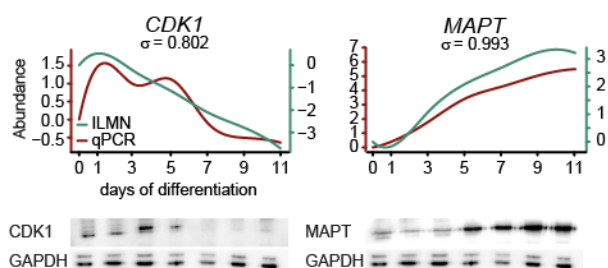


Figure 2 Validation of neuronal differentiation.

Neuronal differentiation was confirmed at mRNA (top) and protein level (bottom) by decreased expression of the cell division marker CDK1 and increased expression of the neuronal marker MAPT. Abundance or gene expression (\log_2 fold change) normalized to time-point 0 (proliferation) was analyzed using Illumina HumanHT-12 v4 Expression BeadChips (ILMN, turquoise) and real-time RT-PCR (qPCR, red). Western blot images are all from the same blot (reference protein: GAPDH). Figure modified from Chiocchetti, Haslinger et al., 2016.

We performed real-time RT-PCR for ASD risk genes (*SHANK3*, *NRXN1*, *CNTNAP2*, *DHCR7*, *GABRB3* and *GRIK2*), glutamatergic receptors (*GRIN1*, *GRIA2*, *GRM1* and *GRM4*) and dopaminergic markers (*TH* and *DRD4*) that were previously reported to be regulated during neuronal differentiation (Konopka et al., 2012). Analyzing the correlation of real-time RT-PCR and microarray data demonstrated the technical reproducibility of microarray data with correlation coefficients ranging from 0.561 (*GRIA2*) to 0.984 (*NRXN1*; Figure 3).

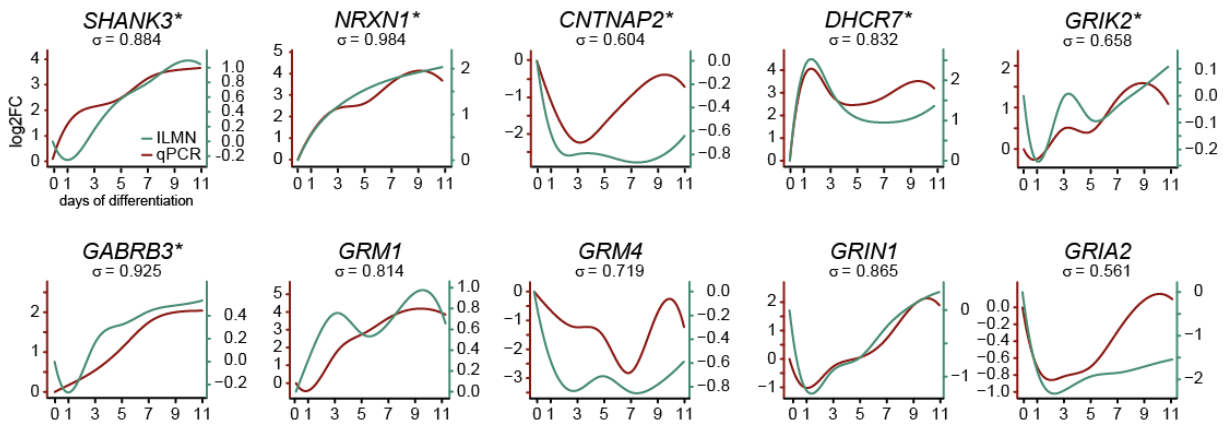


Figure 3 Validation of microarray data.

The correlation values of microarray (ILMN; turquoise) and real-time RT-PCR (qPCR; red) data are shown. Respective log2 fold changes (log2FC) normalized to proliferating state (0 days of differentiation) of selected ASD risk genes (asterisk) and neuronal receptors are shown. For gene descriptions also see List of genes discussed in this study. Figure modified from Chiocchetti, Haslinger et al., 2016.

Markers for neuronal subtypes, including cholinergic, dopaminergic, serotonergic, GABAergic as well as glutamatergic neurons were expressed (Figure 4). The *dopamine transporter 1 (DAT1/SLC6A3)* was not expressed at any stage. The dopaminergic marker tyrosine hydroxylase (*TH*; Figure 4) was not regulated, while the cholinergic markers *acetylcholinesterase (ACHE)* and *vesicular acetylcholine transporter (SLC18A3)* were up-regulated. The *norepinephrine transporter (SLC6A2)* showed down-regulation upon the induction of differentiation. We also observed a modest up-regulation of the glutamatergic transporter *vesicular glutamate transporter 1 (SLC17A7)* and the GABAergic transporter *vesicular GABA transporter (SLC32A1)*. Markers specific for motor neurons were expressed but not regulated during differentiation. Thus, the implemented differentiation protocol yielded an unspecific mixture of neurons.

Finally, we aimed to confirm the differentiation stage achieved by our method: Similar to findings in human brain (Cahoy et al., 2008), the SH-SY5Y neuronal transcriptome, i.e. the genes expressed above microarray background in our cell model included 11,392 out of 20,318 genes targeted on the microarray (see dataset published in Chiocchetti et al., 2016). The CoNTEXT framework (Stein et al., 2014) was implemented to estimate differentiation stage and brain-regional identity of our cell model as published in Chiocchetti et al., 2016. Expression signature of SH-SY5Y cells differentiated using continuous RA and BDNF was reminiscent of brain tissue developed for at least 16-19 weeks post-conception (Stages 5-8; accuracy > 96%) and was most likely to be of a cortical identity (accuracy > 90%; Figure 5).

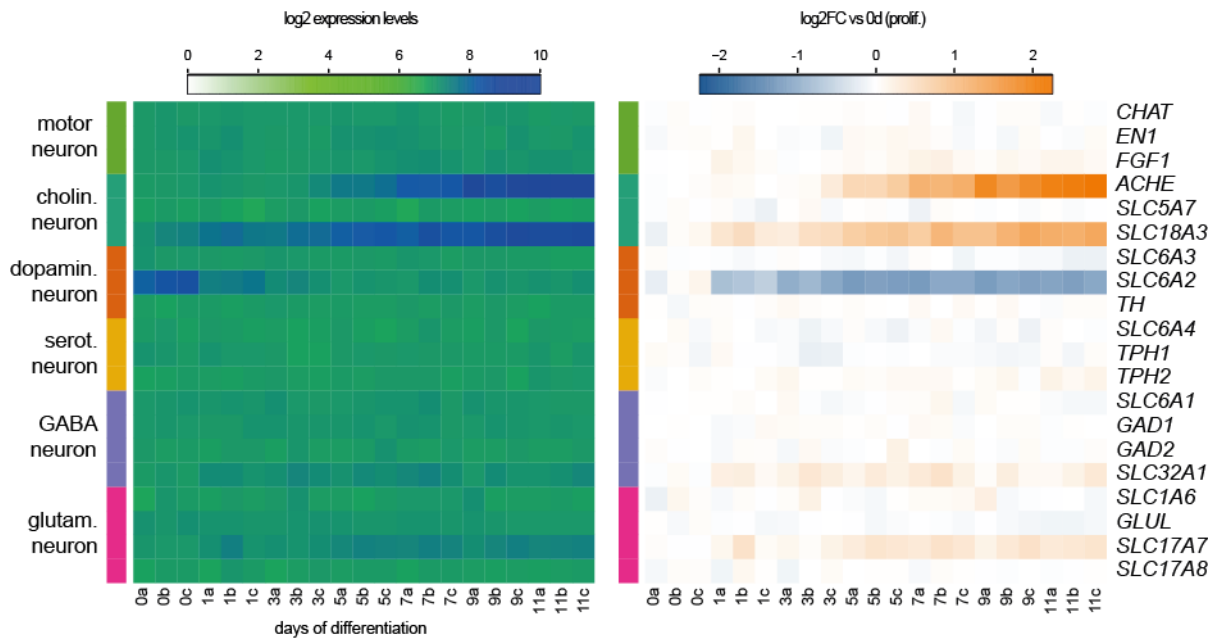


Figure 4 Expression of neuronal markers.

Expression of neuronal markers for motor neurons, cholinergic, dopaminergic, serotonergic, GABAergic and glutamatergic markers during neuronal differentiation are shown as log₂ expression values (left panel) and as log₂ fold change (FC) compared to undifferentiated cells (right panel). Up-regulation of the cholinergic markers *acetylcholinesterase (ACHE)* and *vesicular acetylcholine transporter (SLC18A3)* as well as a mild up-regulation of *GABA vesicular transporter (SLC32A1)* and *vesicular glutamate transporter 1 (SLC17A7)* was observed. The *norepinephrine transporter (SLC6A2)* was down-regulated. For gene descriptions see List of genes discussed in this study. For gene descriptions also see List of genes discussed in this study. Figure modified from Chiocchetti, Haslinger et al., 2016.

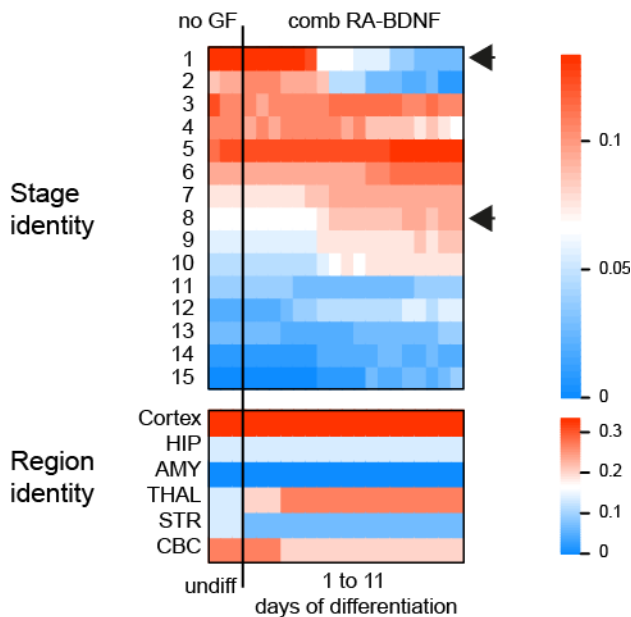


Figure 5 Evaluation of neuronal differentiation.

CoNTExt analysis revealed that mRNA expression of SH-SY5Y cells differentiated with a continuous application of BDNF and RA was most similar to the cortical area and reminiscent of 16-19 weeks post conception (Stage 5) or above. GF: Growth factor. RA: Retinoic acid. BDNF: Brain derived neurotrophic factor. HIP: Hippocampus. AMY: Amygdala. THAL: Thalamus. STR: Striatum. CBC: Cerebellar Cortex. Figure modified from Chiocchetti, Haslinger et al., 2016.

4.1.2 Identification of genes implicated in neuronal differentiation

To robustly identify the subset of genes regulated during neural development three complementary statistical approaches were implemented: Differential gene expression (DEX) analysis identifies genes by comparing two time-points, dynamic time warping (DTW) analysis identifies genes that are regulated across a temporal trajectory, and independent component analysis (ICA) extracts individual processes and underlying genes (for details see Chiocchetti et al., 2016). Combining all genes identified through DEX, DTW and ICA analyses yielded 6,262 genes implicated in neuronal differentiation. Of these, 299 were identified in all three analyses (Figure 6).

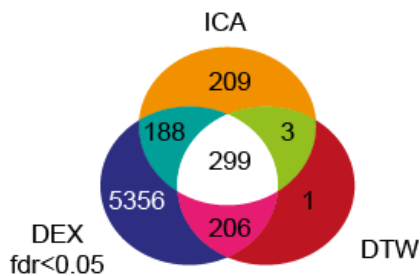


Figure 6 Differentially regulated genes during SH-SY5Y neuronal differentiation.

Overlap of gene-sets identified through linear regression DEX (FDR < 0.05), DTW and ICA (for details also see Chiocchetti et al., 2016). DEX: Differential expression. DTW: Dynamic time warping. ICA: Parallel independent component analysis. FDR: False discovery rate. Figure published in Chiocchetti, Haslinger et al., 2016.

4.1.3 Co-expression network analysis

Weighted gene co-expression network analysis (WGCNA) identified 20 regulatory modules (Figure 7a). As shown in detail in Chiocchetti et al., 2016, modules up-regulated early during neuronal differentiation were enriched for processes involved in membrane remodeling (magenta), protein stabilization (lightcyan) or axonal guidance (pink). Modules up-regulated during early phases of differentiation only were related to inflammatory response (lightyellow) and cellular fatty acid metabolism (darkgrey). Late activated modules were associated with synaptic transmission (blue) or dendrite development (darkgreen). In contrast, early down-regulated modules were attributed to cell division (black) or mitochondrial organization (grey60, brown). Modules inhibited at later stages also included genes associated with cell cycle regulation (turquoise) and DNA metabolic processes (cyan, purple). Modules associated with splicing (darkturquoise) or cell projection and transcriptional regulation were undulating over time. Modules enriched for ASD risk genes as defined by overlaps with AutismKB or SFARI gene include the early up-regulated lightcyan, orange and pink modules (Figure 7b).

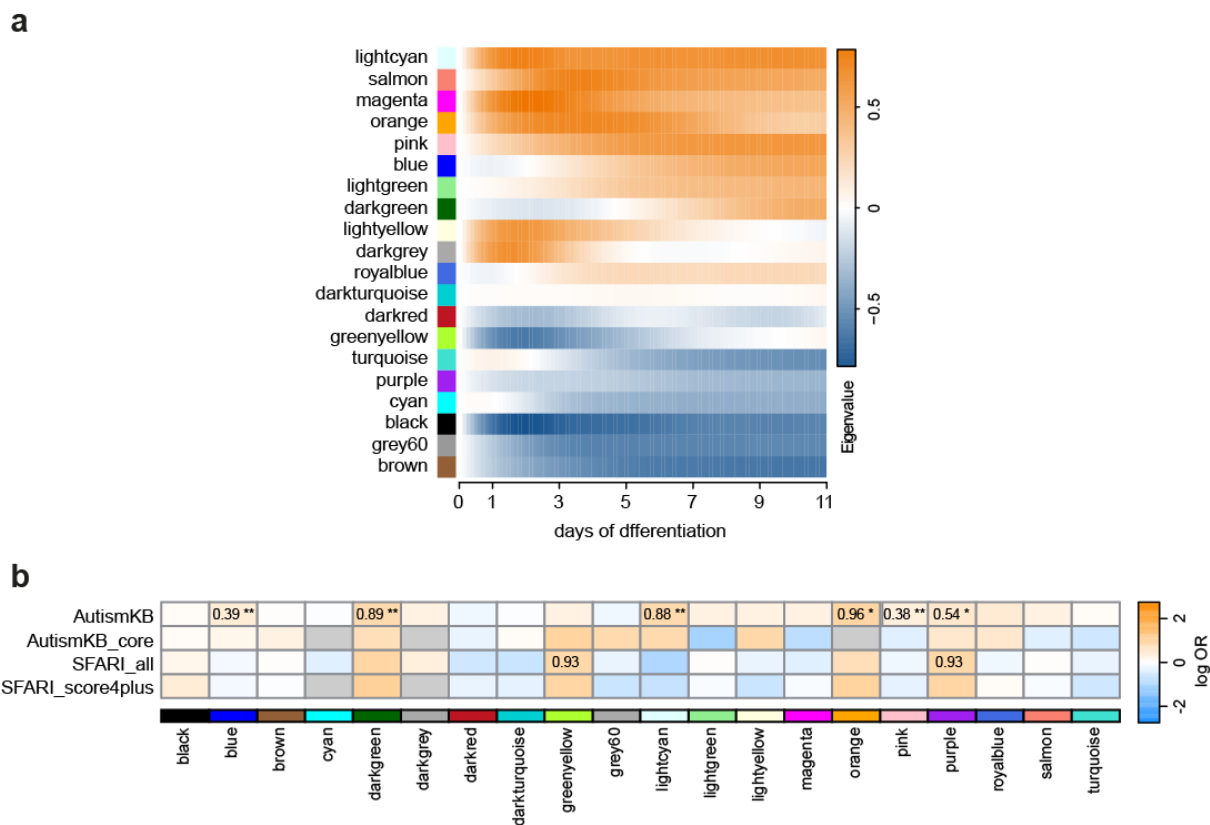


Figure 7 Regulation of WGCNA modules and risk gene enrichment analysis.

(a) WGCNA modules and their regulation over the time course of neuronal differentiation. Colors correspond to the 20 identified modules. (b) ASD risk genes were tested for enrichment in the identified modules using gene lists extracted from AutismKB or SFARI gene. Log-transformed odds ratios are shown if the respective false discovery rate (FDR) < 0.1. Asterisks mark significance: *FDR < 0.05; **FDR < 0.01. Figure modified from Chiocchetti, Haslinger et al., 2016.

4.2 QPRT as candidate gene for functional validation

4.2.1 QPRT is differentially regulated during neuronal differentiation

To identify Chr16p11.2 genes implicated in neuronal differentiation, we tested the 29 genes located in Chr16p11.2 for overlaps with the 6,262 genes differentially regulated during SH-SY5Y neuronal differentiation. We found 9 genes to be differentially regulated in one of the three approaches (*SULT1A3* in ICA; *MVP*, *SEZ6L2*, *KCTD13*, *TMEM219*, *ALDOA*, *GDPD3* and *CORO1A* in DEX) and one gene in two approaches (*HIRIP3* in DEX and ICA). The gene *QPRT* was the only gene identified in all three approaches and therefore considered as robustly differentially regulated during neuronal differentiation. *QPRT* is part of the early up-regulated orange module involved in immune response (see Chiocchetti et al., 2016) and enriched for ASD candidate genes (Figure 7b).

Furthermore, of the genes located in the Chr16p11.2 region, *QPRT* was one of the highest expressed genes during SH-SY5Y neuronal differentiation and the one with the highest regulatory fold change after induction of differentiation (0/proliferation vs 2 days of differentiation: \log_2 FC = 0.22; $p = 1.10E-03$; Figure 8).

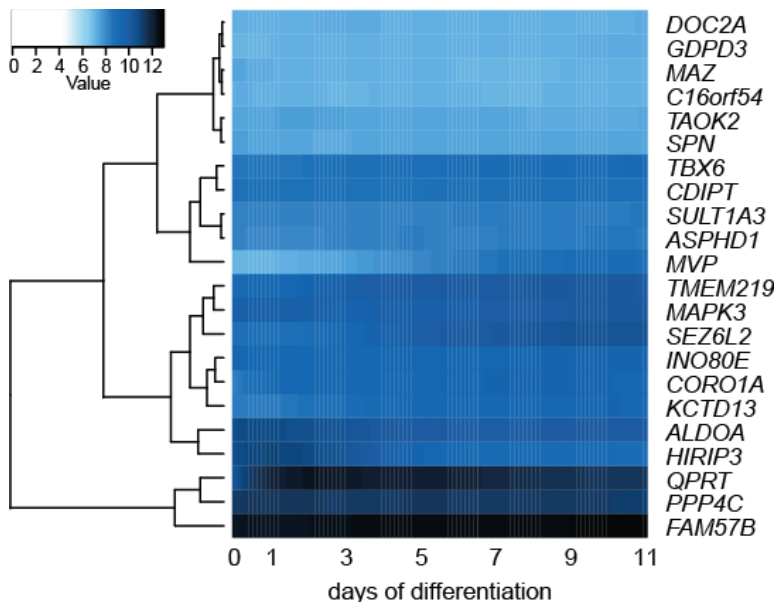


Figure 8 Expression of 16p11.2 genes.

Pattern of expressed genes located in the chromosomal region 16p11.2. *QPRT* shows high expression and the highest regulatory fold change of all genes located in Chr16p11.2 after the start of differentiation. For gene descriptions see List of genes discussed in this study.

4.2.2 *QPRT* correlates with neuronal morphology during neuronal differentiation

QPRT RNA expression during SH-SY5Y differentiation showed significant correlation between microarray and real-time RT-PCR data ($\rho = 0.88$; $p = 0.0098$; Figure 9a). Further, we compared the expression data of *QPRT* (ILMN and qPCR) as well as of the WGCNA modules and tested them for their correlation with morphological parameters as assessed by Sholl analysis during 11 days of neuronal differentiation (Figure 9b). Both, *QPRT* expression and the eigenvalue of its associated module (MEorange as published in Chiochetti et al., 2016) significantly correlated with the average number of intersections, i. e. a measure for neuritic complexity (*QPRT* microarray/ILMN: $\rho = 0.86$, FDR = $8.16E-05$; *QPRT* RT-PCR/qPCR: $\rho = 0.54$, FDR = 0.020; MEorange: $\rho = 0.93$, FDR = $1.71E-07$; Figure 9b).

In summary, we report a correlative association between *QPRT* expression and a measure for development of neurite complexity during *in vitro* neuronal differentiation of wild type SH-SY5Y cells. To investigate if the correlation of *QPRT* expression with neuritic complexity is causal or secondary, i.e. due to the progressive neurite growth over time, we performed functional inhibition analysis of *QPRT*.

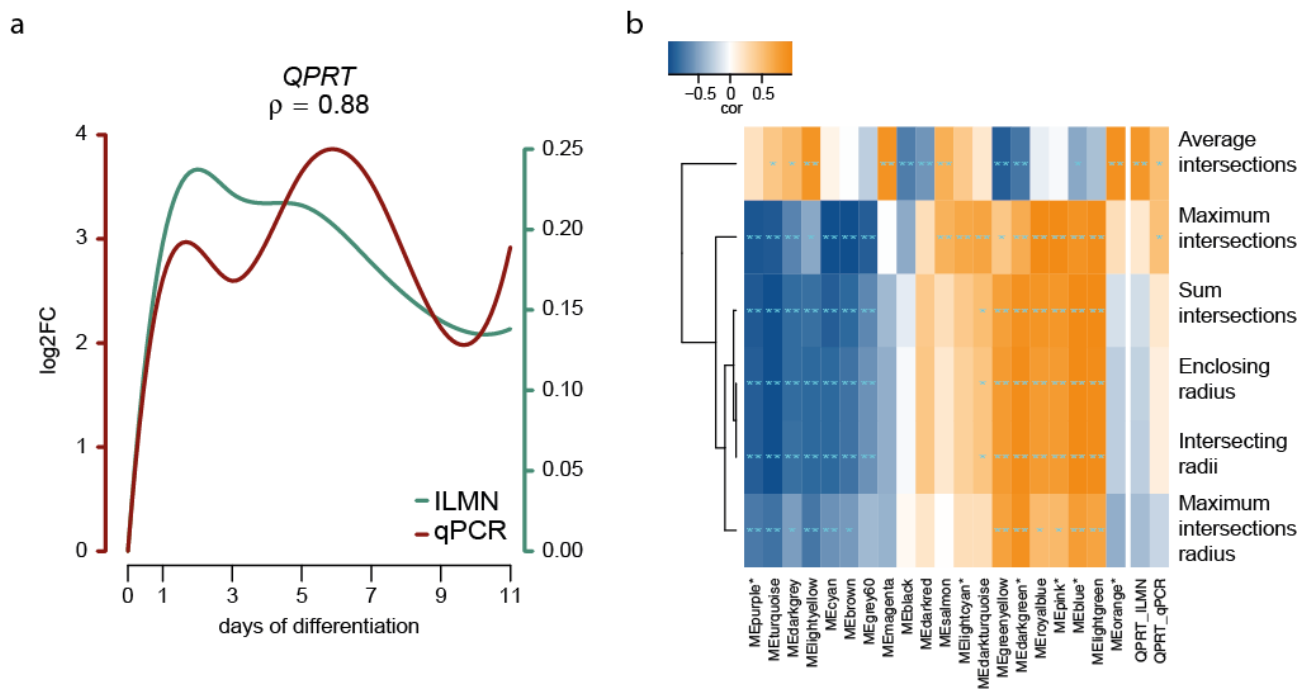


Figure 9 Correlation of *QPRT* expression with morphological parameters.

(a) *QPRT* expression as assessed by microarray (ILMN) and real-time RT-PCR (qPCR) showed significant correlation during 11 days of neuronal differentiation. (b) *QPRT* expression (ILMN and qPCR) as well as the regulation of the module harboring *QPRT*, MEorange, correlate significantly with the morphological parameter average intersections, reflecting the neuritic complexity. Asterisks mark the module eigengene (ME) of modules enriched for ASD risk genes as defined by AutismKB. Average intersections: Sum of all intersections divided by the number of intersecting radii. Maximum intersections: Maximum number of intersections. Sum intersections: Sum of all intersections per cell. Enclosing radius: Outer radius intersecting the cell; indicating the cell's total size. Intersecting radii: Number of radii intersecting one cell. Maximum intersections radius: Radial distance of the maximum number of intersections from the cell body; indicates the site of a cell's highest branching density. This figure has been submitted to *Molecular Autism* as Haslinger et al. and is currently under review.

4.2.3 Validation of 16p11.2 CNVs

To test the hypothesis that a deletion of the 16p11.2 region affects expression of *QPRT* we screened previously collected Illumina bead array data (unpublished data) and identified five individuals with suggestive CNVs in 16p11.2. Here, we show validation of a *de novo* 16p11.2 deletion (Figure 10) in one proband compared to his non-carrier parents and an unrelated control (Figure 11; unpublished data). For this family, LCLs were available and used for functional validation of *QPRT* in the following.

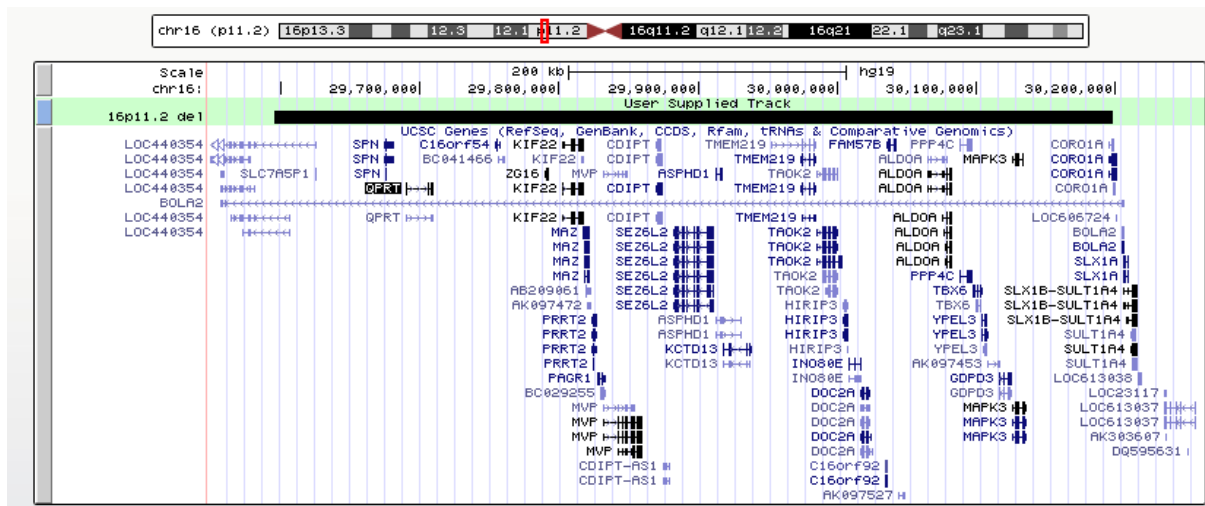


Figure 10 16p11.2 deletion. Idiogram taken from the UCSC genome browser (<https://genome.ucsc.edu>). The black bar shows the patient-specific 16p11.2 deletion. Genes located in the respective genomic region are listed below the bar, *QPRT* is surrounded by a black box. For gene descriptions see List of genes discussed in this study.

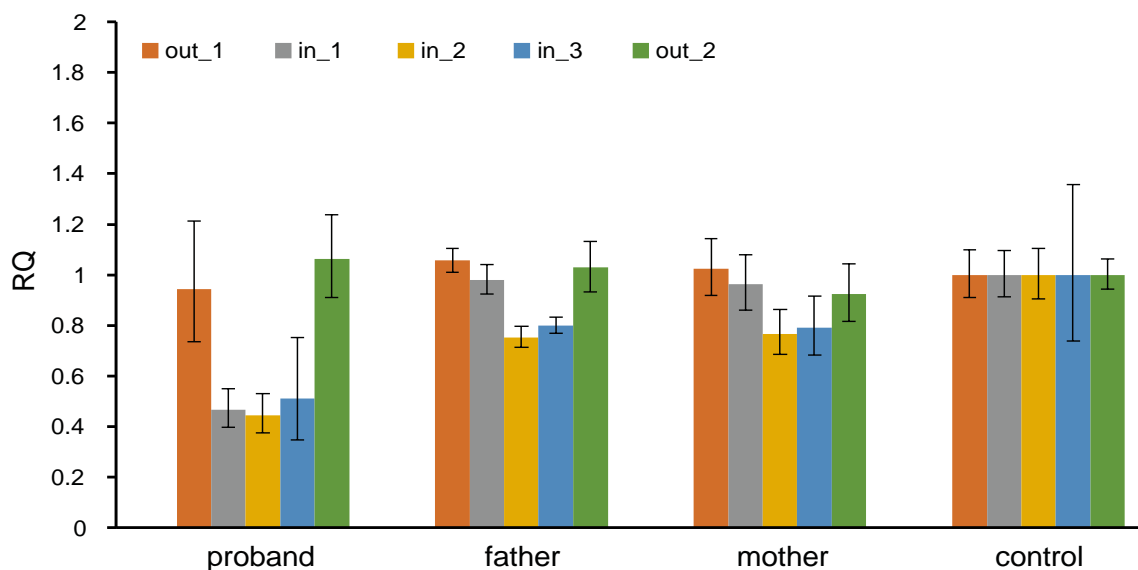


Figure 11 Validation of 16p11.2 deletion. Using real-time PCR, the deletion of Chr16p11.2 was validated in one carrier when compared to his non-carrier parents and normalized to an unrelated control. Outside primers (out_1 and out_2) were designed surrounding the deletion while in_1 to in_3 were located in the deleted region as identified by Illumina bead arrays. RQ: Relative quantification.

4.2.4 Validation of *QPRT* expression in 16p11.2 deletion carrier

To replicate previous reports (Blumenthal et al., 2014) of altered *QPRT* expression in 16p11.2 CNV carriers we compared *QPRT* expression in a patient specific LCL of a deletion carrier and his unaffected parents. We confirmed a dosage-dependent expression of *QPRT* at mRNA level (16p11.2 deletion carrier vs. non-carrier parents; logFC = -0.68, $p = 0.014$; Figure 12).

In summary, we report a correlative association between *QPRT* expression and neuronal development. This confirmed us to test if *QPRT* is causally linked to neuronal differentiation by functional analyses.

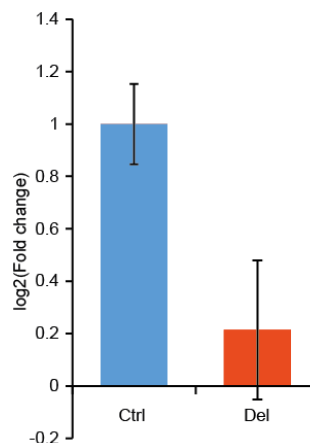


Figure 12 *QPRT* expression in LCLs of a 16p11.2 deletion carrier and control cell lines. *QPRT* is expressed in a gene dosage dependent manner on mRNA level (16p11.2 deletion carrier compared to parental controls). This figure has been submitted to *Molecular Autism* as Haslinger et al. and is currently under review.

4.3 Functional validation of *QPRT* in SH-SY5Y

4.3.1 siRNA mediated knock down (KD) of *QPRT*

All three siRNAs targeting three different sites of *QPRT* (named here siQ1-siQ3) induced a decrease in *QPRT* protein as confirmed by Western Blot (Figure 13). At neuromorphological level, KD cell lines compared to control cell lines (siCtrl) showed a significant decrease of the maximum intersections radius, in that the site of highest branching density was shifted closer towards the soma (p siQ1: 0.027, siQ2: 0.001, siQ3: 3.8E-04; Means[SD] siCtrl: 103.98[115.54]; siQ1: 56.50[80.53]; siQ2: 56.29[97.17]; siQ3: 41.51[76.70]). Overall cell size or the enclosing radius, did not change (all $p > 0.6$; Means[SD] siCtrl: 349.60[223.68]; siQ1: 286.98[125.05]; siQ2: 270.06[135.62]; siQ3: 293.81[176.86]; Figure 13). In addition to the significant reductions of the maximum intersections radius, KD cells also showed a trend for decreases of the overall sum of intersections (p siQ1: 0.396, siQ2: 0.064, siQ3: 0.064; Means[SD] siCtrl: 726.43[650.78]; siQ1: 553.86[356.01]; siQ2: 470.85[307.45]; siQ3: 516.05[505.19]) or the average intersections per cell (p siQ1: 0.957, siQ2: 0.132, siQ3: 0.054; Means[SD] siCtrl: 2.14[1.37]; siQ1: 1.99[0.77]; siQ2: 1.82[0.78]; siQ3: 1.76[0.94]).

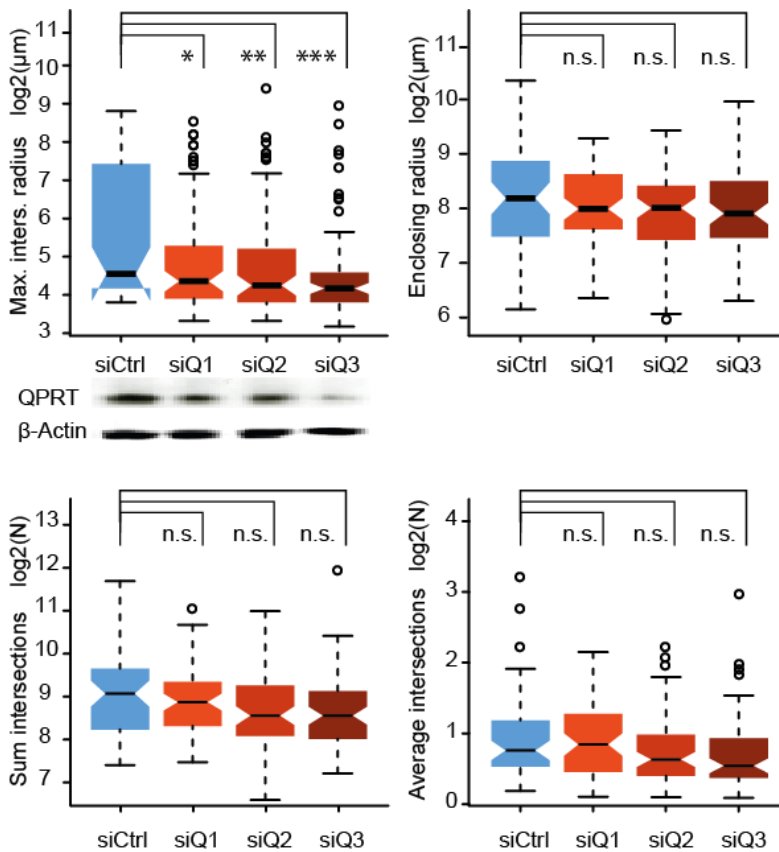


Figure 13 Morphological alterations upon reduction of *QPRT*.

SH-SY5Y cells were transfected with a non-targeting siRNA (siCtrl) and three different siRNAs targeting *QPRT* (siQ1-siQ3). After transfection, cells were differentiated and analyzed at protein level (bottom) to confirm the KD of *QPRT*. Further, cells were morphologically analyzed utilizing Sholl analysis at 11 days of differentiation. Upon *QPRT*-KD cells showed a significant decrease of the maximum intersections radius when compared to the non-targeting control, i.e. the maximum complexity of neurites was significantly closer to the cell soma. None of the three KDs differed with respect to enclosing radius when compared to the non-target control, i.e. the length of the neurites was not different. Maximum intersections radius: Radial distance of the maximum number of intersections from the cell body; indicates the site of a cell's highest branching density. Enclosing radius: Outer radius intersecting the cell; indicates the cell's total size. Sum intersections: Sum of all intersections per cell. Average intersections: Sum of all intersections divided by the number of intersecting radii. All p-values were corrected for multiple testing using Benjamini-Hochberg correction. This figure has been submitted to *Molecular Autism* as Haslinger et al. and is currently under review.

4.3.2 Chemical inhibition of QPRT

Cells exposed to an inhibitor of QPRT, the chemical phthalic acid (PA), showed an increased cell death upon start of differentiation, and thus no end-point morphological analysis was performed. Application of PA for 3 days led to a dosage dependent increase of cell death during differentiation (5mM PA: FC = 1.81, $p = 0.019$; 10mM PA: FC = 4.21, $p = 0.039$) but not during proliferation (5mM PA: FC = 0.73, $p = 0.432$; 10mM PA: FC = 0.68, $p = 0.355$; Figure 14). This finding suggested that loss of *QPRT* is causally linked to

differentiation deficits. Therefore, we aimed at further elucidating the functional role of QPRT inducing a stable loss of *QPRT*.

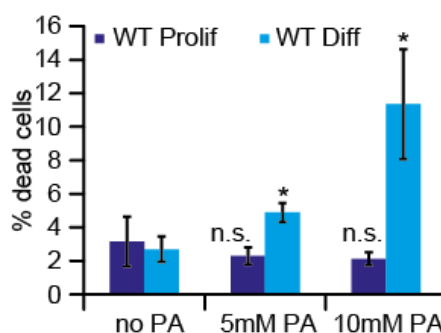


Figure 14 Chemical inhibition of QPRT. Application of the QPRT inhibitor phthalic acid (PA) for 3 days led to a significant increase of cell death in differentiating wild type (WT) SH-SY5Y cells. In proliferating cells QPRT inhibition did not change the rate of cell death. This figure has been submitted to *Molecular Autism* as Haslinger et al. and is currently under review.

4.3.3 CRISPR/Cas9 mediated knock out (KO) of QPRT

4.3.3.1 Generation and viability

Here, we generated two *QPRT-KO* cell lines, del268T and ins395A (NM_014298), both inducing frameshifts leading to premature stop codons (Figure 15). Both showed a significant loss of *QPRT* expression at mRNA level (proliferating cell lines: del268T: below detection limits, ins395A: FC = 0.17, $p = 0.046$; 2 days of differentiation: del268T: FC = 0.13, $p = 0.003$; ins395A: FC = 0.15, $p = 0.003$; all compared to the empty control vector (eCtrl; Figure 16) as well as descriptively at protein level in proliferating state (Figure 16). While the eCtrl and both *QPRT-KO* cell lines were comparably growing during proliferation, both KO cell lines died upon differentiation. After 3 days of differentiation we observed a significant increase of cell death in the KO cell lines when compared to eCtrl cells harboring the empty control vector (eCtrl to del268T: FC = 2.23, $p = 8.2E-04$; eCtrl to ins395A: FC = 1.76, $p = 5.2E-04$; Figure 17a), after 9 days of differentiation merely no differentiating KO cells were detected under the microscope (Figure 17b).



Figure 15 Sequencing of QPRT-KO cell lines.

Results confirmed the generation of indels (red triangles) leading to frameshifts. (a) del268T (QPRT^{-/-} NM_014298 del268T; Ex.1; premature stop codon at position 580) and (b) ins395A (QPRT^{-/-} NM_014298 ins395A; Ex.2; premature stop codon at position 593). Sequencing of the eCtrl (empty control vector) for both of the targeting regions did not show any mutations. This figure has been submitted to *Molecular Autism* as Haslinger et al. and is currently under review.

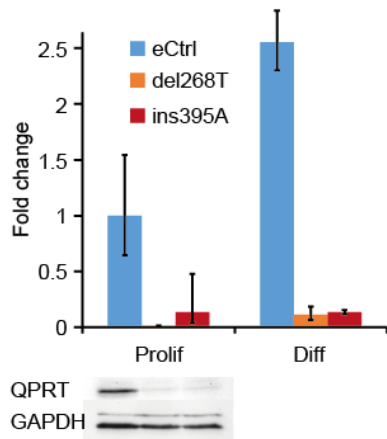


Figure 16 QPRT expression in generated KO and control cell lines.

Loss of QPRT was confirmed for both del268T and ins395A on RNA level (top) for cells after proliferation or 2 days of differentiation. For proliferating cells, KO was furthermore descriptively confirmed at protein level (bottom). This figure has been submitted to *Molecular Autism* as Haslinger et al. and is currently under review.

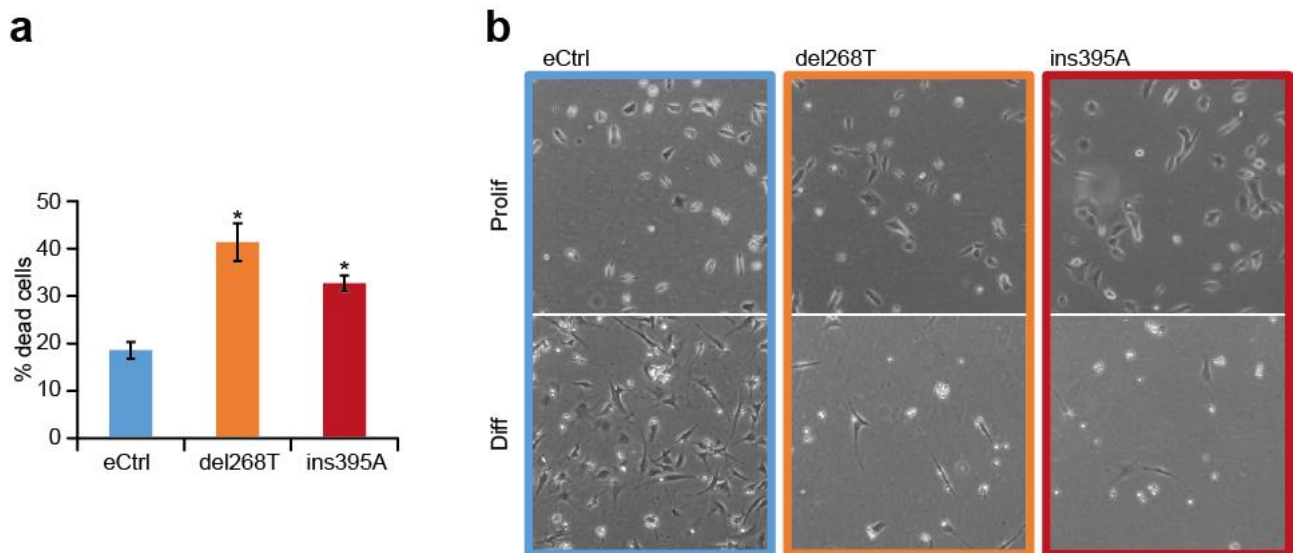


Figure 17 Viability of QPRT-KO cell lines.

(a) Percentage of cell death was assessed by performing viability assays after 3 days of differentiation showing a significant increase of cell death in both generated QPRT-KO cell lines. (b) KO of QPRT led to observable cell death during differentiation (9 days) but not during proliferation. This figure has been submitted to *Molecular Autism* as Haslinger et al. and is currently under review.

4.3.3.2 Mimicking and rescue experiments using small compounds

We hypothesized that loss of *QPRT* might lead to increased levels of its neurotoxic substrate quinolinic acid (QUIN). Thus, we exposed wild type cells to elevated QUIN levels. However, we did neither observe an increase in cell death during proliferation (all $p > 0.3$ for 5 μ M and 250 μ M QUIN) nor during differentiation (all $p > 0.3$ for 5 μ M and 250 μ M QUIN; Figure 18) compared to vehicle only (0 μ M).

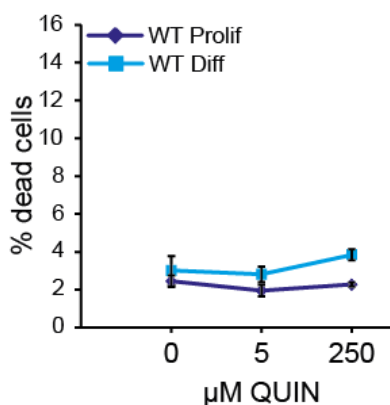


Figure 18 Application of QUIN to proliferating and differentiating SH-SY5Y wild type cells. Propidium iodide (PI) viability assays did not show a significant increase of cell death upon QUIN application during proliferation or differentiation. This figure has been submitted to *Molecular Autism* as Haslinger et al. and is currently under review.

In addition, we tried to rescue the *QPRT-KO* effect by inhibiting the effector pathways downstream of QUIN, i.e. inhibit a potentially induced neurotoxicity by hyperactivation of NMDA-R as well as replenish NAD^+ , the downstream metabolite of *QPRT* and the final outcome of the kynurenine pathway. Neither the NMDA-R antagonist MK801 (both *QPRT-KO* compared to eCtrl: FC > 1.7, $p < 3.9\text{E-}03$ for 0 μ M; FC > 1.6, $p < 0.04$ for 6 μ M; FC > 1.6, $p < 1.5\text{E-}03$ for 12 μ M) nor inhibition of the NMDA-R downstream enzyme NOS1 by L-NAME (both *QPRT-KO* compared to eCtrl: FC > 1.3, $p < 0.05$ for 0mM; FC > 1.3, $p < 0.02$ for 0.5mM; FC > 1.5, $p < 0.01$ for 1mM) nor supplying NAD^+ , the downstream product of tryptophan catabolism (both *QPRT-KO* compared to eCtrl: FC > 1.3, $p < 9\text{E-}03$ for 0mM; FC > 1.3, $p < 1.6\text{E-}03$ for 5mM; del268T compared to eCtrl: FC = 1.20, $p = 0.1$; ins395A compared to eCtrl: FC = 1.54, $p = 0.009$ for 10mM) resulted in a significant reduction of cell death for both of the KO cell lines upon differentiation (Figure 19).

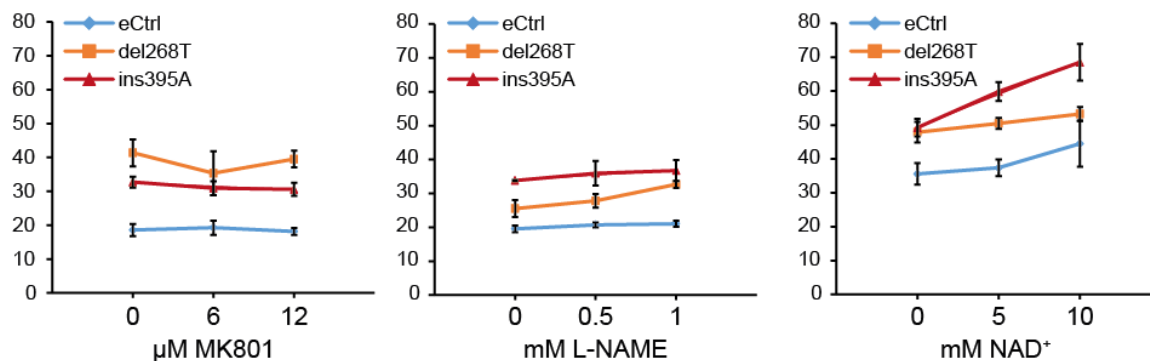


Figure 19 Rescue experiments of *QPRT-KO* induced cell death.

Neither the NMDA-R antagonist MK801 nor the NOS1 inhibitor L-NAME could rescue the increased cell death. Furthermore, application of the more downstream target NAD⁺ could not rescue *QPRT-KO*-induced cell death during differentiation. This figure has been submitted to *Molecular Autism* as Haslinger et al. and is currently under review.

4.3.3.3 Metabolite analysis

To test if loss of *QPRT* results in an altered metabolite profile of the kynurenine pathway we implemented UHPLC and GC/MS analysis. We were able to detect tryptophan, kynurenine, kynurenic acid, 3-hydroxykynurenine, anthranilic acid and picolinic acid. Quinolinic acid (QUIN) could not be detected in any of the samples, while 3-hydroxyanthranilic acid could only be detected in the differentiated (eCtrl and both of the *KO*) cell lines only. However, no significant changes could be observed in any of the metabolites when comparing both of the *QPRT-KO* cell lines to the control cell lines (Figure 20).

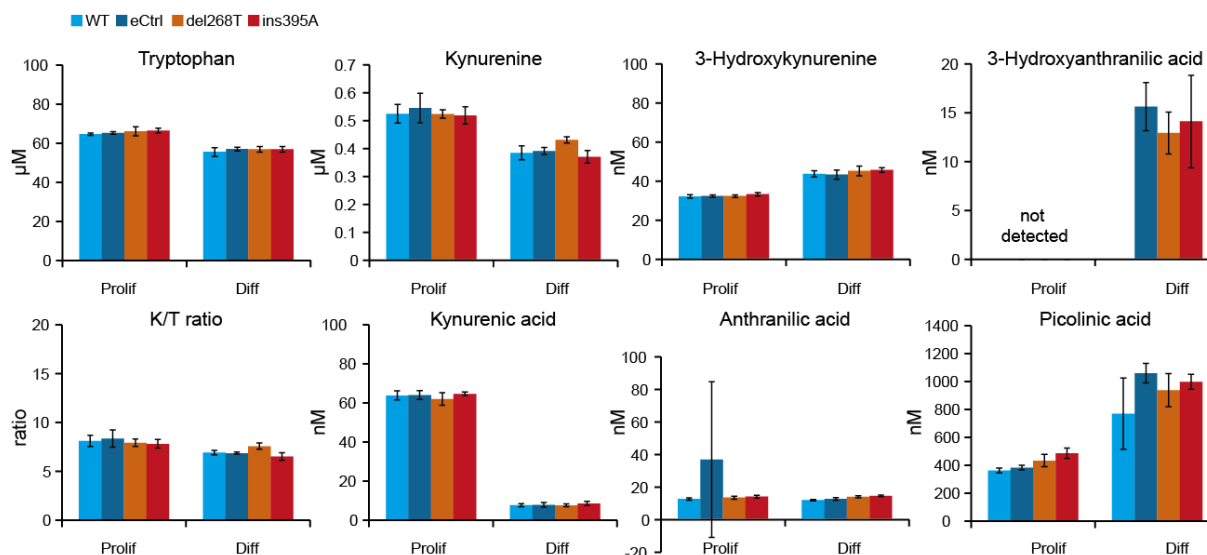


Figure 20 Metabolite analysis of *QPRT-KO* cells.

Tryptophan, kynurenine, kynurenic acid, 3-hydroxykynurenine, anthranilic acid and picolinic acid were measurable in all tested samples. QUIN could not be detected in any of the samples, while 3-hydroxyanthranilic acid could be detected in the 3 days differentiated (eCtrl and both of the *KO*) cell lines only. However, no significant changes could be observed in any of the metabolites when comparing both of the *QPRT-KO* cell lines to the control cell lines. K/T ratio: Ratio of kynurenine and tryptophan. This figure has been submitted to *Molecular Autism* as Haslinger et al. and is currently under review.

4.3.3.4 MACE transcriptome analysis of *QPRT-KO*

Since in our cell model the effect of *QPRT-KO* on neuronal differentiation was not related to changes in the kynurenine pathway or the neurotoxic effects of QUIN, we aimed to further elucidate the effect of the knockout on differentiating cells implementing a transcriptome wide analysis. Overall, we were able to measure expression of 32,739 transcripts. Statistical analysis identified 269 differentially regulated genes (103 up-regulated and 166 down-regulated; Figure 21, see supplementary table provided separately on disk) expressed in all three replicates of both KO cell lines, all with an FDR ≤ 0.05 . The 12 genes (Table 2) with an absolute $\log_2(\text{FC})$ value > 2.5 were technically validated using real-time RT-PCR with an average correlation between RNA sequencing data and real-time RT-PCR of $\rho = 0.91$ (SD = 0.10). *QPRT-KO* was also confirmed (eCtrl vs del268T: $\log_2\text{FC} = -2.44$, FDR = $1.07\text{E-}207$; eCtrl vs ins395A: $\log_2\text{FC} = -3.17$, FDR = $9.88\text{E-}291$). Of the genes coding for components of the kynurenine pathway, only *NMNAT2* was significantly down-regulated upon *QPRT-KO* (eCtrl vs del268T: $\log_2\text{FC} = -0.70$, FDR = $2.10\text{E-}07$; eCtrl vs ins395A: $\log_2\text{FC} = -1.51$, FDR = $6.70\text{E-}28$). The gene coding for the ASD implicated protein *NLGN3* was suggestively down-regulated in the del268T only (eCtrl vs del268T: $\log_2\text{FC} = -0.43$, FDR = $6.58\text{E-}02$; eCtrl vs ins395A $\log_2\text{FC} = -0.09$, FDR = $9.15\text{E-}01$) and was thus not considered to be regulated upon KO of *QPRT*.

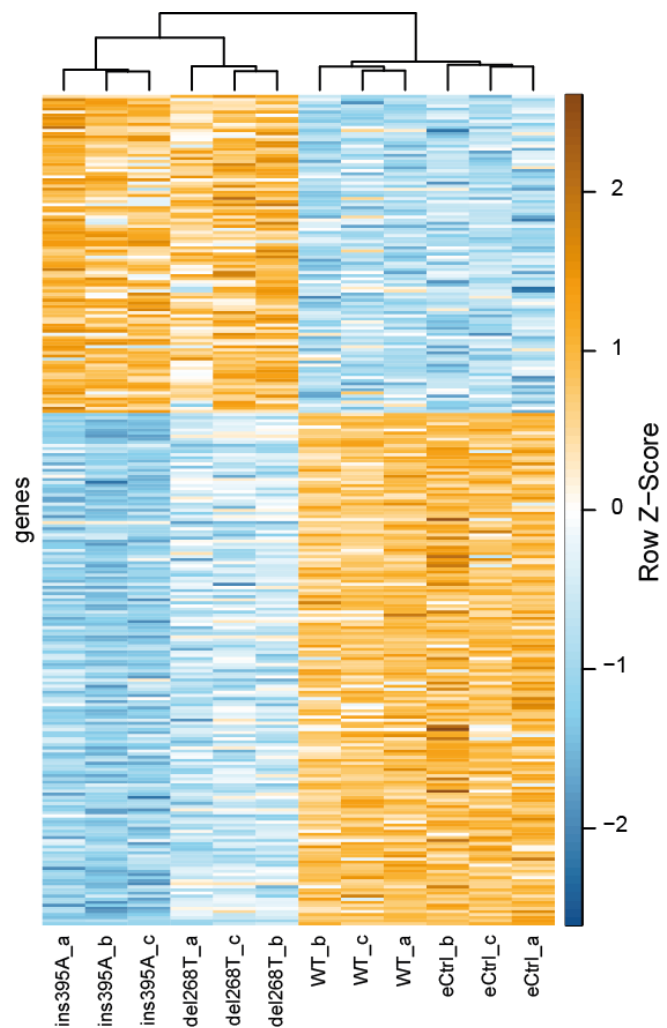


Figure 21 Heatmap of genes differentially expressed in *QPRT-KO* cells.

Upon KO of *QPRT* 269 genes were significantly differentially expressed between both of the KO and the eCtrl cell line (FDR ≤ 0.05) but not between the controls (wild type and eCtrl, FDR > 0.1). Overall, ins395A descriptively showed stronger effects than del268T. This figure has been submitted to *Molecular Autism* as Haslinger et al. and is currently under review.

The genes up-regulated upon KO of *QPRT* were enriched (all p-values < 0.05, Figure 22) for the GO annotated biological processes “neurotransmitter secretion”, “negative regulation of cell growth” and “negative regulation of cytoskeleton organization” among others. Genes down-regulated in KO cell lines showed enrichment for GO terms including “positive regulation of neuron differentiation”, “positive regulation of dendritic spine development” as well as “synapse organization” (Figure 22). Furthermore, down-regulated genes were also enriched for “ion transmembrane transport”, including “potassium transport”, as well as for glutamatergic signaling like “glutamate secretion” and “regulation of glutamate receptor signaling pathway” (Figure 22). We also observed significant enrichment for ASD genes among highly differentially regulated candidates. Of the 269 differentially regulated genes 15 were listed in the SFARI gene database (<https://gene.sfari.org/database/human-gene>) with an evidence score of 4 or better ($p = 9.2E-04$, odds ratio OR[95% confidence interval] OR = 2.68[1.47-4.54]): *CELFB4*, *PCCB*, *APP*, *GALNT14*, *SHANK1*, *SLC7A3*, *GABRB3*, *CTNNA1*, *SDC2*, *SNTG2*, *CHD2*, *CNTNAP2*, *ABAT*, *KCNQ3*, *PAX5* (all but *PCCB* and *CHD2* are down-regulated; for a list of gene descriptions see List of genes discussed in this study). When looking at the 12 differentially regulated genes with a FC > 2.5, three down-regulated genes are reported in SFARI: *gamma-aminobutyric acid type A receptor beta 3 subunit (GABRB3)*, *potassium voltage-gated channel subfamily Q member 3 (KCNQ3)*, *syntrophin gamma 2 (SNTG2)* and *contactin associated protein like 2 (CNTNAP2)*. A total of eleven out of 166 down-regulated genes and one gene of 103 up-regulated genes showed a $|\log_2FC| > 2.5$ (Table 2). Literature search for these twelve highly regulated genes revealed that six had been published in the context of ASD before and three (*KCNQ3*, *GABRB3*, *SNTG2*) are listed in the SFARI database with an evidence score of 4 or better (Table 2).

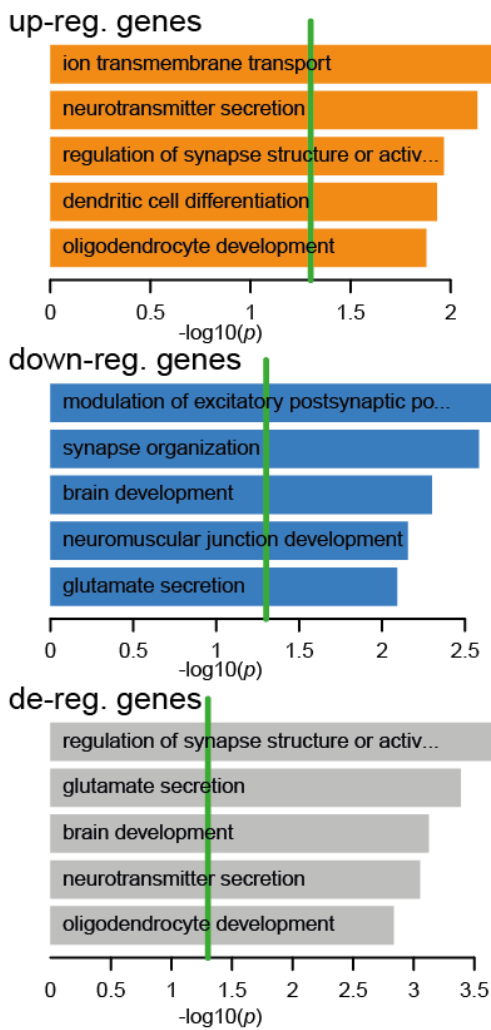


Figure 22 GO-term enrichment for differentially expressed genes upon KO of *QPRT*.

Up-regulated genes were associated with GO terms including neurotransmitter secretion, negative regulation of cell growth and negative regulation of cytoskeleton organization (all $p < 0.05$). Genes down-regulated upon *QPRT-KO* were enriched for GO-terms involved in processes of neuronal development (positive regulation of neuron differentiation, positive regulation of dendritic spine development and synapse organization (all $p < 0.04$)) and neurotransmitter transport (potassium transport, as well as for glutamatergic processes like glutamate secretion and regulation of glutamate receptor signaling pathway (all $p < 0.05$)). De-regulated genes were enriched for processes like neurotransmitter secretion and brain development (all $p < 0.05$). All p-values account for the hierarchical structure of the gene ontology (GO) and can thus be considered as corrected for multiple testing. This figure has been submitted to *Molecular Autism* as Haslinger et al. and is currently under review.

Table 2 Differentially expressed genes upon QPRT-KO with $|\log_2FC| > 2.5$

Gene	Chr	del268T vs eCtrl		ins395A vs eCtrl		WT vs eCtrl		SFARI score	ASD literature
		FDR	log ₂ FC	FDR	log ₂ FC	FDR	log ₂ FC		
COX17	3q13.33	3.33E-138	-5.94	1.78E-154	-5.63	0.30	-0.13	/	/
GUCA1A	6p21.1	4.56E-41	-5.38	3.97E-46	-5.88	0.20	0.26	/	/
COX17P1	13q14.13	1.09E-84	-5.19	5.82E-93	-5.28	0.59	-0.11	/	/
VSTM2A	7p11.2	1.81E-10	-5.00	6.36E-12	-5.28	0.61	-0.27	/	/
KCNQ3	8q24.22	5.77E-04	-4.76	1.25E-03	-3.04	0.46	0.49	3	Role for KCNQ3 in epilepsy and autism (Guglielmi et al., 2015)
CCK	3p22.1	2.56E-04	-3.18	5.97E-05	-3.13	0.17	0.68	/	Candidate gene for Asperger's in a microdeletion case study (Iourov et al., 2015)
GABRB3	15q12	3.04E-43	-3.00	9.43E-54	-3.58	0.80	0.04	2	CNV Chr15q11-13 implicated in ASD; Polymorphisms associated with ASD (Buxbaum et al., 2002; Varghese et al., 2017)
BRINP1	9q33.1	8.93E-09	-2.92	2.09E-09	-2.85	0.20	-0.53	/	-/- mice: autism-like behavior including reduced sociability and altered vocalization (Berkowicz et al., 2016)
LINC01760	1p21.3	1.02E-02	2.74	4.93E-03	2.62	0.95	-0.30	/	/
SNTG2	2p25.3	7.04E-04	-2.71	5.06E-07	-5.58	0.72	0.22	4	Region linked with ID (Bulayeva et al., 2015), associated with ASD (Rosenfeld et al., 2010); Interaction partner of neurotrophins, interaction altered by ASD associated mutations (Yamakawa et al., 2007)
ARHGAP20	11q23.1	1.63E-09	-2.65	4.08E-15	-3.93	0.45	-0.30	/	/
SRRM4	12q24.23	1.29E-18	-2.61	2.25E-26	-3.40	0.54	-0.20	/	-/+ mice: multiple autistic-like features (Quesnel-Vallières et al., 2016)

Abbrev.: COX17: cytochrome C oxidase copper chaperone. GUCA1A: Guanylate cyclase activator 1A. COX17P1: COX17, cytochrome C oxidase copper chaperone pseudogene 1. VSTM2A: V-set and transmembrane domain containing 2A. KCNQ3: Potassium voltage-gated channel subfamily Q member 3. CCK: Cholecystokinin. GABRB3: Gamma-aminobutyric acid type A receptor beta3 subunit. BRINP1: BMP/retinoic acid inducible neural specific 1. LINC01760: Long intergenic non-protein coding RNA 1760. SNTG2: Synaptrophin gamma 2. ARHGAP20: Rho GTPase activating protein 20. SRRM4: Serine/arginine repetitive matrix 4. Chr: Chromosomal region. del268T: CRISPR/Cas9 induced mutation (deletion of one nucleotide) in exon 2 of QPRT. ins395A: CRISPR/Cas9 induced mutation (insertion of one nucleotide) in exon 2 of QPRT. eCtrl: Control cell line with empty CRISPR/Cas9 control vector. WT: Wild type SH-SY5Y cell line untreated. FDR: False discovery rate. log₂FC: Log₂ fold change. SFARI score: Score in the SFARI database (<https://gene.sfari.org/database/human-gene/>); a smaller score means higher evidence). ASD literature: Pubmed was searched for "gene & autism" and "gene & ASD". ASD: Autism spectrum disorder. ID: Intellectual disability. This table has been submitted to Molecular Autism as Haslinger et al. and is currently under review.

4.3.3.5 Gene network analysis

At gene network level we identified 20 co-regulated modules upon KO. Here, *QPRT* was co-regulated within a module associated with neurotransmitter secretion and synaptic vesicle transport as well as negative regulation of neurogenesis ($p < 0.04$). Overall, the eigenvalue of this module was not different between controls and KOs. Here, we identified one co-regulated gene set (darkgrey, Figure 23) to be associated with *QPRT-KO* as it was significantly down-regulated in both KO cell lines when compared to the control cell lines (KOs versus eCtrl or WT, all $p < 8E-07$). GO term enrichment analysis of this module again revealed processes involved in brain development and synaptic transmission and plasticity ($p < 0.05$; Figure 23), confirming the association of *QPRT-KO* with neuronal development.



Figure 23 Regulation of the darkgrey gene set.

This module was identified as *QPRT-KO* associated module harboring genes down-regulated upon *QPRT-KO* when comparing both KO cell lines to wild type and eCtrl cells (all $p < 8E-07$; left panel). GO term enrichment analysis (right panel) of this module again revealed processes involved in brain development and synaptic transmission and plasticity ($p < 0.05$), confirming the association of *QPRT-KO* with neuronal development. This figure has been submitted to *Molecular Autism* as Haslinger et al. and is currently under review.

4.3.3.6 Translation to developmental brain expression data

Finally, we aimed to translate the effects of *QPRT-KO* onto the spatial and temporal gene expression network of the brain using previously published data (Kang et al., 2011). In this previous work the authors reported 29 gene modules (termed “Kang-Module” in the following) that are co-regulated during the development of human brain regions. We observed that the *QPRT-KO* induced down-regulated genes were strongly enriched in the Kang-Modules number 1 (odds ratio OR[95% confidence interval] OR = 8.86[3.12-20.45], $p = 5.76E-04$), number 2 (OR = 5.96[3.55-9.75], $p = 2.21E-09$), number 10 (OR = 69.92[20.70-188.44], $p = 2.64E-07$), number 15 (OR = 14.58[6.00-30.72], $p = 1.57E-06$) and number 20 (OR = 7.13[4.40-11.40],

$p = 7.74E-13$) while the *QPRT-KO* up-regulated genes were enriched in Kang-Modules number 2 (OR = 23.20[11.25-49.97], $p = 1.07E-16$) and number 20 (OR = 3.54[1.46-7.76], $p = 4.18E-02$). Kang-Module 17 was enriched for *QPRT-KO* induced de-regulated genes in general, i.e. for the merged lists of up- and down-regulated genes (OR = 20.41[2.33-82.57], $p = 2.45E-02$; Figure 24a). By plotting the eigengene value of the Kang-Modules over time for each region we observed that number 1 showed strong early up-regulation in the hippocampus (HIP) and the amygdala (AMY) during embryonal development while it was down-regulated in all tested brain regions after birth (Figure 24b). Kang-Module 1 was also slightly up-regulated in embryonal development in parts of the frontal cortex (orbitofrontal cortex (OFC), dorsolateral prefrontal cortex (DFC) and medial prefrontal cortex (MFC)), the striatum (STR) and the cerebellar cortex (CBC). Kang-Module 2 was overall down-regulated prenatally and showed up-regulation after birth, with maximum expression between the ages of 6 and 14 i.e. during middle and late childhood in OFC, MFC, posterior inferior parietal cortex (IPC), primary auditory (A1) cortex (A1C), inferior temporal cortex (ITC), primary visual (V1) cortex (V1C) and STR. Kang-Module 10 was only expressed in the CBC with a peak around the age of 6 years, while Kang-Module 15 was strongly down-regulated during embryonal development in the CBC. The low expression of Kang-Module 15 in the CBC was stable across the tested time course, and it was slightly up-regulated in other brain regions, showing peaks between the years 6 and 14 in OFC, DFC, ventrolateral prefrontal cortex (VFC), MFC, IPC, A1C, ITC and V1C. Kang-Module 17 showed a constant active expression in the CBC over time with a peak during early development in the CBC. Kang-Module 20 was an overall early up-regulated gene network down-regulated after the age of ~2 years, showing the strongest down-regulation between the years 6 and 14 in OFC, MFC, IPC, A1C, ITC, V1C and STR.

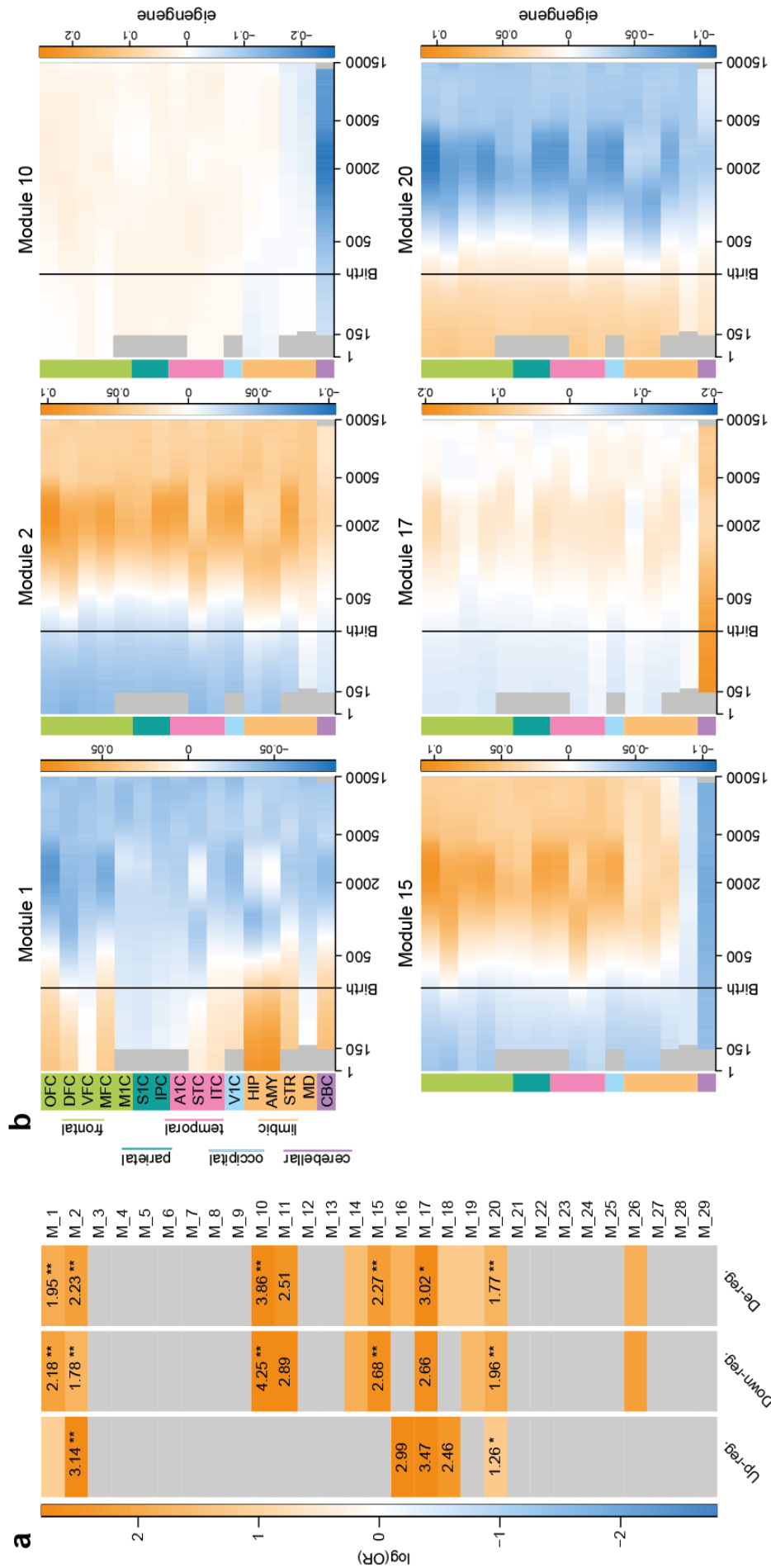


Figure 24 Translation of QPRT-KO induced gene expression profile to human development. (a) Modules enriched for QPRT-KO de-regulated genes. A total of 29 modules (in the following termed “Kang-Modules”) identified by Kang and colleagues (Kang et al., 2011) were tested for enrichment with genes differentially regulated in QPRT-KO de-regulated genes. Down-regulated genes were strongly enriched in the Kang-Module number 1, 10, 15 and 20 while up-regulated genes were enriched in Kang-Module number 2 and 20. Kang-Module 17 was enriched for de-regulated genes in general, i.e. for the merged lists of up- and down-regulated genes. (b) Regulation of modules enriched for QPRT-KO implicated genes during brain development. Kang-Modules 15 (enriched for QPRT-KO induced down-regulated genes), 2 and 20 (both enriched for genes up- and down-regulated) were strongly regulated during early infancy (~2 years), especially in the dorsolateral prefrontal cortex, the superior temporal cortex, hippocampus and amygdala. Kang-Module 10 was down-regulated in the cerebellum while it was enriched for genes down-regulated in QPRT-KO cells. Kang-Module 17 was enriched for de-regulated genes and showed an up-regulation of genes expressed in the cerebellum. Kang-Module 1 showed strong regulation of the hippocampus and the amygdala, parts of the frontal cortex and the cerebellum. This module was enriched for genes down-regulated in QPRT-KO cells. OFC: Orbital prefrontal cortex. DFC: Dorsolateral prefrontal cortex. VFC: Ventrolateral prefrontal cortex. MFC: Medial prefrontal cortex. M1C: Primary motor (M1) cortex. S1C: Primary somatosensory (S1) cortex. IPC: Posterior inferior parietal cortex. A1C: Primary auditory (A1) cortex. STC: Superior temporal cortex. ITC: Inferior temporal cortex. V1C: Primary visual (V1) cortex. HIP: Hippocampus. AMY: Amygdala. STR: Striatum. MD: Mediodorsal nucleus of the thalamus. CBC: Cerebellar cortex. This figure has been submitted to *Molecular Autism* as Haslinger et al. and is currently under review.

5 Discussion

In part, the discussion presented here was published in Chiocchetti, Haslinger et al., 2016 and has been submitted to *Molecular Autism* as Haslinger et al., with the revised manuscript currently being under review.

5.1 Suitability of the SH-SY5Y neuroblastoma model

As it was questioned before, we here confirmed the suitability of the neuroblastoma cell line SH-SY5Y to study neuronal differentiation *in vitro*. The utility of the SH-SY5Y cellular model to investigate this process depends on how well it models *in vivo* development (Stein et al., 2014). Our improved differentiation protocol and transcriptome analysis confirmed the capacity of these cells to model cortical development upon differentiation. As we discussed in the publication resulting from this work here (Chiocchetti et al., 2016), one major limitation of this model is its origin from a tumor as the cells were isolated from a bone marrow biopsy of a four-year-old girl with a metastatic neuroblastoma. Tumor derived cell lines have a highly active, dysregulated cell cycle, which might bias the interpretability of cell cycle associated findings. The cell line shows some well described cytogenetic aberrations including several CNVs and a trisomy of chromosome 7 (Yusuf et al., 2013). However, to our knowledge the reported CNVs do not span our region of interest, namely Chr16p11.2, as well as major genes associated with neuronal differentiation and neuropsychiatric disorders.

The result of the CoNTEXT algorithm showed that SH-SY5Y cells treated with a combination of retinoic acid (RA) and brain derived neurotrophic factor (BDNF) were differentiated towards developmental stages 5-8 which is beyond the stages achieved using established protocols (Nishida et al., 2008; Korecka et al., 2013). In addition, we observed preservation of ASD-relevant modules, i.e. glutamatergic and GABAergic pathways. However, none of the established differentiation protocols retrieved cells showing preservation of modules associated with synaptic transmission. In conclusion, SH-SY5Y cells may not allow investigating all functional aspects of neurons, however, the continuous exposure of SH-SY5Y cells to RA and BDNF applied here improved differentiation and thus allows investigating genes relevant in early cortical

development and exploring regulatory networks associated with psychiatric disorders (Chiocchetti et al., 2016).

5.2 Selection of the candidate gene *QPRT* located in the ASD-associated CNV region

Chr16p11.2

Several studies analyzed the impact of 16p11.2 genes or CNVs. In this study here, we selected the gene *quinolinate phosphoribosyltransferase (QPRT)* for functional validation and report an effect on neuronal differentiation. This gene was the only gene fulfilling our selection criteria, i.e. high expression and significant association with neuronal differentiation in SH-SY5Y cells in all three statistical tests as well as significant correlation with neuromorphological parameters. While a previously described gene of this region, *FAM57B* (Blaker-Lee et al., 2012), showed the highest expression values, it was not significantly regulated over time. Similarly, *KCTD13* (Blaker-Lee et al., 2012; Golzio et al., 2012; Escamilla et al., 2017), was significantly regulated during SH-SY5Y neuronal differentiation in only one of the three applied tests and showed relatively low expression levels.

Thus, the only 16p11.2 gene robustly regulated during neuronal differentiation in SH-SY5Y was *QPRT*. Its early and strong up-regulation after the induction of neuronal differentiation suggested its involvement in the underlying processes. This hypothesis was supported by the finding of a significant correlation between *QPRT* expression at mRNA level and the development of SH-SY5Y neuritic complexity. Finally, as expected from previous findings (Blumenthal et al., 2014), *QPRT* was expressed in a gene dosage dependent manner in the lymphoblastoid cell line of a Chr16p11.2 deletion carrier when compared to his non-carrier parents, which is suggesting to result in a change of function.

The gene *QPRT* is coding for an enzyme of the kynurenine pathway which is part of the catabolism of tryptophan ultimately resulting in the production of NAD^+ . The role of *QPRT* is to catabolize quinolinic acid (QUIN), which is a potent neuronal excitotoxin as it acts as NMDA-R agonist. QUIN itself is generated non-enzymatically from its precursor alpha-amino-beta-carboxy-muconate-epsilon-semialdehyde (ACMS), which also serves as precursor for the neuroprotectant picolinic acid. A reduction of *QPRT* is suggested to lead to

an accumulation of QUIN. This accumulation over-activates NMDA-R resulting in an increased production of both intracellular Ca^{2+} and nitric oxide (NO) which in turn may induce neuronal cell death (Braidy et al., 2009). Furthermore, altered QUIN levels were also reported to lead to a change in NAD^+ production (Braidy et al., 2011) which in turn could impact on Poly (ADP-ribose) polymerase (PARP) activity (Sahm et al., 2013). Taken together, our findings combined with the reported function of *QPRT* assured us to functionally validate *QPRT* in order to elucidate its potential role in the pathology of the Chr16p11.2 deletion syndrome.

5.3 The functional impact of *QPRT*

5.3.1 Reduction of *QPRT* induced subtle morphological changes of differentiated SH-SY5Y cells while a complete loss was lethal

Our first approach, i.e. a reduction of *QPRT* rather than a total loss, in general better reflects the heterozygous status of 16p11.2 deletion carriers. In previous studies, alterations of 16p11.2 gene dosage led to subtle changes of neuronal morphology as reported from mouse models of Chr16p11.2 (Blizinsky et al., 2016) and iPSC cells generated from 16p11.2 CNV carriers (Deshpande et al., 2017; also see Table 1). In detail, differentiation of iPSCs generated from heterozygous 16p11.2 deletion carriers resulted in neurons with an increase in total dendrite length and dendritic complexity accompanied by a decrease of synaptic density which seemed to be compensated for by an increase in synaptic strength (Deshpande et al., 2017). Although the gene dosage of *QPRT* assumingly is comparable between the cell lines generated by Deshpande et al. and our study here, the results of their and our study can not be fully compared as Deshpande and colleagues in contrast to our SH-SY5Y single gene study (i) performed functional analysis for the whole 16p11.2 region and (ii) used iPSCs differentiated into neurons. Still, both studies resulted in alterations of neuronal complexity *in vitro*. Taken together, these findings suggested a hemizygous deletion of 16p11.2 or reduced expression of *QPRT* to induce an aberration of neuronal development. We suggest that specifically reduction of *QPRT* might underlie the observed alterations of neuronal complexity.

A complete loss of Chr16p11.2 is supposedly lethal as to our knowledge there are no functional studies or reports of complete losses identified in ASD patients. The abovementioned KO mouse for *QPRT* was

generated to study Parkinson's disease (Fukuoka et al., 2012; Campbell et al., 2014) and niacin deficiency (Terakata et al., 2012). These animals exhibited neurodegeneration in the striatum suggested to be induced by an accumulation of QUIN (Fukuoka et al., 1998). No other histological differences were observed in the brain (Terakata et al., 2012). ASD-like behaviors were not studied but the animals showed no growth or developmental abnormalities (Terakata et al., 2012).

In contrast to *QPRT-KO* mice, the complete loss of *QPRT* was lethal for differentiating but not proliferating SH-SY5Y cells. We thus suggest that the viability of *QPRT-KO* mice relies on coping mechanisms at systems level, e.g. urinary excretion of excess QUIN or that the effect observed in SH-SY5Y KO cells is independent of QUIN and induced by alterations of neuronal processes (see following section 5.3.2).

Thus, our findings suggested that the level of QPRT protein in the KD cells is sufficient for survival of differentiating cells while the complete loss of QPRT is lethal for differentiating SH-SY5Y cells.

5.3.2 Neuronal cell death of SH-SY5Y induced by QPRT loss was independent of QUIN

We further elucidated the processes underlying cell death upon differentiation in *QPRT-KO* cells in a metabolite and transcriptomic assay and excluded the involvement of QUIN or the kynurenine pathway. This is in contrast to the current literature, which suggests a loss of QPRT to be lethal due to an accumulation of QUIN. Only one of the genes coding for proteins of the kynurenine pathway, *NMNAT2*, was differentially expressed upon KO of *QPRT*. This enzyme acts as an axonal maintenance factor down-stream of QPRT. Reduction of *NMNAT2* levels was found to cause axonal degeneration in superior cervical ganglia neurons (Gilley and Coleman, 2010) and axonal outgrowth deficits in *NMNAT2-KO* mice (Hicks et al., 2012). *NMNAT2* is influenced by MAPK signaling which promotes axonal degeneration by speeding the turnover of *NMNAT2* (Gerdtts et al., 2016; Walker et al., 2017). Considering the fact that *MAPK3* is also located in Chr16p11.2 and that a deletion of this region reduces *MAPK3* expression, the reduced *NMNAT2* availability could be alleviated in 16p11.2 deletion carriers by slowing down the *NMNAT2* turnover mediated by *MAPK3*. However, it remains unclear why *NMNAT2* is the only enzyme of the kynurenine pathway showing differential expression after KO of *QPRT*.

In contrast to the studies in animals or patients discussed above, we investigated the loss of *QPRT* at cellular level only. SH-SY5Y cells may not be able to produce QUIN at all, as it was mostly found to be produced by microglia and macrophages (Guillemin, 2012). Also, depending on the brain region, neurons exhibit differing sensitivity to QUIN, e.g. neurons of the cerebellum were shown to be less sensitive than those within the striatum or hippocampus (Guillemin, 2012). Furthermore, although the SH-SY5Y cells under study here do express some NMDA-R subunits it is possible that QUIN exhibits its excitotoxic effects to different extents depending on the expressed receptor subtype configuration (Guillemin, 2012). However, since cell death was only observed in differentiating cells and could be replicated in the chemically and genetically induced models for *QPRT* loss, we suggest that other, QUIN independent mechanisms of *QPRT* might be inhibited. Nevertheless, the overlaps of the functional effects of *QPRT* loss reported here and the findings in mouse models or ASD patients remain to be elucidated.

5.3.3 Overlap of ASD and epilepsy: Genes differentially regulated upon KO of *QPRT* in SH-SY5Y converged on synaptic functions with a suggested impact on E/I balance

Our findings of the transcriptomic approach overall suggested the loss of the ASD candidate gene *QPRT* to impact on neuronal viability via an increased negative regulation of cytoskeleton organization as well as an inhibition of neuronal differentiation and dendritic spine development. The reduced neuritic complexity observed in our KD model for *QPRT* specifically mirrored this functional role in these processes. Similarly, copy number changes of the whole 16p11.2 region were found to alter the expression of synaptic genes in lymphoblastoid cell lines as well (Blumenthal et al., 2014). The functional association of *QPRT* with ASD was further affirmed by the overlap of genes de-regulated upon KO of *QPRT* with ASD candidate genes extracted from SFARI (<https://gene.sfari.org>; see 4.3.3.4 and Table 2).

Among the most interesting candidate genes differentially expressed upon *QPRT-KO* is the gene *potassium voltage-gated channel subfamily Q member 3 (KCNQ3)* located at Chr8q24.22. This ASD candidate gene is down-regulated upon *QPRT-KO*. It encodes a protein regulating neuronal excitability by repolarizing the cell

membrane after action potentials. Variants of this gene were found to be implicated in the development of ASD and epilepsies (Gilling et al., 2013).

Another ASD risk gene down-regulated in *QPRT-KO* cells is the *solute carrier family 7 member 3 (SLC7A3)*, located at ChrXq13.1 and coding for the sodium-independent cationic amino acid transporter CAT-3. This protein is specifically expressed in the developing brain and four different missense variants were identified in individuals with ASD (Nava et al., 2015). Functional analysis revealed two of these four variants to cause severe or moderate loss of CAT-3 function potentially impacting on NO and mTOR signaling (Nava et al., 2015).

The gene *chromodomain helicase DNA binding protein 2 (CHD2)* at Chr15q26.1 is one of the two ASD candidate genes up-regulated in *QPRT-KO* cells and is involved in epilepsy (Caputo et al., 2018) as well as in the development of cortical inhibitory interneurons (Meganathan et al., 2017).

Another gene down-regulated upon *QPRT-KO* is the gene *4-aminobutyrate aminotransferase (ABAT)* which is involved in the catabolism of GABA and located at Chr16p13.2. In line with this finding, children with ASD exhibit elevated GABA levels in urine (Cohen, 2001) and plasma (Cohen, 2001; Dhossche et al., 2002; Russo, 2013) while the opposite is the case for epilepsy (Cohen, 2001). Although, as discussed by Dhossche et al., 2002, the relation of GABA levels in plasma with those of the brain and cerebrospinal fluid are unclear, alterations of GABA levels were suggested to be shared between the etiologies of ASD and seizures (Olsen and Avoli, 1997; Tanaka et al., 2012). This is also in line with the repeated reports of an E/I imbalance in ASD and epilepsy (Ben-Ari et al., 2012; Dickinson et al., 2016; Bozzi et al., 2017).

Paired box 5 (PAX5), an ASD candidate gene down-regulated upon loss of *QPRT* located at Chr9p13.2, codes for a transcription factor implicated in neuronal development. *PAX5-KO* in GABAergic neurons of mice led to an enlargement of lateral ventricles at seven weeks of age ultimately resulting in death of the mice one to two weeks afterwards (Ohtsuka et al., 2013).

Furthermore, a member of the SHANK family, *SHANK1*, located at Chr19q13.33, was down-regulated upon *KO* of *QPRT*. SHANK proteins (*SHANK1*, *SHANK2* and *SHANK3*) are scaffold proteins enriched in the postsynaptic density (PSD) of excitatory glutamatergic synapses. These proteins are required for

synaptogenesis and synaptic function and have recurrently been shown to be implicated in the etiology of ASD (Jiang and Ehlers, 2013). KO mice for SHANK1 exhibit an altered PSD protein composition, smaller dendritic spines as well as weaker basal synaptic transmission (Hung et al., 2008; Sungur et al., 2017).

The gene *CUGBP elav-like family member 4 (CELF4)*, located at Chr18q12.2, deletions of which have been identified in ASD patients, was down-regulated upon KO of *QPRT*. *CELF4* codes for an RNA binding protein that was found to regulate a vast set of mRNAs, especially a specific set coding for proteins involved in synaptic neurotransmission in both pre- and postsynapses (Wagnon et al., 2012). Of note, over 30% of ASD candidate genes were found in the mRNA set bound by CELF4 when cross-referenced to the ASD risk gene database AutDB (Basu et al., 2009; Wagnon et al., 2012). In mice, CELF4 is predominantly expressed in excitatory neurons located in the cortex and the hippocampus but sparsely in highly GABAergic neurons as found in the striatum (Wagnon et al., 2011). Lack of CELF4 during embryology led to a complex seizure phenotype in *CELF4-KO* mice. As seizures associated with epilepsy are considered to arise from alterations of synaptic transmission during development, the authors furthermore studied temporal and spatial KO of CELF4. Both, deletion of CELF4 in adulthood or from excitatory neurons only, was sufficient to induce convulsive seizures. The deletion of CELF4 resulted in a boost of excitatory synaptic transmission, indicating increased glutamate release or an increase of glutamatergic synapses (Wagnon et al., 2011).

Another gene down-regulated upon KO of *QPRT* is the Alzheimer's disease-implicated gene β -A4 amyloid protein precursor (APP) located at Chr21q21.3. KO mice for APP exhibited reduced branching of both dendrites and axons in cultured hippocampal neurons resulting in reduced synapse formation (Southam et al., 2018).

Syndecan 2 (SDC2) at Chr8q22.1 codes for a protein localized to dendritic spines and required for spinogenesis (filopodium-spine transition) as it facilitates the targeting of NMDA-R via a Ca^{2+} dependent interaction with calcium/calmodulin-dependent serine protein kinase (CASK) and Lin-7 homolog B, crumbs cell polarity complex component (LIN7B; Hu and Hsueh, 2014).

We also found *contactin associated protein like 2 (CNTNAP2)*, a well replicated risk gene for ASD (Peñagarikano and Geschwind, 2012) located at Chr7q35-36.1, to be down-regulated in *QPRT-KO* cells.

CNTNAP2 is a member of the presynaptic neurexin family and mediates interactions between neurons and glia during nervous system development. Furthermore, *CNTNAP2* is located at the juxtaparanodes of myelinated axons and required for the localization of Kv1-family potassium channels in differentiating axons to stabilize the conduction of action potentials (Scott et al., 2017). Studies of *CNTNAP2-KO* mice suggested a role for *CNTNAP2* in brain development and neuronal differentiation as the mice showed aberrant neuronal migration as well as a reduction of GABAergic interneurons (Peñagarikano et al., 2011). Another KO mouse study reports *CNTNAP2-KO* mice to exhibit altered excitatory synaptic transmission in the neocortex, as well as repetitive behavior at the phenotypic level (Scott et al., 2017). A more recent study reports a role for *CNTNAP2* in already-formed interneuron dendritic trees via the interaction with CASK, which is also a known ASD risk gene (Gao et al., 2018). In a former study, our group reports *CNTNAP2* promoter variants reducing transcription to be risk factors for ASD (Chiocchetti et al., 2015).

The gene *syntrophin gamma 2 (SNTG2)* is also down-regulated in *QPRT-KO* cells and codes for a synaptic scaffolding protein involved in actin and PDZ domain binding. *SNTG2* is located in 2p25.3, a region linked to intellectual disability (Bulayeva et al., 2015) and implicated in ASD (Rosenfeld et al., 2010; Lovrečić et al., 2018). The protein SNTG2 was shown to interact with neuroligins 3 and 4X at the inhibitory synapse (Yamakawa et al., 2007) and this interaction was weakened by ASD-associated mutations, e.g. NLGN3inR737C, where an arginine at the intracellular part of NLGN3 is exchanged to a cysteine (Yan et al., 2005a; Yamakawa et al., 2007). NLGN3 is found at the postsynapse of both GABAergic and glutamatergic synapses (Budreck and Scheiffele, 2007) and plays a role in synaptogenesis and glia-neuron interaction. Interestingly, QPRT was also found to physically interact with NLGN3 (Shen et al., 2015). Although the function of the interaction between NLGN3 and QPRT is still unclear, it is likely that QPRT is involved in the formation of the postsynaptic density of GABAergic and glutamatergic neurons. NLGN3 variants associated with ASD might thus also be linked to loss of QPRT function through an altered binding at the postsynaptic density.

QPRT-KO also led to inhibition of *gamma-aminobutyric acid type A receptor beta 3 subunit (GABRB3)*, which is a well replicated ASD risk gene (Buxbaum et al., 2002). *GABRB3* is located on Chr15q11-13, a region

strongly implicated in ASD, and codes for a subunit of the inhibitory GABA receptor (La Torre-Ubieta et al., 2016). Reduced expression of inhibitory GABA signals shifts the E/I balance to the excitatory side (Pizzarelli and Cherubini, 2011) as observed in KO mice for GABRB3 (DeLorey et al., 1998). These mice exhibited several phenotypes similar to that seen in ASD patients including EEG abnormalities and seizures, learning deficits or hyperactivity (DeLorey et al., 1998). A down-regulation of GABRB3 upon KO of QPRT could furthermore impair synaptic transmission and postsynaptic scaffolding of inhibitory synapses via gephyrin (GPHN) which in turn interacts with members of the neuroligin family, especially NLGN2 (Poulopoulos et al., 2009; Pizzarelli and Cherubini, 2011). It is suggested that at excitatory synapses NLGN3 can bind to neurexins on its own while it needs to build heterodimers with NLGN2 for proper function at the inhibitory synapse (Nguyen et al., 2016). The function of NLGN2-NLGN3 heterodimers in *QPRT-KO* could further be altered as the down-regulation of GABRB3 may also impair the scaffolding protein GPHN needed for synaptic transmission.

Finally, *catenin beta 1 (CTNNB1)* is down-regulated in *QPRT-KO* cells. The gene located at Chr3p22.1 is coding for the protein β -catenin which on the one hand plays a role in transcription and on the other hand mediates the formation of cell-cell-junctions. It plays an additional role in neurons, where it regulates the size and localization of synaptic vesicle clusters at the presynapse via the interaction with PDZ proteins (Bamji et al., 2003; Maguschak and Ressler, 2012; Wisniewska, 2013). At the postsynaptic site β -catenin interacts with the synaptic scaffolding molecule (S-SCAM) which in turn interacts with NMDA-R and neuroligins (Nishimura et al., 2002) and regulates the excitatory postsynaptic strength (Okuda et al., 2007). A recent study in mouse reports Wnt/ β -catenin signaling to increase the expression of NLGN3 as endogenous β -catenin binds to sequences in the promoter of NLGN3 (Medina et al., 2018). Furthermore, activation of Wnt/ β -catenin increased NLGN3 clustering and its co-localization with PSD-95, suggesting a role for this pathway in E/I balance (Medina et al., 2018). We therefore hypothesize that loss of QPRT may not only affect the direct interaction with NLGN3 but can further impact on its function via the down-regulation of Wnt/ β -catenin signaling.

Here, we report various ASD candidate genes differentially regulated upon KO of *QPRT* also being involved in the etiology of epilepsy, corroborating the findings that 40% of 16p11.2 deletion carriers are diagnosed with comorbid epilepsy (Shinawi et al., 2010). Overall, ASD candidate genes down-regulated upon KO of *QPRT* were predominantly involved in processes of synapse formation and organization as well as neurotransmission in both GABAergic and glutamatergic synapses. The down-regulated candidate genes furthermore impacted on neurite outgrowth and spinogenesis, while one of the two up-regulated candidates was involved in the generation of inhibitory interneurons. Ultimately, the disturbance of these processes suggestively results in an imbalance of excitation (E) and inhibition (I), a process highly discussed in both ASD and epilepsy (Bozzi et al., 2017).

Approaches to measure or identify E/I imbalance include the accession of frequencies of GABAergic and glutamatergic receptors in *post mortem* brains as well as *in vivo* MRI studies measuring GABA and glutamate levels (Dickinson et al., 2016). Although there is evidence for both, an increased relative excitation over inhibition and the opposite in ASD (Dickinson et al., 2016), the imbalance towards an increased excitation (hyperexcitability) is suggested to contribute higher to the comorbidity of ASD and epilepsy (Dickinson et al., 2016; Bozzi et al., 2017). The reported imbalances were identified in different brain regions during development and can arise from or impact on the molecular, cellular and circuit level (Dickinson et al., 2016). At the level of neural transmission, cellular abnormalities are reported from various parts of this system: neurotransmitter generation, release, reception and re-uptake (Dickinson et al., 2016). Further, findings in ASD included alterations of especially GABA receptor densities (Coghlan et al., 2012). Interestingly, in the adult brain GABA is mostly acting as an inhibitory neurotransmitter while it was found to additionally act excitatory in the developing brain (Sibilla and Ballerini, 2009).

A small metabolic study comparing blood plasma of 15 children with ASD to that of 12 age-matched healthy siblings identified disturbances of the kynurenine pathway, i.e. elevated levels of QUIN and kynurenine accompanied by a decrease of the neuroprotective picolinic acid, suggested to result in an imbalance of excitation and inhibition (Lim et al., 2015). Of note, to our knowledge these children were only analyzed and excluded for mutations in *TSC* or *FMR1* but not for e.g. CNVs including their state of 16p11.2 copy

numbers. The findings need to be repeated for bigger sample sizes of individuals tested for their genetic background to clarify whether alterations of the kynurenine system are observed in individuals with ASD in general and if these alterations differ from the ones in carriers of 16p11.2 CNVs.

5.3.4 Neuronal cell death of SH-SY5Y induced by *QPRT* loss: Suggested mechanisms

ASD is categorized as neurodevelopmental disorder meaning that the perturbations of the various neuronal systems which lead to the disorder are arising during different phases of brain development. In general, cell death of a subset of immature neurons is an important process during brain development while other progenitor cells will enter pro-survival pathways (Pfisterer and Khodosevich, 2017). Again, perturbations of these developmental processes induced by genetic mutations like the deletion of Chr16p11.2 or as seen in our study the death of neuronal cells induced by KO of *QPRT* may be involved in the etiology of ASD. A review on E/I imbalance also highlights the role of processes of neural development including synapse formation and function (Rubenstein and Merzenich, 2003). A down-regulation of genes involved in the formation and maintenance of synapses as observed in our KO-model for *QPRT* may lead to alterations of neurotransmission and circuit function and can further influence neuronal survival (Rubenstein and Merzenich, 2003).

Fricker et al., 2018 reviewed the various processes involved in neuronal cell death and defined them either by the stimuli inducing death (e.g. excitotoxicity) or by the mechanism executing cell death (e.g. apoptosis). Regarding apoptotic processes, genes differentially up-regulated upon KO of *QPRT* were indeed enriched for the GO-term “apoptotic process involved in morphogenesis”. In our cell model, we excluded QUIN-induced excitotoxicity, however, there are several other options discussed in Fricker et al., 2018: One is neuronal cell death during development and its prevention by survival factors. Neurotrophic factors (e.g. NGF, BDNF, NT3-5) and the respective kinases are essential for neurons and their absence leads to apoptotic cell death (Rubenstein and Merzenich, 2003; Fricker et al., 2018). The here applied differentiation method is based on BDNF but neither BDNF nor the gene *NTRK2* coding for its receptor Trkb are differentially expressed in our KO cell lines. It remains to be elucidated if downstream mediators of this pathway are disturbed upon KO of *QPRT*. Another option is axon death and cell death induced by axotomy

(Fricker et al., 2018). This mechanism includes the action of *NMNAT2* which is down-regulated upon KO of *QPRT*. Blocking of *NMNAT2* expression was shown to result in the generation of short axons only (Fricker et al., 2018). It remains to be established whether the *QPRT-KO* induced reduction of *NMNAT2* is underlying the here observed effects. Additionally, the authors discuss the mechanism of cell death induced by cell cycle re-entry. Usually, differentiated neurons are considered as postmitotic. There are cases where neurons would re-enter the cell cycle, e.g. after DNA damage (Fricker et al., 2018), which is usually resulting in neuronal cell death (Walton et al., 2018). In our cell model we observed enrichment for the process “negative regulation of mitotic cell cycle” in down-regulated genes and “positive regulation of mitotic nuclear division” in up-regulated genes. The observed death of differentiating *QPRT-KO* cells might be related to perturbations of the cell cycle or their inhibited capacity to exit the cell cycle.

In addition, although *NLGN3* itself is not differentially regulated upon KO of *QPRT*, we hypothesize that due to the described variants the interaction between *NLGN3* and *QPRT* is altered which in turn could impair *NLGN3* in its function suggestively resulting in disturbed synaptogenesis. A potential perturbation of *NLGN3* function is not only possible due to *QPRT* itself but could also be mediated via other genes that are down-regulated upon KO of *QPRT*. As discussed above, the proteins encoded by *SNTG2* and *CNNTB1* could also impact on the function of *NLGN3*.

5.3.5 Translation to human brain development: Expression patterns induced by *QPRT-KO* impacted on neuron-specific markers, developmental processes and brain regions previously associated with ASD

Finally, by translating the *in vitro* transcriptomic effects of *QPRT-KO* to the gene-networks active during human brain development (Kang et al., 2011) we observed differentially regulated genes to be enriched in modules previously associated with cell cycle regulation (Kang-Module 1), transcription factors regulating progenitor cell fate (Kang Module 20), neuronal development (Kang-Module 10 and 20), morphogenesis (Kang Modules 17 and 2) and synaptic transmission (Kang-Module 2 and 15). These findings mirrored the functions of the above discussed ASD-candidate genes affected by loss of *QPRT* which again indicated a role

for *QPRT* in these processes. In addition, the Kang-Modules identified to be affected by *QPRT-KO* were also reported to be highly co-expressed ($\rho \geq 0.68$) with markers for glutamatergic (Kang-Module 10) and GABAergic neurons (Kang-Module 2 and 15) or astrocytes (Kang-Module 2). This further supported our conclusion drawn from the single ASD related genes differentially regulated upon KO of *QPRT*.

To understand the potential neural consequences of *QPRT-KO*, it is essential to compare the brain regions indicated by our transcriptomic translational approach to results of brain imaging studies. Overall, the *QPRT* implicated functional networks were associated with brain regions that have been previously discussed in the context of ASD. However, few consistent imaging findings are available for ASD, and thus only findings from meta-analyses are discussed here.

Genes down-regulated upon *QPRT* KO were enriched in a negatively regulated gene set relevant for the cerebellum. In addition, the activated module for cerebellar development was also enriched for differentially regulated genes. Interestingly, a meta-analysis of fMRI studies in ASD confirmed that the cerebellum is differentially inhibited during face processing and activated during non-face processing tasks when comparing ASD cases to controls (Patriquin et al., 2016). It remains to be tested if alterations of the *QPRT* implicated gene-network are directly related to this phenomenon.

The same meta-analysis also reported an increased activity in the superior temporal cortex during non-face processing tasks in ASD (Patriquin et al., 2016). This again is translatable to our findings of an altered gene network regulating development of the superior temporal cortex. Furthermore, the transcriptomic approach suggested that reduced availability of *QPRT* inhibits networks involved in development of the prefrontal cortex, the middle frontal gyrus, the hippocampus and the amygdala. Again, the meta-analysis referenced above confirmed a reduced activation of the middle frontal gyrus during face processing tasks paralleled by an increase in activation during non-face processing tasks. Regarding social brain activity, the authors reported lower activation of the hippocampus in ASD while the amygdala showed altered activation in both directions (Patriquin et al., 2016).

At structural level an increased prefrontal grey matter in probands with high functioning autism has been confirmed (DeRamus and Kana, 2015). Considering our enrichment analyses we hypothesize that this again

may originate from an altered regulatory network of the early infancy and childhood prefrontal cortex development as suggested in this study here.

Although interpreting these findings in detail would go beyond the scope and suitability of this study here, the suggested altered neurotransmission induced by KO of *QPRT* may also impact on the discussed brain regions and lead to imbalances of excitation and inhibition during critical phases of neuronal development (Rubenstein and Merzenich, 2003).

5.4 Limitations of the study

To validate the gene dosage dependent expression of *QPRT* at mRNA level we only had access to lymphoblastoid cell lines of one 16p11.2 deletion carrier and his parents. However, our findings mirror previous reports of a gene dosage dependent expression of genes located in 16p11.2 (Blumenthal et al., 2014).

Although the here applied differentiation method yielded a more mature SH-SY5Y neuronal phenotype as reported from other studies, our model does not allow investigating all functional aspects of neurons. Our cells are suggested to exhibit limited synaptic function as they did express genes of synaptic pathways but they did not show preservation of modules associated with synaptic transmission (Chiocchetti et al., 2016). The fact that the applied cell line is not able to build functional synapses is a critical point for the interpretation of our results as our main finding is based on an altered synaptic transmission upon KO of *QPRT*. We suggest repeating the findings in neuronal cell lines reaching a more mature neuronal stage, e.g. human neuronal progenitor cells.

In addition, when analyzing the overlap of differentially expressed genes in *QPRT-KO* cells with ASD candidate genes the conclusion of enrichment for neuronal genes can be biased. ASD genes are known to frequently play a role in synaptic function and thus several publications specifically focused on these genes. Still, it has to be noted that the same processes were also found when we look at all (i.e. systems level) of the genes differentially regulated upon KO of *QPRT*. There, down-regulated genes, suggestively reduced in their function, again were involved in processes including synapse organization as well as glutamate

secretion under the top 10 GO terms independent of their previous involvement in ASD. Up-regulated genes are as well involved in processes like neurotransmitter secretion or dendritic differentiation. Although these associations were significant, it has to be considered that they were not under the top enriched GO terms.

Here, we exclude alterations of the kynurenine pathway, like the potential accumulation of QUIN, as underlying mechanism for SH-SY5Y cell death during differentiation upon *QPRT-KO*. Obviously, we are not able to picture this process to an extent as it is possible in mouse models or ASD patients. As discussed above, *QPRT* could have a dual role in patients where its gene dosage reduction on the one hand may lead to an accumulation of QUIN and on the other hand may impact on synapse formation and neurotransmission.

While the here generated KO cell lines showed an almost complete loss of *QPRT*, patients carrying a deletion of Chr16p11.2 are hemizygous for the deletion meaning that they still express the region harboring *QPRT* on one allele. The genes and pathways affected by KO of *QPRT* ultimately leading to neuronal cell death may be affected in a milder form in ASD patients suggestively resulting in similar effects as observed in our KD model. In addition, it has to be considered that in patients not only *QPRT* is affected by gene dosage changes but also its neighboring genes located in Chr16p11.2 which could alter the functional impact of *QPRT*. More studies will be needed to reveal the interplay of the individual genes located in this region.

5.5 Outlook

To further elucidate the function of *QPRT* and its role in ASD etiology, there is a need to repeat our findings in neuronal cells that reach a more mature state, e.g. human neuronal progenitor cell lines. Specifically, gene networks involved in synaptic function and neurotransmission were shown to be fully preserved in this neuronal cell model (Stein et al., 2014) while these networks cannot be fully depicted in SH-SY5Y cells. In CNV carriers, *QPRT* is not deleted as single gene but together with its surrounding genes in Chr16p11.2. Therefore, the generation and characterization of iPSCs of 16p11.2 deletion carriers can reveal the

functional impact of *QPRT* when compared to the deletion of *QPRT* alone. In addition, overexpressing *QPRT* in these cells can disclose the effect of a wild type *QPRT* gene dose in the surrounding of the 16p11.2 deletion. Furthermore, the application of overexpression experiments allows investigating the functional impact of duplications which were not under study here.

In addition, the *QPRT-KO* mouse model is of great interest for our studies. This model allows to study the functional effect of *QPRT* loss not only at cellular level to validate our findings presented here but it furthermore is an option to study the possible dual role of *QPRT* with its involvement in neurotransmission and the systems-wide effect of the kynurenine pathway.

To further understand the phenotype observed in *QPRT-KO* cells, the investigation and comparison of *QPRT* variants would be an interesting follow-up study, although to our knowledge there are none described.

More studies are needed to elucidate the role of the interaction between *QPRT* and *NLGN3* as the latter is a very promising and highly discussed ASD candidate gene involved in synaptogenesis. As already discussed above, we hypothesize that due to the described variants the interaction between *NLGN3* and *QPRT* is altered which in turn could impair *NLGN3* in its function. In addition, the down-regulation of *SNTG2* and *CNNTB1* upon KO of *QPRT* could also impact on the function of *NLGN3*.

6 Conclusions

Here, we report *quinolinate phosphoribosyltransferase (QPRT)*, a gene located in the ASD-associated 16p11.2 CNV region, to be essential for and causally related to *in vitro* neuronal differentiation of SH-SY5Y cells. While knock down of *QPRT* only resulted in slight alterations of neuritic complexity, a complete loss as well as chemical inhibition led to cell death during differentiation but not proliferation. This corroborates previous reports where alterations of 16p11.2 gene dosage resulted in subtle changes of neuromorphology in mouse models and human cell lines as well as *post mortem* findings of a disturbed neuronal development in ASD in general.

In contrast to the available literature on *QPRT* and its substrate *QUIN* we could not find alterations of the kynurenine pathway in the here generated SH-SY5Y *QPRT-KO* cellular model. Rather, the complete loss of

QPRT impacted on ASD candidate genes converging on functions in synapse formation and stability as well as neurotransmission in both glutamatergic and GABAergic synapses. All but two of the differentially expressed genes were down-regulated upon KO of *QPRT*, predicting a reduced function. In addition, our findings further support the previously suggested link between QPRT and the ASD candidate protein NLGN3, which needs further characterization in future studies. In general, genes down-regulated upon KO of *QPRT* were involved in processes including synapse organization as well as glutamate secretion. Finally, the finding of synaptic processes was mirrored by the results of our translational approach of human brain development.

We conclude that the availability of QPRT is linked to genes implicated in the formation, function and existence of functional synapses. Further, we hypothesize that an interplay of the down-regulation of genes implicated in the development and function of synapses and the various apoptotic mechanisms including aberrations of axonal outgrowth as well as an inhibited capacity of exiting the cell cycle leads to the here observed cell death of differentiating SH-SY5Y *QPRT-KO* cells. We further hypothesize that in patients QPRT could have a dual role: First, as suggested in our transcriptomic approach here, loss of QPRT impacts on several genes regulating synaptic functions which may lead to E/I imbalances ultimately resulting in neuronal cell death. Second, as observed in *QPRT-KO* mice, QPRT loss leads to an accumulation of the excitotoxin QUIN which suggestively also induces neuronal cell death. In carriers of 16p11.2 deletions an interplay of both mechanisms could lead to the observed phenotype.

The findings of our study partially revealed how the KO of a single gene can impact on the etiology of this complex disease and helped to further understand the underlying mechanisms of ASD and related disorders. To confirm these results and the neurodevelopmental role of *QPRT* in the etiology of ASD in general, further studies in human neuronal progenitor cells or animal models are needed.

7 Appendix

7.1 Supplementary tables

7.1.1 List of antibodies used in this study

Primary		
Antibody	Dilution	Supplier
rabbit anti-CDK1	1:500	GeneTex
rabbit anti-MAPT	1:500	GeneTex
mouse anti-QPRT	1:1,000	Abcam
mouse anti-GAPDH	1:2,500	Santa Cruz
anti-ACTB	1:10,000	Sigma Aldrich
Secondary		
Antibody	Dilution	Supplier
goat anti-rabbit poly-HRP	1:5,000	Pierce
goat anti-mouse poly-HRP	1:5,000	Pierce
anti-mouse IgG HRP	1:5,000	Santa Cruz

For gene descriptions also see List of genes discussed in this study.

7.1.2 List of real-time PCR primers used in this study

Primer	Forward	Reverse	UPL probe
out_1	ttgttgcaaacagcattc	aaacatacatggggtgaagagg	12
in_1	acgtccattcactgcaacac	agtgactggtgctggttagg	61
in_2	gaagaaccattgcctaattgga	aagcaggaaaagcctcatca	89
in_3	acagtgctcgaaaggatgat	ccacaagaccgcaaagtca	64
out_2	cctactgccaagacagcaga	gggatgggtaaggacga	21
reference_SNCA	ttactttcatgtctaagggtgga	ggggctgacctcaagattc	35
reference_CSF3R	tggtgactggagatggtgag	gaagaggggagggtccataa	23

For gene descriptions also see List of genes discussed in this study.

7.1.3 List of real-time RT-PCR primers used in this study

Gene	RefSeq-Nr.	Forward	Reverse	UPL probe
<i>ARHGAP20</i>	NM_020809.3	tgagatgtgacactagagagaatgc	ctcatttagctcattttccaagc	63
<i>BRINP1</i>	NM_014618.2	aaaagtacggcaccaccct	catatacatggtaaagcctct	5
<i>CCK</i>	NM_000729.5	ctttcactgaccagaacactg	cggtgaagtggctctg	80
<i>CDK1</i>	NM_001786	tgatctgaagaaatactggattcta	caatcccctgtaggattgg	79
<i>CNTNAP2</i>	NM_001786	cctggagctctacagccagt	tcacccattcatctcaa	26
<i>COX17</i>	NM_005694.1	aagatgccgggtctggt	ttcttctcttctcgatgataca	2
<i>COX17P1</i>	ENST00000535895	caagtgcagcagggtctc	aaagatgccgggtctggt	2
<i>CUX2</i>	NM_015267.3	cgatcaactggtccaca	ggatcaaggctggctcatc	22
<i>DHCR7</i>	NM_001360	gccatggtcaagggtctac	ttgtaaaagaaattgctgtgaat	60
<i>DRD4</i>	NM_000797.3	gctctctgctactccgaggt	cgcacaggtgaagatgga	66
<i>GABRB3</i>	NM_000814.5	tgagctcccgcagttctc	cagtgcagctcaggataggc	54
<i>GAPDH</i>	NM_002046.3	agccacatcgctcagacac	gcccaatacgaccaaacc	60
<i>GRIA2</i>	NM_000826.3	actgacacccacatcgac	tcgaaaactgggagcagaaa	10
<i>GRIK2</i>	NM_021956.4	tgatattctcaaggaaccacac	tcacagcaaactggaatgcaa	73
<i>GRIN1</i>	NM_001185091.1	ccgatgtccatctactcg	tgactggtgggagtaggg	4
<i>GRM1</i>	NM_000838.3	atgtctctgcagtccacacg	cagaatgggagatacagagg	44
<i>GRM4</i>	NM_000841.1	tgaccacctgcaccttagaa	actgtcttctccgctcacc	74
<i>GUCA1A</i>	NM_000409.4	caggacctcgagcagctct	gagtctccactaaatccttgag	66
<i>GUSB</i>	NM_000181.3	cgccctgctatctgtattc	gatgaggaactggctcttg	5
<i>KCNQ3</i>	NM_004519.3	aagggtcagcattcaccttc	tgatgtggatggtctggcta	14
<i>LINC01760</i>	NR_135588.1	aggcaactactagactaagggtga	tgatttctcaaagcagacaa	4
<i>MAPT</i>	NM_016835	accacagccaccttctct	cagccatcctggtcaaagt	55
<i>NLGN3</i>	NM_018977.3	cccaacgaagactgtctctacc	cctcgccctgttcttagc	88
<i>NMNAT2</i>	NM_015039.3	acacctggcagacgacct	gggtgttgacattggagagg	71
<i>NRXN1</i>	NM_001135659	ccggagccaggaactaga	tggaaggattgtatgttcttagc	63
<i>POLR2F</i>	NM_001135659	gatgaagggtatagactggtg	ccagaggggaggatctcg	2
<i>PSMD7</i>	NM_002811.4	cacgtgaccagtgaaattgg	ccaccgtcgtgtcttgata	6
<i>QPRT</i>	NM_014298.3	tggaagtggaatgcagcag	gaactggccttcagcac	82
<i>SHANK3</i>	NM_033517	cacggaccaagtctgtaggg	gtcttgcacgaggtgctc	11
<i>SNTG2</i>	NM_018968.3	ttttcaacgtggagctggtg	gctgcacatgtatgtctgga	7
<i>SRRM4</i>	NM_194286.3	gctcctctatgccagcac	gagagcgggagtaggacctt	65
<i>TH</i>	NM_199292.2	cctggtcaccaagttcgac	gtacacctggcggagaagc	85
<i>VSTM2A</i>	NM_182546.3	ctggagatccaatgggtggt	ctgtccgggtctctgtcg	39

For gene descriptions also see List of genes discussed in this study.

7.1.4 sgRNAs and sequencing primers for CRISPR/Cas9

sgRNAs were designed using the tool crispr.mit.edu/:

Ex. 2.1 5' **CACCGCAGTTGAGTTGGGTAAATA** 3'
 3' CGTCAACTCAACCCATTTAT**CAAA** 5'

Ex. 2.2 5' **CACCGCAGCGGGCCAGCGTGTGA** 3'
 3' CGTCGCCCGGTCGCACAACT**CAAA** 5'

Oligos were ordered from Sigma Aldrich and cloned into pSpCas9(BB)-2A-Puro (PX459) V2.0 (Plasmid #62988; Addgene).

Primer used for Sanger-Sequencing:

Ex. 2.1/Ex. 2.2_fw GAGAGGCAGCCAACTCAA
 Ex. 2.1/Ex. 2.2_rv ACCAGGAGCCCATACTTCT

7.2 Supplementary methods

7.2.1 ImageJ macros for Sholl analysis

7.2.1.1 Make binary for soma 20x

```
run("Set Scale...", "distance=404 known=100 pixel=1 unit=µm");
setMinAndMax(150, 255);
call("ij.ImagePlus.setDefault16bitRange", 0);
run("Subtract Background...", "rolling=25 sliding");
run("Despeckle");
run("8-bit");
setAutoThreshold("Otsu dark");
run("Make Binary");
```

7.2.1.2 Make binary for sholl 20x

```
run("Set Scale...", "distance=404 known=100 pixel=1 unit=µm");
setMinAndMax(17, 100);
call("ij.ImagePlus.setDefault16bitRange", 0);
run("Subtract Background...", "rolling=25 sliding");
run("Despeckle");
run("8-bit");
setAutoThreshold("Triangle dark");
run("Make Binary");
```

7.2.1.3 Analysis soma area

```
run("Create Selection");  
run("Measure");
```

7.2.1.4 Analysis sholl area

```
run("Create Selection");  
run("Measure");
```

7.2.1.5 Analysis sholl

```
run("Sholl Analysis...", "starting=5 ending=NaN radius_step=1 samples=3  
samples_integration=Mean sholl=Intersections fit polynomial=[5th degree]  
background=228");  
close();
```

7.2.2 Metabolite analysis

For subsequent metabolite analysis, samples were sent to and analyzed by Prof. Gilles J. Guillemin and Dr. Chai K. Lim (Macquarie University, Australia). The methods have previously been described in their original publications (Lim et al., 2015; Lim et al., 2017a) as copied here: Prior to analysis, culture media and serum samples were deproteinized with trichloroacetic acid at a final concentration of 5 % (w+v) in equal volume. Samples were incubated for 5 min, vortexed and then centrifuged (4°C) for 10 min at 12,000 rpm. Supernatant was extracted, filtered with syringe filters (0.22µm) and subsequently injected into analyzers. Concurrent quantification of tryptophan (TRP), kynurenine (KYN), 3-hydroxykynurenine (3-HK), 3-hydroxyanthranilic acid (3HAA), and anthranilic acid (AA) was carried out in accordance to Lim et al., 2017a. An Agilent 1290 infinity ultra-high-performance liquid chromatography (UHPLC) system coupled with temperature controlled autosampler and column compartment, diode array detector and fluorescence detector were used for the analysis of these metabolites with a 20µL sample injection volume. Separation of metabolites was performed under stable temperature of 38°C for 12 min, using 0.1mM sodium acetate (pH 4.65) as mobile phase, with an isocratic flow rate of 0.75ml/min in an Agilent Eclipse Plus C18 reverse-phase column (2.1mm x 150mm, 1.8µm particle size). 3HK and KYN were detected using an UV wavelength of 365nm with a retention time of 1.2 and 3.1 min, respectively. TRP, 3HAA and AA were

detected using fluorescence intensity set at Ex/Em wavelength of 280/438 nm for TRP and 320/438 nm for 3HAA and AA. Mixed standards of all metabolites were used for a six-point calibration curve in order to interpolate the quantity of the sample readout. Agilent OpenLAB CDS Chemstation (Edition C.01.04) was used to analyze the chromatograms. The inter- and intra-assay coefficient of variation was within the acceptable range of 3-7%.

Kynurenic acid (KA) detection was carried out using UHPLC with a gradient mobile phase comprising 50mM sodium acetate buffer spiked with 25mM zinc acetate (dihydrate) to enhance fluorescence intensity and 2.25% acetonitrile as organic modifier (solvent A), and 10% acetonitrile (solvent B). Each sample (10 μ L) was injected into a Poroshell RRHT C-18, 1.8 μ m 2.1 \times 100mm column (Agilent Technologies, Inc, Santa Clara, CA) maintained at 38°C for a 12 min run time at a unison flowrate of 0.75 ml/min. The gradient elution comprised 100% solvent A for 3 min and then 50% solvent A and 50% solvent B for 2 min, followed by 100% solvent B for 2 min and 100% solvent A (run time of 10 min). This gradient ensured sufficient time for KA retention while minimizing potential build-up of pressure due to precipitation of the high salt buffer. Fluorescence was used for detection of KA (excitation and emission wavelengths of 344nm and 388nm, respectively with a retention time of 1.5 min). Agilent OpenLAB CDS ChemStation (Edition C.01.04) was used to analyze the chromatograms.

Picolinic acid (PIC) and quinolinic acid (QUIN) were detected using gas chromatography–mass spectrometry (GC/MS) as previously described in Lim et al., 2015. Separation of PIC and QUIN were achieved using a DB-5MS column, 0.25 μ m film thickness, 0.25mm \times 30m capillary column (Agilent Technologies, Inc, Santa Clara, CA) with a 1 μ L injection volume of the derivatized sample. Quantification of PIC and QUIN concentrations were analyzed using Agilent GC/MSD ChemStation software (Edition 02.02.1431) and interpolated from the established six-point calibration curves based on the abundance count ratio of the metabolites to their corresponding deuterated internal standards within each standard and sample. The intra- and inter-assay coefficient of variability was within the acceptable range (4–8% for UHPLC assays, 7-10% for GC/MS assays) calculated from the repeated measures of the metabolite standards incorporated during the sequence run.

8 References

- Alexa, A., Rahnenführer, J., and Lengauer, T. (2006). Improved scoring of functional groups from gene expression data by decorrelating GO graph structure. *Bioinformatics (Oxford, England)* 22, 1600-1607.
- Amaral, D.G., Schumann, C.M., and Nordahl, C.W. (2008). Neuroanatomy of autism. *Trends in neurosciences* 31, 137-145.
- American Psychiatric Association (1994). *Diagnostic and Statistical Manual of Mental Disorders, Fourth Edition (DSM-IV)*.
- American Psychiatric Association (2013). *Diagnostic and Statistical Manual of Mental Disorders, Fifth Edition (DSM-5™)*.
- An, J.Y., and Claudianos, C. (2016). Genetic heterogeneity in autism: From single gene to a pathway perspective. *Neuroscience and biobehavioral reviews* 68, 442-453.
- Angelakos, C.C., Watson, A.J., O'Brien, W.T., Krainock, K.S., Nickl-Jockschat, T., and Abel, T. (2017). Hyperactivity and male-specific sleep deficits in the 16p11.2 deletion mouse model of autism. *Autism research : official journal of the International Society for Autism Research* 10, 572-584.
- Anney, R., Klei, L., Pinto, D., Regan, R., Conroy, J., Magalhaes, T.R., Correia, C., Abrahams, B.S., Sykes, N., and Pagnamenta, A.T., et al. (2010). A genome-wide scan for common alleles affecting risk for autism. *Human Molecular Genetics* 19, 4072-4082.
- Anney, R.J.L., Ripke, S., Anttila V., and Grove, J. (2017). Meta-analysis of GWAS of over 16,000 individuals with autism spectrum disorder highlights a novel locus at 10q24.32 and a significant overlap with schizophrenia. *Molecular autism* 8, 21.
- Bamji, S.X., Shimazu, K., Kimes, N., Huelsken, J., Birchmeier, W., Lu, B., and Reichardt, L.F. (2003). Role of beta-catenin in synaptic vesicle localization and presynaptic assembly. *Neuron* 40, 719-731.
- Basu, S.N., Kollu, R., and Banerjee-Basu, S. (2009). AutDB: a gene reference resource for autism research. *Nucleic Acids Res.* 37, 6.
- Baudouin, S.J., Gaudias, J., Gerharz, S., Hatstatt, L., Zhou, K., Punnakkal, P., Tanaka, K.F., Spooren, W., Hen, R., and Zeeuw, C.I. de, et al. (2012). Shared synaptic pathophysiology in syndromic and nonsyndromic rodent models of autism. *Science (New York, N.Y.)* 338, 128-132.
- Ben-Ari, Y., Khalilov, I., Kahle, K.T., and Cherubini, E. (2012). The GABA excitatory/inhibitory shift in brain maturation and neurological disorders. *The Neuroscientist : a review journal bringing neurobiology, neurology and psychiatry* 18, 467-486.
- Ben-Reuven, L., and Reiner, O. (2016). Modeling the autistic cell: iPSCs recapitulate developmental principles of syndromic and nonsyndromic ASD. *Development, growth & differentiation*.
- Berg, J.M., and Geschwind, D.H. (2012). Autism genetics: searching for specificity and convergence. *Genome biology* 13, 247.
- Bernardet, M., and Crusio, W.E. (2006). Fmr1 KO mice as a possible model of autistic features. *TheScientificWorldJournal* 6, 1164-1176.
- Billstedt, E., Gillberg, I.C., and Gillberg, C. (2007). Autism in adults: symptom patterns and early childhood predictors. Use of the DISCO in a community sample followed from childhood. *Journal of child psychology and psychiatry, and allied disciplines* 48, 1102-1110.
- Blaker-Lee, A., Gupta, S., McCammon, J.M., Rienzo, G. de, and Sive, H. (2012). Zebrafish homologs of genes within 16p11.2, a genomic region associated with brain disorders, are active during brain

- development, and include two deletion dosage sensor genes. *Disease models & mechanisms* 5, 834-851.
- Blizinsky, K.D., Diaz-Castro, B., Forrest, M.P., Schurmann, B., Bach, A.P., Martin-de-Saavedra, M.D., Wang, L., Csernansky, J.G., Duan, J., and Penzes, P. (2016). Reversal of dendritic phenotypes in 16p11.2 microduplication mouse model neurons by pharmacological targeting of a network hub. *Proceedings of the National Academy of Sciences of the United States of America* 113, 8520-8525.
- Blumenthal, I., Ragavendran, A., Erdin, S., Klei, L., Sugathan, A., Guide, J.R., Manavalan, P., Zhou, J.Q., Wheeler, V.C., and Levin, J.Z., et al. (2014). Transcriptional consequences of 16p11.2 deletion and duplication in mouse cortex and multiplex autism families. *American journal of human genetics* 94, 870-883.
- Bölte, S., and Poustka, F. (2004). Diagnostische Beobachtungsskala für Autistische Störungen (ADOS): Erste Ergebnisse zur Zuverlässigkeit und Gültigkeit. *Zeitschrift für Kinder- und Jugendpsychiatrie und Psychotherapie* 32, 45-50.
- Bourgeron, T. (2015). From the genetic architecture to synaptic plasticity in autism spectrum disorder. *Nature reviews. Neuroscience* 16, 551-563.
- Bozdagi, O., Sakurai, T., Papapetrou, D., Wang, X., Dickstein, D.L., Takahashi, N., Kajiwar, Y., Yang, M., Katz, A.M., and Scattoni, M.L., et al. (2010). Haploinsufficiency of the autism-associated Shank3 gene leads to deficits in synaptic function, social interaction, and social communication. *Mol Autism* 1, 15.
- Bozzi, Y., Provenzano, G., and Casarosa, S. (2017). Neurobiological bases of autism-epilepsy comorbidity: a focus on excitation/inhibition imbalance. *The European journal of neuroscience*.
- Braidy, N., Grant, R., Adams, S., Brew, B.J., and Guillemain, G.J. (2009). Mechanism for quinolinic acid cytotoxicity in human astrocytes and neurons. *Neurotox Res* 16, 77-86.
- Braidy, N., Guillemain, G.J., and Grant, R. (2011). Effects of Kynurenine Pathway Inhibition on NAD Metabolism and Cell Viability in Human Primary Astrocytes and Neurons. *International journal of tryptophan research : IJTR* 4, 29-37.
- Budreck, E.C., and Scheiffele, P. (2007). Neuroligin-3 is a neuronal adhesion protein at GABAergic and glutamatergic synapses. *Eur. J. Neurosci.* 26, 1738-1748.
- Bulayeva, K., Lesch, K.-P., Bulayev, O., Walsh, C., Glatt, S., Gurganova, F., Omarova, J., Berdichevets, I., and Thompson, P.M. (2015). Genomic structural variants are linked with intellectual disability. *Journal of neural transmission (Vienna, Austria : 1996)* 122, 1289-1301.
- Burd, L., Fisher, W., and Kerbeshian, J. (1987). A prevalence study of pervasive developmental disorders in North Dakota. *Journal of the American Academy of Child and Adolescent Psychiatry* 26, 700-703.
- Butler, M.G., Dasouki, M.J., Zhou, X.-P., Talebizadeh, Z., Brown, M., Takahashi, T.N., Miles, J.H., Wang, C.H., Stratton, R., and Pilarski, R., et al. (2005). Subset of individuals with autism spectrum disorders and extreme macrocephaly associated with germline PTEN tumour suppressor gene mutations. *Journal of medical genetics* 42, 318-321.
- Buxbaum, J.D., Silverman, J.M., Smith, C.J., Greenberg, D.A., Kilifarski, M., Reichert, J., Cook, E.H., Fang, Y., Song, C.-Y., and Vitale, R. (2002). Association between a GABRB3 polymorphism and autism. *Molecular psychiatry* 7, 311-316.
- C Yuen, R.K., Merico, D., Bookman, M., L Howe, J., Thiruvahindrapuram, B., Patel, R.V., Whitney, J., Deflaux, N., Bingham, J., and Wang, Z., et al. (2017). Whole genome sequencing resource identifies 18 new candidate genes for autism spectrum disorder. *Nat. Neurosci.* 20, 602-611.
- Cahoy, J.D., Emery, B., Kaushal, A., Foo, L.C., Zamanian, J.L., Christopherson, K.S., Xing, Y., Lubischer, J.L., Krieg, P.A., and Krupenko, S.A., et al. (2008). A transcriptome database for astrocytes, neurons, and

- oligodendrocytes: a new resource for understanding brain development and function. *The Journal of neuroscience : the official journal of the Society for Neuroscience* *28*, 264-278.
- Calderon de Anda, F., Rosario, A.L., Durak, O., Tran, T., Gräff, J., Meletis, K., Rei, D., Soda, T., Madabhushi, R., and Ginty, D.D., et al. (2012). Autism spectrum disorder susceptibility gene TAOK2 affects basal dendrite formation in the neocortex. *Nat Neurosci* *15*, 1022-1031.
- Campbell, B.M., Charych, E., Lee, A.W., and Möller, T. (2014). Kynurenines in CNS disease: regulation by inflammatory cytokines. *Frontiers in neuroscience* *8*, 12.
- Candemir, E., Kollert, L., Weissflog, L., Geis, M., Muller, A., Post, A.M., OLeary, A., Harro, J., Reif, A., and Freudenberg, F. (2016). Interaction of NOS1AP with the NOS-I PDZ domain: Implications for schizophrenia-related alterations in dendritic morphology. *European neuropsychopharmacology : the journal of the European College of Neuropsychopharmacology* *26*, 741-755.
- Caputo, D., Trivisano, M., Vigeveno, F., and Fusco, L. (2018). CHD2-epilepsy. Polygraphic documentation of self-induced seizures due to fixation-off sensitivity. *Seizure* *57*, 8-10.
- Casanova, M.F., van Kooten, Imke A J, Switala, A.E., van Engeland, H., Heinsen, H., Steinbusch, H.W.M., Hof, P.R., Trippe, J., Stone, J., and Schmitz, C. (2006). Minicolumnar abnormalities in autism. *Acta neuropathologica* *112*, 287-303.
- Chang, J., Gilman, S.R., Chiang, A.H., Sanders, S.J., and Vitkup, D. (2015). Genotype to phenotype relationships in autism spectrum disorders. *Nature neuroscience* *18*, 191-198.
- Chen, J.A., Peñagarikano, O., Belgard, T.G., Swarup, V., and Geschwind, D.H. (2015). The emerging picture of autism spectrum disorder: genetics and pathology. *Annual review of pathology* *10*, 111-144.
- Chen, R., Davis, L.K., Guter, S., Wei, Q., Jacob, S., Potter, M.H., Cox, N.J., Cook, E.H., Sutcliffe, J.S., and Li, B. (2017). Leveraging blood serotonin as an endophenotype to identify de novo and rare variants involved in autism. *Molecular autism* *8*, 14.
- Chiocchetti, A.G., Bour, H.S., and Freitag, C.M. (2014). Glutamatergic candidate genes in autism spectrum disorder: an overview. *Journal of neural transmission (Vienna, Austria : 1996)* *121*, 1081-1106.
- Chiocchetti, A.G., Haslinger, D., Stein, J.L., La Torre-Ubieta, L. de, Cocchi, E., Rothamel, T., Lindlar, S., Waltes, R., Fulda, S., and Geschwind, D.H., et al. (2016). Transcriptomic signatures of neuronal differentiation and their association with risk genes for autism spectrum and related neuropsychiatric disorders. *Translational psychiatry* *6*, e864.
- Chiocchetti, A.G., Kopp, M., Waltes, R., Haslinger, D., Duketis, E., Jarczok, T.A., Poustka, F., Voran, A., Graab, U., and Meyer, J., et al. (2015). Variants of the CNTNAP2 5' promoter as risk factors for autism spectrum disorders: a genetic and functional approach. *Molecular psychiatry* *20*, 839-849.
- Christensen, D.L., Baio, J., van Naarden Braun, K., Bilder, D., Charles, J., Constantino, J.N., Daniels, J., Durkin, M.S., Fitzgerald, R.T., and Kurzius-Spencer, M., et al. (2016). Prevalence and Characteristics of Autism Spectrum Disorder Among Children Aged 8 Years—Autism and Developmental Disabilities Monitoring Network, 11 Sites, United States, 2012. *Morbidity and mortality weekly report. Surveillance summaries (Washington, D.C. : 2002)* *65*, 1-23.
- Christensen, J., Grønborg, T.K., Sørensen, M.J., Schendel, D., Parner, E.T., Pedersen, L.H., and Vestergaard, M. (2013). Prenatal valproate exposure and risk of autism spectrum disorders and childhood autism. *JAMA* *309*, 1696-1703.
- Coghlan, S., Horder, J., Inkster, B., Mendez, M.A., Murphy, D.G., and Nutt, D.J. (2012). GABA system dysfunction in autism and related disorders: from synapse to symptoms. *Neuroscience and biobehavioral reviews* *36*, 2044-2055.
- Cohen, B.I. (2001). GABA-transaminase, the liver and infantile autism. *Med. Hypotheses* *57*, 673-674.

- Connolly, J.J., Glessner, J.T., and Hakonarson, H. (2013). A genome-wide association study of autism incorporating autism diagnostic interview-revised, autism diagnostic observation schedule, and social responsiveness scale. *Child development* *84*, 17-33.
- DeLorey, T.M., Handforth, A., Anagnostaras, S.G., Homanics, G.E., Minassian, B.A., Asatourian, A., Fanselow, M.S., Delgado-Escueta, A., Ellison, G.D., and Olsen, R.W. (1998). Mice lacking the beta3 subunit of the GABAA receptor have the epilepsy phenotype and many of the behavioral characteristics of Angelman syndrome. *J. Neurosci.* *18*, 8505-8514.
- DeRamus, T.P., and Kana, R.K. (2015). Anatomical likelihood estimation meta-analysis of grey and white matter anomalies in autism spectrum disorders. *NeuroImage. Clinical* *7*, 525-536.
- Deshpande, A., Yadav, S., Dao, D.Q., Wu, Z.-Y., Hokanson, K.C., Cahill, M.K., Wiita, A.P., Jan, Y.-N., Ullian, E.M., and Weiss, L.A. (2017). Cellular Phenotypes in Human iPSC-Derived Neurons from a Genetic Model of Autism Spectrum Disorder. *Cell reports* *21*, 2678-2687.
- Dhossche, D., Applegate, H., Abraham, A., Maertens, P., Bland, L., Bencsath, A., and Martinez, J. (2002). Elevated plasma gamma-aminobutyric acid (GABA) levels in autistic youngsters. Stimulus for a GABA hypothesis of autism. *Medical science monitor : international medical journal of experimental and clinical research* *8*, PR1-6.
- Dickinson, A., Jones, M., and Milne, E. (2016). Measuring neural excitation and inhibition in autism: Different approaches, different findings and different interpretations. *Brain research* *1648*, 277-289.
- Doers, M.E., Musser, M.T., Nichol, R., Berndt, E.R., Baker, M., Gomez, T.M., Zhang, S.-C., Abbeduto, L., and Bhattacharyya, A. (2014). iPSC-derived forebrain neurons from FXS individuals show defects in initial neurite outgrowth. *Stem cells and development* *23*, 1777-1787.
- Dong, S., Walker, M.F., Carriero, N.J., DiCola, M., Willsey, A.J., Ye, A.Y., Waqar, Z., Gonzalez, L.E., Overton, J.D., and Frahm, S., et al. (2014). De novo insertions and deletions of predominantly paternal origin are associated with autism spectrum disorder. *Cell reports* *9*, 16-23.
- Elsabbagh, M., Divan, G., Koh, Y.-J., Kim, Y.S., Kauchali, S., Marcín, C., Montiel-Nava, C., Patel, V., Paula, C.S., and Wang, C., et al. (2012). Global prevalence of autism and other pervasive developmental disorders. *Autism research : official journal of the International Society for Autism Research* *5*, 160-179.
- Encinas, M., Iglesias, M., Liu, Y., Wang, H., Muhaisen, A., Ceña, V., Gallego, C., and Comella, J.X. (2000). Sequential treatment of SH-SY5Y cells with retinoic acid and brain-derived neurotrophic factor gives rise to fully differentiated, neurotrophic factor-dependent, human neuron-like cells. *J. Neurochem.* *75*, 991-1003.
- Escamilla, C.O., Filonova, I., Walker, A.K., Xuan, Z.X., Holehonnur, R., Espinosa, F., Liu, S., Thyme, S.B., López-García, I.A., and Mendoza, D.B., et al. (2017). Kctd13 deletion reduces synaptic transmission via increased RhoA. *Nature* *551*, 227-231.
- Etherton, M.R., Blaiss, C.A., Powell, C.M., and Südhof, T.C. (2009). Mouse neurexin-1alpha deletion causes correlated electrophysiological and behavioral changes consistent with cognitive impairments. *Proc. Natl. Acad. Sci. U.S.A.* *106*, 17998-18003.
- Fournier, K.A., Hass, C.J., Naik, S.K., Lodha, N., and Cauraugh, J.H. (2010). Motor coordination in autism spectrum disorders: a synthesis and meta-analysis. *Journal of autism and developmental disorders* *40*, 1227-1240.
- Freitag, C.M., Staal, W., Klauck, S.M., Duketis, E., and Waltes, R. (2010). Genetics of autistic disorders: review and clinical implications. *European child & adolescent psychiatry* *19*, 169-178.
- Fricker, M., Tolkovsky, A.M., Borutaite, V., Coleman, M., and Brown, G.C. (2018). Neuronal Cell Death. *Physiological reviews* *98*, 813-880.

- Fukuoka, S.I., Nyaruhucha, C.M., and Shibata, K. (1998). Characterization and functional expression of the cDNA encoding human brain quinolinate phosphoribosyltransferase. *Biochimica et biophysica acta* 1395, 192-201.
- Fukuoka, S.-I., Kawashima, R., Asuma, R., Shibata, K., and Fukuwatari, T. (2012). Quinolinate Accumulation in the Brains of the Quinolinate Phosphoribosyltransferase (QPRT) Knockout Mice.
- Gao, R., Piguel, N.H., Melendez-Zaidi, A.E., Martin-de-Saavedra, M.D., Yoon, S., Forrest, M.P., Myczek, K., Zhang, G., Russell, T.A., and Csernansky, J.G., et al. (2018). CNTNAP2 stabilizes interneuron dendritic arbors through CASK. *Mol. Psychiatry*.
- Gaugler, T., Klei, L., Sanders, S.J., Bodea, C.A., Goldberg, A.P., Lee, A.B., Mahajan, M., Manaa, D., Pawitan, Y., and Reichert, J., et al. (2014). Most genetic risk for autism resides with common variation. *Nat. Genet.* 46, 881-885.
- Gerdtts, J., Summers, D.W., Milbrandt, J., and DiAntonio, A. (2016). Axon Self-Destruction: New Links among SARM1, MAPKs, and NAD⁺ Metabolism. *Neuron* 89, 449-460.
- Gilley, J., and Coleman, M.P. (2010). Endogenous Nmnat2 is an essential survival factor for maintenance of healthy axons. *PLoS biology* 8, e1000300.
- Gilling, M., Rasmussen, H.B., Calloe, K., Sequeira, A.F., Baretto, M., Oliveira, G., Almeida, J., Lauritsen, M.B., Ullmann, R., and Boonen, S.E., et al. (2013). Dysfunction of the Heteromeric KV7.3/KV7.5 Potassium Channel is Associated with Autism Spectrum Disorders. *Frontiers in genetics* 4, 54.
- Glessner, J.T., Li, J., Wang, D., March, M., Lima, L., Desai, A., Hadley, D., Kao, C., Gur, R.E., and Cohen, N., et al. (2017). Copy number variation meta-analysis reveals a novel duplication at 9p24 associated with multiple neurodevelopmental disorders. *Genome medicine* 9, 106.
- Golzio, C., Willer, J., Talkowski, M.E., Oh, E.C., Taniguchi, Y., Jacquemont, S., Reymond, A., Sun, M., Sawa, A., and Gusella, J.F., et al. (2012). KCTD13 is a major driver of mirrored neuroanatomical phenotypes of the 16p11.2 copy number variant. *Nature* 485, 363-367.
- Grayton, H.M., Missler, M., Collier, D.A., and Fernandes, C. (2013). Altered social behaviours in neurexin 1 α knockout mice resemble core symptoms in neurodevelopmental disorders. *PLoS ONE* 8, e67114.
- Grissom, N.M., McKee, S.E., Schoch, H., Bowman, N., Havekes, R., O'Brien, W.T., Mahrt, E., Siegel, S., Commons, K., and Portfors, C., et al. (2017). Male-specific deficits in natural reward learning in a mouse model of neurodevelopmental disorders. *Molecular psychiatry*.
- Guillemin, G.J. (2012). Quinolinic acid, the inescapable neurotoxin. *The FEBS journal* 279, 1356-1365.
- Hanson, E., Bernier, R., Porche, K., Jackson, F.I., Goin-Kochel, R.P., Snyder, L.G., Snow, A.V., Wallace, A.S., Campe, K.L., and Zhang, Y., et al. (2015). The cognitive and behavioral phenotype of the 16p11.2 deletion in a clinically ascertained population. *Biological psychiatry* 77, 785-793.
- Hicks, A.N., Lorenzetti, D., Gilley, J., Lu, B., Andersson, K.-E., Miligan, C., Overbeek, P.A., Oppenheim, R., and Bishop, C.E. (2012). Nicotinamide mononucleotide adenylyltransferase 2 (Nmnat2) regulates axon integrity in the mouse embryo. *PLoS ONE* 7, e47869.
- Horev, G., Ellegood, J., Lerch, J.P., Son, Y.-E.E., Muthuswamy, L., Vogel, H., Krieger, A.M., Buja, A., Henkelman, R.M., and Wigler, M., et al. (2011). Dosage-dependent phenotypes in models of 16p11.2 lesions found in autism. *Proceedings of the National Academy of Sciences of the United States of America* 108, 17076-17081.
- Hu, H.-T., and Hsueh, Y.-P. (2014). Calcium influx and postsynaptic proteins coordinate the dendritic filopodium-spine transition. *Developmental neurobiology* 74, 1011-1029.

- Huang, T.-N., Chuang, H.-C., Chou, W.-H., Chen, C.-Y., Wang, H.-F., Chou, S.-J., and Hsueh, Y.-P. (2014). *Tbr1* haploinsufficiency impairs amygdalar axonal projections and results in cognitive abnormality. *Nat. Neurosci.* *17*, 240-247.
- Hung, A.Y., Futai, K., Sala, C., Valtschanoff, J.G., Ryu, J., Woodworth, M.A., Kidd, F.L., Sung, C.C., Miyakawa, T., and Bear, M.F., et al. (2008). Smaller dendritic spines, weaker synaptic transmission, but enhanced spatial learning in mice lacking *Shank1*. *J. Neurosci.* *28*, 1697-1708.
- Hussman, J.P., Chung, R.-H., Griswold, A.J., Jaworski, J.M., Salyakina, D., Ma, D., Konidari, I., Whitehead, P.L., Vance, J.M., and Martin, E.R., et al. (2011). A noise-reduction GWAS analysis implicates altered regulation of neurite outgrowth and guidance in autism. *Molecular autism* *2*, 1.
- Iossifov, I., O’Roak, B.J., Sanders, S.J., Ronemus, M., Krumm, N., Levy, D., Stessman, H.A., Witherspoon, K.T., Vives, L., and Patterson, K.E., et al. (2014). The contribution of de novo coding mutations to autism spectrum disorder. *Nature* *515*, 216-221.
- Iossifov, I., Ronemus, M., Levy, D., Wang, Z., Hakker, I., Rosenbaum, J., Yamrom, B., Lee, Y.-H., Narzisi, G., and Leotta, A., et al. (2012). De novo gene disruptions in children on the autistic spectrum. *Neuron* *74*, 285-299.
- Ip, J.P.K., Nagakura, I., Petravicz, J., Li, K., Wiemer, E.A.C., and Sur, M. (2018). Major vault protein, a candidate gene in 16p11.2 microdeletion syndrome, is required for the homeostatic regulation of visual cortical plasticity. *The Journal of neuroscience : the official journal of the Society for Neuroscience*.
- Isshiki, M., Tanaka, S., Kuriu, T., Tabuchi, K., Takumi, T., and Okabe, S. (2014). Enhanced synapse remodelling as a common phenotype in mouse models of autism. *Nat Comms* *5*, 4742.
- Jamain, S., Radyushkin, K., Hammerschmidt, K., Granon, S., Boretius, S., Varoquaux, F., Ramanantsoa, N., Gallego, J., Ronnenberg, A., and Winter, D., et al. (2008). Reduced social interaction and ultrasonic communication in a mouse model of monogenic heritable autism. *Proc. Natl. Acad. Sci. U.S.A.* *105*, 1710-1715.
- Jiang, Y.-H., and Ehlers, M.D. (2013). Modeling autism by SHANK gene mutations in mice. *Neuron* *78*, 8-27.
- Kang, H.J., Kawasawa, Y.I., Cheng, F., Zhu, Y., Xu, X., Li, M., Sousa, A.M.M., Pletikos, M., Meyer, K.A., and Sedmak, G., et al. (2011). Spatio-temporal transcriptome of the human brain. *Nature* *478*, 483-489.
- Kemper, T.L., and Bauman, M.L. (1993). The contribution of neuropathologic studies to the understanding of autism. *Neurologic clinics* *11*, 175-187.
- Konopka, G., Wexler, E., Rosen, E., Mukamel, Z., Osborn, G.E., Chen, L., Lu, D., Gao, F., Gao, K., and Lowe, J.K., et al. (2012). Modeling the functional genomics of autism using human neurons. *Mol. Psychiatry* *17*, 202-214.
- Korecka, J.A., van Kesteren, Ronald E., Blaas, E., Spitzer, S.O., Kamstra, J.H., Smit, A.B., Swaab, D.F., Verhaagen, J., Bossers, K., and Lim, K.-L. (2013). Phenotypic Characterization of Retinoic Acid Differentiated SH-SY5Y Cells by Transcriptional Profiling. *PLoS ONE* *8*, e63862.
- Krishnan, A., Zhang, R., Yao, V., Theesfeld, C.L., Wong, A.K., Tadych, A., Volfovsky, N., Packer, A., Lash, A., and Troyanskaya, O.G. (2016). Genome-wide prediction and functional characterization of the genetic basis of autism spectrum disorder. *Nature neuroscience*.
- Kwon, C.-H., Luikart, B.W., Powell, C.M., Zhou, J., Matheny, S.A., Zhang, W., Li, Y., Baker, S.J., and Parada, L.F. (2006). *Pten* regulates neuronal arborization and social interaction in mice. *Neuron* *50*, 377-388.
- La Torre-Ubieta, L. de, Won, H., Stein, J.L., and Geschwind, D.H. (2016). Advancing the understanding of autism disease mechanisms through genetics. *Nature medicine* *22*, 345-361.
- Lai, M.-C., Lombardo, M.V., and Baron-Cohen, S. (2014). Autism. *Lancet (London, England)* *383*, 896-910.

- Langfelder, P., and Horvath, S. (2007). Eigengene networks for studying the relationships between co-expression modules. *BMC Syst Biol* 1, 54.
- Lartseva, A., Dijkstra, T., and Buitelaar, J.K. (2014). Emotional language processing in autism spectrum disorders: a systematic review. *Frontiers in human neuroscience* 8, 991.
- Lee, E.-J., Lee, H., Huang, T.-N., Chung, C., Shin, W., Kim, K., Koh, J.-Y., Hsueh, Y.-P., and Kim, E. (2015). Trans-synaptic zinc mobilization improves social interaction in two mouse models of autism through NMDAR activation. *Nat Comms* 6, 7168.
- Levy, D., Ronemus, M., Yamrom, B., Lee, Y.-H., Leotta, A., Kendall, J., Marks, S., Lakshmi, B., Pai, D., and Ye, K., et al. (2011). Rare de novo and transmitted copy-number variation in autistic spectrum disorders. *Neuron* 70, 886-897.
- Li, Z., He, X., and Feng, J. (2013). 16p11.2 is required for neuronal polarity. *WJNS* 03, 221-227.
- Lim, C.K., Bilgin, A., Lovejoy, D.B., Tan, V., Bustamante, S., Taylor, B.V., Bessede, A., Brew, B.J., and Guillemin, G.J. (2017a). Kynurenine pathway metabolomics predicts and provides mechanistic insight into multiple sclerosis progression. *Scientific reports* 7, 41473.
- Lim, C.K., Essa, M.M., Paula Martins, R. de, Lovejoy, D.B., Bilgin, A.A., Waly, M.I., Al-Farsi, Y.M., Al-Sharbati, M., Al-Shaffae, M.A., and Guillemin, G.J. (2015). Altered kynurenine pathway metabolism in autism: Implication for immune-induced glutamatergic activity. *Autism research : official journal of the International Society for Autism Research*.
- Lim, C.-S., Hoang, E.T., Viar, K.E., Stornetta, R.L., Scott, M.M., and Zhu, J.J. (2014). Pharmacological rescue of Ras signaling, GluA1-dependent synaptic plasticity, and learning deficits in a fragile X model. *Genes & development* 28, 273-289.
- Lim, E.T., Uddin, M., Rubeis, S. de, Chan, Y., Kamumbu, A.S., Zhang, X., D’Gama, A.M., Kim, S.N., Hill, R.S., and Goldberg, A.P., et al. (2017b). Rates, distribution and implications of postzygotic mosaic mutations in autism spectrum disorder. *Nature neuroscience* 20, 1217-1224.
- Liu, X.-Q., Paterson, A.D., and Szatmari, P. (2008). Genome-wide linkage analyses of quantitative and categorical autism subphenotypes. *Biological psychiatry* 64, 561-570.
- Livak, K.J., and Schmittgen, T.D. (2001). Analysis of relative gene expression data using real-time quantitative PCR and the 2^{-Delta Delta C(T)} Method. *Methods* 25, 402-408.
- Lopez, S.J., Dunaway, K., Islam, M.S., Mordaunt, C., Vogel Ciernia, A., Meguro-Horike, M., Horike, S.-I., Segal, D.J., and Lasalle, J.M. (2017). UBE3A-mediated regulation of imprinted genes and epigenome-wide marks in human neurons. *Epigenetics* 12, 982-990.
- Lord, C., Rutter, M., DiLavore, P.C., Risi, S., Gotham, K., and Bishop, S. (2012). *Autism diagnostic observation schedule—Second edition (ADOS-2)*. Los Angeles: Western Psychological Services.
- Lord, C., Rutter, M., Goode, S., Heemsbergen, J., Jordan, H., Mawhood, L., and Schopler, E. (1989). Autism diagnostic observation schedule: a standardized observation of communicative and social behavior. *Journal of autism and developmental disorders* 19, 185-212.
- Lord, C., Rutter, M., and Le Couteur, A. (1994). Autism Diagnostic Interview-Revised: a revised version of a diagnostic interview for caregivers of individuals with possible pervasive developmental disorders. *Journal of autism and developmental disorders* 24, 659-685.
- Love, M.I., Huber, W., and Anders, S. (2014). Moderated estimation of fold change and dispersion for RNA-seq data with DESeq2. *Genome biology* 15, 550.
- Lovrečić, L., Rajar, P., Volk, M., Bertok, S., Gnidovec Stražičar, B., Osredkar, D., Jekovec Vrhovšek, M., and Peterlin, B. (2018). Diagnostic efficacy and new variants in isolated and complex autism spectrum disorder using molecular karyotyping. *Journal of applied genetics* 59, 179-185.

- Ma, D., Salyakina, D., Jaworski, J.M., Konidari, I., Whitehead, P.L., Andersen, A.N., Hoffman, J.D., Slifer, S.H., Hedges, D.J., and Cukier, H.N., et al. (2009). A genome-wide association study of autism reveals a common novel risk locus at 5p14.1. *Annals of human genetics* *73*, 263-273.
- Maguschak, K.A., and Ressler, K.J. (2012). The dynamic role of beta-catenin in synaptic plasticity. *Neuropharmacology* *62*, 78-88.
- Maillard, A.M., Ruef, A., Pizzagalli, F., Migliavacca, E., Hippolyte, L., Adaszewski, S., Dukart, J., Ferrari, C., Conus, P., and Männik, K., et al. (2015). The 16p11.2 locus modulates brain structures common to autism, schizophrenia and obesity. *Molecular psychiatry* *20*, 140-147.
- Manolio, T.A., Collins, F.S., Cox, N.J., Goldstein, D.B., Hindorff, L.A., Hunter, D.J., McCarthy, M.I., Ramos, E.M., Cardon, L.R., and Chakravarti, A., et al. (2009). Finding the missing heritability of complex diseases. *Nature* *461*, 747-753.
- Mariani, J., Coppola, G., Zhang, P., Abyzov, A., Provini, L., Tomasini, L., Amenduni, M., Szekely, A., Palejev, D., and Wilson, M., et al. (2015). FOXP1-Dependent Dysregulation of GABA/Glutamate Neuron Differentiation in Autism Spectrum Disorders. *Cell* *162*, 375-390.
- Marshall, C.R., Noor, A., Vincent, J.B., Lionel, A.C., Feuk, L., Skaug, J., Shago, M., Moessner, R., Pinto, D., and Ren, Y., et al. (2008). Structural variation of chromosomes in autism spectrum disorder. *American journal of human genetics* *82*, 477-488.
- Mazzucchelli, C., Vantaggiato, C., Ciamei, A., Fasano, S., Pakhotin, P., Krezel, W., Welzl, H., Wolfer, D.P., Pagès, G., and Valverde, O., et al. (2002). Knockout of ERK1 MAP kinase enhances synaptic plasticity in the striatum and facilitates striatal-mediated learning and memory. *Neuron* *34*, 807-820.
- McBride, K.L., Varga, E.A., Pastore, M.T., Prior, T.W., Manickam, K., Atkin, J.F., and Herman, G.E. (2010). Confirmation study of PTEN mutations among individuals with autism or developmental delays/mental retardation and macrocephaly. *Autism research : official journal of the International Society for Autism Research* *3*, 137-141.
- McCammon, J.M., Blaker-Lee, A., Chen, X., and Sive, H. (2017). The 16p11.2 homologs fam57ba and doc2a generate certain brain and body phenotypes. *Human Molecular Genetics* *26*, 3699-3712.
- McCarthy, M.I., Abecasis, G.R., Cardon, L.R., Goldstein, D.B., Little, J., Ioannidis, J.P.A., and Hirschhorn, J.N. (2008). Genome-wide association studies for complex traits: consensus, uncertainty and challenges. *Nat. Rev. Genet.* *9*, 356-369.
- McCarthy, S.E., Makarov, V., Kirov, G., Addington, A.M., McClellan, J., Yoon, S., Perkins, D.O., Dickel, D.E., Kusenda, M., and Krastoshevsky, O., et al. (2009). Microduplications of 16p11.2 are associated with schizophrenia. *Nature genetics* *41*, 1223-1227.
- Medina, M.A., Andrade, V.M., Caracci, M.O., Avila, M.E., Verdugo, D.A., Vargas, M.F., Ugarte, G.D., Reyes, A.E., Opazo, C., and Ferrari, G.V. de (2018). Wnt/ β -catenin signaling stimulates the expression and synaptic clustering of the autism-associated Neurologin 3 gene. *Transl Psychiatry* *8*, 45.
- Meganathan, K., Lewis, E.M.A., Gontarz, P., Liu, S., Stanley, E.G., Elefanty, A.G., Huettner, J.E., Zhang, B., and Kroll, K.L. (2017). Regulatory networks specifying cortical interneurons from human embryonic stem cells reveal roles for CHD2 in interneuron development. *Proc. Natl. Acad. Sci. U.S.A.* *114*, E11180-E11189.
- Meguro-Horike, M., Yasui, D.H., Powell, W., Schroeder, D.I., Oshimura, M., Lasalle, J.M., and Horike, S.-I. (2011). Neuron-specific impairment of inter-chromosomal pairing and transcription in a novel model of human 15q-duplication syndrome. *Human Molecular Genetics* *20*, 3798-3810.
- Modabbernia, A., Velthorst, E., and Reichenberg, A. (2017). Environmental risk factors for autism: an evidence-based review of systematic reviews and meta-analyses. *Molecular autism* *8*, 13.

- Moy, S.S., Nadler, J.J., Perez, A., Barbaro, R.P., Johns, J.M., Magnuson, T.R., Piven, J., and Crawley, J.N. (2004). Sociability and preference for social novelty in five inbred strains: an approach to assess autistic-like behavior in mice. *Genes, brain, and behavior* 3, 287-302.
- Muotri, A.R. (2016). The Human Model: Changing Focus on Autism Research. *Biological psychiatry* 79, 642-649.
- Nakatani, J., Tamada, K., Hatanaka, F., Ise, S., Ohta, H., Inoue, K., Tomonaga, S., Watanabe, Y., Chung, Y.J., and Banerjee, R., et al. (2009). Abnormal behavior in a chromosome-engineered mouse model for human 15q11-13 duplication seen in autism. *Cell* 137, 1235-1246.
- Nava, C., Rupp, J., Boissel, J.-P., Mignot, C., Rastetter, A., Amiet, C., Jacquette, A., Dupuits, C., Bouteiller, D., and Keren, B., et al. (2015). Hypomorphic variants of cationic amino acid transporter 3 in males with autism spectrum disorders. *Amino acids* 47, 2647-2658.
- Neitzel, H. (1986). A routine method for the establishment of permanent growing lymphoblastoid cell lines. *Human genetics* 73, 320-326.
- Nguyen, Q.-A., Horn, M.E., and Nicoll, R.A. (2016). Distinct roles for extracellular and intracellular domains in neuroligin function at inhibitory synapses. *eLife* 5.
- Nishida, Y., Adati, N., Ozawa, R., Maeda, A., Sakaki, Y., and Takeda, T. (2008). Identification and classification of genes regulated by phosphatidylinositol 3-kinase- and TRKB-mediated signalling pathways during neuronal differentiation in two subtypes of the human neuroblastoma cell line SH-SY5Y. *BMC research notes* 1, 95.
- Nishimura, W., Yao, I., Iida, J., Tanaka, N., and Hata, Y. (2002). Interaction of synaptic scaffolding molecule and Beta -catenin. *J. Neurosci.* 22, 757-765.
- Ohtsuka, N., Badurek, S., Busslinger, M., Benes, F.M., Minichiello, L., and Rudolph, U. (2013). GABAergic neurons regulate lateral ventricular development via transcription factor Pax5. *Genesis (New York, N.Y. : 2000)* 51, 234-245.
- Okuda, T., Yu, L.M.Y., Cingolani, L.A., Kemler, R., and Goda, Y. (2007). beta-Catenin regulates excitatory postsynaptic strength at hippocampal synapses. *Proc. Natl. Acad. Sci. U.S.A.* 104, 13479-13484.
- Olsen, R.W., and Avoli, M. (1997). GABA and epileptogenesis. *Epilepsia* 38, 399-407.
- O'Roak, B.J., Deriziotis, P., Lee, C., Vives, L., Schwartz, J.J., Girirajan, S., Karakoc, E., Mackenzie, A.P., Ng, S.B., and Baker, C., et al. (2011). Exome sequencing in sporadic autism spectrum disorders identifies severe de novo mutations. *Nature genetics* 43, 585-589.
- Oswald, F., Klöble, P., Ruland, A., Rosenkranz, D., Hinz, B., Butter, F., Ramljak, S., Zechner, U., and Herlyn, H. (2017). The FOXP2-Driven Network in Developmental Disorders and Neurodegeneration. *Frontiers in cellular neuroscience* 11, 212.
- Patriquin, M.A., DeRamus, T., Libero, L.E., Laird, A., and Kana, R.K. (2016). Neuroanatomical and neurofunctional markers of social cognition in autism spectrum disorder. *Human brain mapping* 37, 3957-3978.
- Peça, J., Feliciano, C., Ting, J.T., Wang, W., Wells, M.F., Venkatraman, T.N., Lascola, C.D., Fu, Z., and Feng, G. (2011). Shank3 mutant mice display autistic-like behaviours and striatal dysfunction. *Nature* 472, 437-442.
- Peñagarikano, O., Abrahams, B.S., Herman, E.I., Winden, K.D., Gdalyahu, A., Dong, H., Sonnenblick, L.I., Gruver, R., Almajano, J., and Bragin, A., et al. (2011). Absence of CNTNAP2 leads to epilepsy, neuronal migration abnormalities, and core autism-related deficits. *Cell* 147, 235-246.
- Peñagarikano, O., and Geschwind, D.H. (2012). What does CNTNAP2 reveal about autism spectrum disorder? *Trends in molecular medicine* 18, 156-163.

- Petroni, D., Tsai, J., Mondal, D., and George, W. (2013). Attenuation of low dose methylmercury and glutamate induced-cytotoxicity and tau phosphorylation by an N-methyl-D-aspartate antagonist in human neuroblastoma (SHSY5Y) cells. *Environmental toxicology* 28, 700-706.
- Pfisterer, U., and Khodosevich, K. (2017). Neuronal survival in the brain. Neuron type-specific mechanisms. *Cell death & disease* 8, e2643.
- Pinto, D., Delaby, E., Merico, D., Barbosa, M., Merikangas, A., Klei, L., Thiruvahindrapuram, B., Xu, X., Ziman, R., and Wang, Z., et al. (2014). Convergence of genes and cellular pathways dysregulated in autism spectrum disorders. *Am. J. Hum. Genet.* 94, 677-694.
- Pinto, D., Pagnamenta, A.T., Klei, L., Anney, R., Merico, D., Regan, R., Conroy, J., Magalhaes, T.R., Correia, C., and Abrahams, B.S., et al. (2010). Functional impact of global rare copy number variation in autism spectrum disorders. *Nature* 466, 368-372.
- Pizzarelli, R., and Cherubini, E. (2011). Alterations of GABAergic signaling in autism spectrum disorders. *Neural plasticity* 2011, 297153.
- Polyak, A., Kubina, R.M., and Girirajan, S. (2015). Comorbidity of intellectual disability confounds ascertainment of autism: implications for genetic diagnosis.
- Portmann, T., Yang, M., Mao, R., Panagiotakos, G., Ellegood, J., Dolen, G., Bader, P.L., Grueter, B.A., Goold, C., and Fisher, E., et al. (2014). Behavioral abnormalities and circuit defects in the basal ganglia of a mouse model of 16p11.2 deletion syndrome. *Cell reports* 7, 1077-1092.
- Poulopoulos, A., Aramuni, G., Meyer, G., Soykan, T., Hoon, M., Papadopoulos, T., Zhang, M., Paarmann, I., Fuchs, C., and Harvey, K., et al. (2009). Neuroligin 2 drives postsynaptic assembly at perisomatic inhibitory synapses through gephyrin and collybistin. *Neuron* 63, 628-642.
- Poustka, F., Lisch, S., Rühl, D., Sacher, A., Schmötzer, G., and Werner, K. (1996). The standardized diagnosis of autism, Autism Diagnostic Interview-Revised: interrater reliability of the German form of the interview. *Psychopathology* 29, 145-153.
- Pucilowska, J., Vithayathil, J., Tavares, E.J., Kelly, C., Karlo, J.C., and Landreth, G.E. (2015). The 16p11.2 deletion mouse model of autism exhibits altered cortical progenitor proliferation and brain cytoarchitecture linked to the ERK MAPK pathway. *The Journal of neuroscience : the official journal of the Society for Neuroscience* 35, 3190-3200.
- Ran, F.A., Hsu, P.D., Wright, J., Agarwala, V., Scott, D.A., and Zhang, F. (2013). Genome engineering using the CRISPR-Cas9 system. *Nature protocols* 8, 2281-2308.
- Rasband, M.N. (2010). The axon initial segment and the maintenance of neuronal polarity. *Nature reviews. Neuroscience* 11, 552-562.
- Raymond, G.V., Bauman, M.L., and Kemper, T.L. (1996). Hippocampus in autism: a Golgi analysis. *Acta Neuropathol.* 91, 117-119.
- Richter, M., Murtaza, N., Scharrenberg, R., White, S.H., Johanns, O., Walker, S., Yuen, R.K.C., Schwanke, B., Bedürftig, B., and Henis, M., et al. (2018). Altered TAOK2 activity causes autism-related neurodevelopmental and cognitive abnormalities through RhoA signaling. *Molecular psychiatry*.
- Ristanović, D., Milosević, N.T., and Stulić, V. (2006). Application of modified Sholl analysis to neuronal dendritic arborization of the cat spinal cord. *J. Neurosci. Methods* 158, 212-218.
- Rosenfeld, J.A., Ballif, B.C., Torchia, B.S., Sahoo, T., Ravnan, J.B., Schultz, R., Lamb, A., Bejjani, B.A., and Shaffer, L.G. (2010). Copy number variations associated with autism spectrum disorders contribute to a spectrum of neurodevelopmental disorders. *Genetics in medicine : official journal of the American College of Medical Genetics* 12, 694-702.

- Rubeis, S. de, He, X., Goldberg, A.P., Poultney, C.S., Samocha, K., Cicek, A.E., Kou, Y., Liu, L., Fromer, M., and Walker, S., et al. (2014). Synaptic, transcriptional and chromatin genes disrupted in autism. *Nature* *515*, 209-215.
- Rubenstein, J.L.R., and Merzenich, M.M. (2003). Model of autism. Increased ratio of excitation/inhibition in key neural systems. *Genes, brain, and behavior* *2*, 255-267.
- Russo, A.J. (2013). Correlation Between Hepatocyte Growth Factor (HGF) and Gamma-Aminobutyric Acid (GABA) Plasma Levels in Autistic Children. *Biomarker insights* *8*, 69-75.
- Rutter, M., Le Couteur, A., and Lord, C. (2003). Autism diagnostic interview-revised. Western Psychological Services.
- Sahm, F., Oezen, I., Opitz, C.A., Radlwimmer, B., Deimling, A. von, Ahrendt, T., Adams, S., Bode, H.B., Guillemin, G.J., and Wick, W., et al. (2013). The endogenous tryptophan metabolite and NAD⁺ precursor quinolinic acid confers resistance of gliomas to oxidative stress. *Cancer research* *73*, 3225-3234.
- Sakaguchi, G., Manabe, T., Kobayashi, K., Orita, S., Sasaki, T., Naito, A., Maeda, M., Igarashi, H., Katsuura, G., and Nishioka, H., et al. (1999). Doc2alpha is an activity-dependent modulator of excitatory synaptic transmission. *The European journal of neuroscience* *11*, 4262-4268.
- Salyakina, D., Ma, D.Q., Jaworski, J.M., Konidari, I., Whitehead, P.L., Henson, R., Martinez, D., Robinson, J.L., Sacharow, S., and Wright, H.H., et al. (2010). Variants in several genomic regions associated with asperger disorder. *Autism research : official journal of the International Society for Autism Research* *3*, 303-310.
- Sanders, S.J., Ercan-Sencicek, A.G., Hus, V., Luo, R., Murtha, M.T., Moreno-De-Luca, D., Chu, S.H., Moreau, M.P., Gupta, A.R., and Thomson, S.A., et al. (2011). Multiple recurrent de novo CNVs, including duplications of the 7q11.23 Williams syndrome region, are strongly associated with autism. *Neuron* *70*, 863-885.
- Sanders, S.J., He, X., Willsey, A.J., Ercan-Sencicek, A.G., Samocha, K.E., Cicek, A.E., Murtha, M.T., Bal, V.H., Bishop, S.L., and Dong, S., et al. (2015). Insights into Autism Spectrum Disorder Genomic Architecture and Biology from 71 Risk Loci. *Neuron* *87*, 1215-1233.
- Sanders, S.J., Murtha, M.T., Gupta, A.R., Murdoch, J.D., Raubeson, M.J., Willsey, A.J., Ercan-Sencicek, A.G., DiLullo, N.M., Parikshak, N.N., and Stein, J.L., et al. (2012). De novo mutations revealed by whole-exome sequencing are strongly associated with autism. *Nature* *485*, 237-241.
- Schmeisser, M.J., Ey, E., Wegener, S., Bockmann, J., Stempel, A.V., Kuebler, A., Janssen, A.-L., Udvardi, P.T., Shiban, E., and Spilker, C., et al. (2012). Autistic-like behaviours and hyperactivity in mice lacking ProSAP1/Shank2. *Nature* *486*, 256-260.
- Scott, R., Sánchez-Aguilera, A., van Elst, K., Lim, L., Dehorter, N., Bae, S.E., Bartolini, G., Peles, E., Kas, M.J.H., and Bruining, H., et al. (2017). Loss of Cntnap2 Causes Axonal Excitability Deficits, Developmental Delay in Cortical Myelination, and Abnormal Stereotyped Motor Behavior. *Cereb. Cortex*.
- Sener, E.F., Canatan, H., and Ozkul, Y. (2016). Recent Advances in Autism Spectrum Disorders: Applications of Whole Exome Sequencing Technology. *Psychiatry investigation* *13*, 255-264.
- Shcheglovitov, A., Shcheglovitova, O., Yazawa, M., Portmann, T., Shu, R., Sebastiano, V., Krawisz, A., Froehlich, W., Bernstein, J.A., and Hallmayer, J.F., et al. (2013). SHANK3 and IGF1 restore synaptic deficits in neurons from 22q13 deletion syndrome patients. *Nature* *503*, 267-271.
- Shen, C., Huo, L.-r., Zhao, X.-l., Wang, P.-r., and Zhong, N. (2015). Novel interactive partners of neuroligin 3: new aspects for pathogenesis of autism. *Journal of molecular neuroscience : MN* *56*, 89-101.

- Sheridan, S.D., Theriault, K.M., Reis, S.A., Zhou, F., Madison, J.M., Daheron, L., Loring, J.F., and Haggarty, S.J. (2011). Epigenetic characterization of the FMR1 gene and aberrant neurodevelopment in human induced pluripotent stem cell models of fragile X syndrome. *PLoS ONE* 6, e26203.
- Shinawi, M., Liu, P., Kang, S.-H.L., Shen, J., Belmont, J.W., Scott, D.A., Probst, F.J., Craigen, W.J., Graham, B.H., and Pursley, A., et al. (2010). Recurrent reciprocal 16p11.2 rearrangements associated with global developmental delay, behavioural problems, dysmorphism, epilepsy, and abnormal head size. *Journal of medical genetics* 47, 332-341.
- Sibilla, S., and Ballerini, L. (2009). GABAergic and glycinergic interneuron expression during spinal cord development: dynamic interplay between inhibition and excitation in the control of ventral network outputs. *Progress in neurobiology* 89, 46-60.
- Simonoff, E., Pickles, A., Charman, T., Chandler, S., Loucas, T., and Baird, G. (2008). Psychiatric disorders in children with autism spectrum disorders: prevalence, comorbidity, and associated factors in a population-derived sample. *Journal of the American Academy of Child and Adolescent Psychiatry* 47, 921-929.
- Smalley, S.L. (1998). Autism and tuberous sclerosis. *Journal of autism and developmental disorders* 28, 407-414.
- Smoller, J.W., Ripke, S., Lee, P.H., and Neale, B. (2013). Identification of risk loci with shared effects on five major psychiatric disorders: a genome-wide analysis. *A genome-wide analysis. Lancet (London, England)* 381, 1371-1379.
- Southam, K.A., Stennard, F., Pavez, C., and Small, D.H. (2018). Knockout of Amyloid β Protein Precursor (APP) Expression Alters Synaptogenesis, Neurite Branching and Axonal Morphology of Hippocampal Neurons. *Neurochemical research*.
- Spielman, R.S., McGinnis, R.E., and Ewens, W.J. (1993). Transmission test for linkage disequilibrium. The insulin gene region and insulin-dependent diabetes mellitus (IDDM). *Am. J. Hum. Genet.* 52, 506-516.
- Spreckelmeyer, K.N., Krach, S., Kohls, G., Rademacher, L., Irmak, A., Konrad, K., Kircher, T., and Gründer, G. (2009). Anticipation of monetary and social reward differently activates mesolimbic brain structures in men and women. *Social cognitive and affective neuroscience* 4, 158-165.
- Stein, J.L. (2015). Copy number variation and brain structure: lessons learned from chromosome 16p11.2. *Genome medicine* 7, 13.
- Stein, J.L., de la Torre-Ubieta, Luis, Tian, Y., Parikshak, N.N., Hernández, I.A., Marchetto, M.C., Baker, D.K., Lu, D., Hinman, C.R., and Lowe, J.K., et al. (2014). A quantitative framework to evaluate modeling of cortical development by neural stem cells. *Neuron* 83, 69-86.
- Steinman, K.J., Spence, S.J., Ramocki, M.B., Proud, M.B., Kessler, S.K., Marco, E.J., Green Snyder, L., D'Angelo, D., Chen, Q., and Chung, W.K., et al. (2016). 16p11.2 deletion and duplication: Characterizing neurologic phenotypes in a large clinically ascertained cohort. *American journal of medical genetics. Part A* 170, 2943-2955.
- Stoner, R., Chow, M.L., Boyle, M.P., Sunkin, S.M., Mouton, P.R., Roy, S., Wynshaw-Boris, A., Colamarino, S.A., Lein, E.S., and Courchesne, E. (2014). Patches of disorganization in the neocortex of children with autism. *N. Engl. J. Med.* 370, 1209-1219.
- Sungur, A.Ö., Schwarting, R.K.W., and Wöhr, M. (2017). Behavioral phenotypes and neurobiological mechanisms in the Shank1 mouse model for autism spectrum disorder. A translational perspective. *Behavioural brain research*.
- Sztainberg, Y., and Zoghbi, H.Y. (2016). Lessons learned from studying syndromic autism spectrum disorders. *Nature neuroscience* 19, 1408-1417.

- Takahashi, K., and Yamanaka, S. (2006). Induction of pluripotent stem cells from mouse embryonic and adult fibroblast cultures by defined factors. *Cell* 126, 663-676.
- Tanaka, M., DeLorey, T.M., Delgado-Escueta, A., and Olsen, R.W. (2012). Jasper's Basic Mechanisms of the Epilepsies. *GABRB3, Epilepsy, and Neurodevelopment* (Bethesda (MD)).
- Terakata, M., Fukuwatari, T., Sano, M., Nakao, N., Sasaki, R., Fukuoka, S.-I., and Shibata, K. (2012). Establishment of true niacin deficiency in quinolinic acid phosphoribosyltransferase knockout mice. *J. Nutr.* 142, 2148-2153.
- Tick, B., Bolton, P., Happé, F., Rutter, M., and Rijdsdijk, F. (2016). Heritability of autism spectrum disorders: a meta-analysis of twin studies. *Journal of child psychology and psychiatry, and allied disciplines* 57, 585-595.
- Torres, F., Barbosa, M., and Maciel, P. (2016). Recurrent copy number variations as risk factors for neurodevelopmental disorders: critical overview and analysis of clinical implications. *Journal of medical genetics* 53, 73-90.
- Tsai, P.T., Hull, C., Chu, Y., Greene-Colozzi, E., Sadowski, A.R., Leech, J.M., Steinberg, J., Crawley, J.N., Regehr, W.G., and Sahin, M. (2012). Autistic-like behaviour and cerebellar dysfunction in Purkinje cell Tsc1 mutant mice. *Nature* 488, 647-651.
- Urbach, A., Bar-Nur, O., Daley, G.Q., and Benvenisty, N. (2010). Differential modeling of fragile X syndrome by human embryonic stem cells and induced pluripotent stem cells. *Cell Stem Cell* 6, 407-411.
- van Rooij, D., Anagnostou, E., Arango, C., Auzias, G., Behrmann, M., Busatto, G.F., Calderoni, S., Daly, E., Deruelle, C., and Di Martino, A., et al. (2018). Cortical and Subcortical Brain Morphometry Differences Between Patients With Autism Spectrum Disorder and Healthy Individuals Across the Lifespan: Results From the ENIGMA ASD Working Group. *The American journal of psychiatry* 175, 359-369.
- Wagnon, J.L., Briese, M., Sun, W., Mahaffey, C.L., Curk, T., Rot, G., Ule, J., and Frankel, W.N. (2012). CELF4 regulates translation and local abundance of a vast set of mRNAs, including genes associated with regulation of synaptic function. *PLoS Genet.* 8, e1003067.
- Wagnon, J.L., Mahaffey, C.L., Sun, W., Yang, Y., Chao, H.-T., and Frankel, W.N. (2011). Etiology of a genetically complex seizure disorder in Celf4 mutant mice. *Genes, brain, and behavior* 10, 765-777.
- Walker, L.J., Summers, D.W., Sasaki, Y., Brace, E.J., Milbrandt, J., and DiAntonio, A. (2017). MAPK signaling promotes axonal degeneration by speeding the turnover of the axonal maintenance factor NMNAT2. *eLife* 6.
- Waltes, R., Duketis, E., Knapp, M., Anney, R.J.L., Huguet, G., Schlitt, S., Jarczok, T.A., Sachse, M., Kämpfer, L.M., and Kleinböck, T., et al. (2014). Common variants in genes of the postsynaptic FMRP signalling pathway are risk factors for autism spectrum disorders. *Human genetics* 133, 781-792.
- Walton, C.C., Zhang, W., Patiño-Parrado, I., Barrio-Alonso, E., Garrido, J.-J., and Frade, J.M. (2018). Checkpoint signaling abrogation after cell cycle reentry reveals that differentiated neurons are mitotic cells.
- Wang, K., Zhang, H., Ma, D., Bucan, M., Glessner, J.T., Abrahams, B.S., Salyakina, D., Imielinski, M., Bradfield, J.P., and Sleiman, P.M.A., et al. (2009). Common genetic variants on 5p14.1 associate with autism spectrum disorders. *Nature* 459, 528-533.
- Wang, X., McCoy, P.A., Rodriguiz, R.M., Pan, Y., Je, H.S., Roberts, A.C., Kim, C.J., Berrios, J., Colvin, J.S., and Bousquet-Moore, D., et al. (2011). Synaptic dysfunction and abnormal behaviors in mice lacking major isoforms of Shank3. *Hum. Mol. Genet.* 20, 3093-3108.
- Weiner, D.J., Wigdor, E.M., Ripke, S., Walters, R.K., Kosmicki, J.A., Grove, J., Samocha, K.E., Goldstein, J.I., Okbay, A., and Bybjerg-Grauholm, J., et al. (2017). Polygenic transmission disequilibrium confirms that

- common and rare variation act additively to create risk for autism spectrum disorders. *Nature genetics* **49**, 978-985.
- Weintraub, K. (2011). The prevalence puzzle: Autism counts. *Nature* **479**, 22-24.
- Weiss, L.A., Arking, D.E., Daly, M.J., and Chakravarti, A. (2009). A genome-wide linkage and association scan reveals novel loci for autism. *Nature* **461**, 802-808.
- Werling, D.M., Lowe, J.K., Luo, R., Cantor, R.M., and Geschwind, D.H. (2014). Replication of linkage at chromosome 20p13 and identification of suggestive sex-differential risk loci for autism spectrum disorder. *Molecular autism* **5**, 13.
- WHO (1992). Icd-10: The Icd-10 Classification of Mental and Behavioural Disorders: clinical descriptions and diagnostic guidelines. http://books.google.de/books?hl=de&lr=&id=QiWPj_23ei4C&oi=fnd&pg=PR5&dq=International+classification+of+mental+and+behavioral+disorders&ots=Enpb6WC4TM&sig=-4T6S907FHA00ayiyTioW4zKMJU. 27.03.2013.
- Wisniewska, M.B. (2013). Physiological role of β -catenin/TCF signaling in neurons of the adult brain. *Neurochemical research* **38**, 1144-1155.
- Won, H., Lee, H.-R., Gee, H.Y., Mah, W., Kim, J.-I., Lee, J., Ha, S., Chung, C., Jung, E.S., and Cho, Y.S., et al. (2012). Autistic-like social behaviour in Shank2-mutant mice improved by restoring NMDA receptor function. *Nature* **486**, 261-265.
- Woodbury-Smith, M., and Scherer, S.W. (2018). Progress in the genetics of autism spectrum disorder. *Developmental medicine and child neurology*.
- Xia, K., Guo, H., Hu, Z., Xun, G., Zuo, L., Peng, Y., Wang, K., He, Y., Xiong, Z., and Sun, L., et al. (2014). Common genetic variants on 1p13.2 associate with risk of autism. *Molecular psychiatry* **19**, 1212-1219.
- Xia, N., Zhang, P., Fang, F., Wang, Z., Rothstein, M., Angulo, B., Chiang, R., Taylor, J., and Reijo Pera, R.A. (2016). Transcriptional comparison of human induced and primary midbrain dopaminergic neurons. *Scientific reports* **6**, 20270.
- Yamakawa, H., Oyama, S., Mitsuhashi, H., Sasagawa, N., Uchino, S., Kohsaka, S., and Ishiura, S. (2007). Neuroligins 3 and 4X interact with syntrophin-gamma2, and the interactions are affected by autism-related mutations. *Biochemical and biophysical research communications* **355**, 41-46.
- Yan, J., Oliveira, G., Coutinho, A., Yang, C., Feng, J., Katz, C., Sram, J., Bockholt, A., Jones, I.R., and Craddock, N., et al. (2005a). Analysis of the neuroligin 3 and 4 genes in autism and other neuropsychiatric patients. *Molecular psychiatry* **10**, 329-332.
- Yan, Q.J., Rammal, M., Tranfaglia, M., and Bauchwitz, R.P. (2005b). Suppression of two major Fragile X Syndrome mouse model phenotypes by the mGluR5 antagonist MPEP. *Neuropharmacology* **49**, 1053-1066.
- Yousaf, A., Duketis, E., Jarczok, T., Sachse, M., Biscaldi, M., Degenhardt, F., Herms, S., Chichon, S., Klauck, S.M., and Ackermann, J., et al. (2018). Mapping the genetics of neuropsychological traits to the molecular network of the human brain using a data integrative approach.
- Yusuf, M., Leung, K., Morris, K.J., and Volpi, E.V. (2013). Comprehensive cytogenomic profile of the in vitro neuronal model SH-SY5Y. *Neurogenetics* **14**, 63-70.
- Zheng, T., Xu, S.Y., Zhou, S.Q., Lai, L.Y., and Le Li (2013). Nicotinamide adenine dinucleotide (NAD⁺) repletion attenuates bupivacaine-induced neurotoxicity. *Neurochemical research* **38**, 1880-1894.
- Zhernakov, A., Rotter, B., Winter, P., Borisov, A., Tikhonovich, I., and Zhukov, V. (2017). Massive Analysis of cDNA Ends (MACE) for transcript-based marker design in pea (*Pisum sativum* L.). *Genomics data* **11**, 75-76.

9 Ein riesiges Danke

[Redacted text block]

[Redacted text block]

[Redacted text block]

[Redacted text block]

[REDACTED]

[REDACTED]

[REDACTED]

[REDACTED]

[REDACTED]

[Redacted text line]

[Redacted text block]

[Redacted text block 1]

[Redacted text block 2]

[Redacted text block 3]

[Redacted text block 4]

[Redacted text block 5]

11 List of publications

Publications resulting from the thesis project presented here are highlighted in bold.

Loss of the Chr16p11.2 ASD candidate gene QPRT leads to aberrant neuronal differentiation. Denise Haslinger, Regina Waltes, Afsheen Yousaf, Silvia Lindlar, Ines Schneider, Chai K. Lim, Meng-Miao Tsai, Boyan K. Garvalov, Amparo Acker-Palmer, Till Acker, Gilles J. Guillemin, Simone Fulda, Christine M. Freitag, Andreas G. Chiocchetti; under review at *Molecular Autism* (2018); **attached**

Common functional variants of the glutamatergic system in Autism spectrum disorder with high and low intellectual abilities. Andreas G. Chiocchetti, Afsheen Yousaf, Hanna S. Bour, Denise Haslinger, Regina Waltes, Eftikia Duketis, Tomasz A. Jarczok, Michael Sachse, Monica Biscaldi, Franziska Degenhardt, Stefan Herms, Sven Cichon, Jörg Ackermann, Ina Koch, Sabine M. Klauck, Christine M. Freitag; *Journal of Neural Transmission* (2018)

Transcriptomic signatures of neuronal differentiation and their association with risk genes for autism spectrum and related neuropsychiatric disorders. Andreas G. Chiocchetti, Denise Haslinger, Jason L. Stein, Luis de la Torre-Ubiera, Enrico Cocchi, Thomas Rothämel, Silvia Lindlar, Regina Waltes, Simone Fulda, Daniel H. Geschwind, Christine M. Freitag; *Translational Psychiatry* (2016)

Summaries of plenary, symposia, and oral sessions at the XXII World Congress of Psychiatric Genetics, Copenhagen, Denmark, 12-16 October 2014. Monica Aas, Gabriëlla A.M. Blokland, Samuel J.R.A. Chawner, Shing-Wan Choi, Jose Estrada, Annika Forsingdal, Maximilian Friedrich, Suhas Ganesham, Lynsey Hall, Denise Haslinger, Laura Huckins, Erik Loken, Stefanie Malan-Müller, Joanna Martin, Zuzanna Misiewicz, Luca Pagliaroli; Antonio F. Pardiñas, Claudia Pisanu, Giorgia Quadri, Marcos L. Santoro, Alex D. Shaw, Siri Ranlund, Jie Song, Martin Tesli, Maria Tropeano, Monique van der Voet, Kate Wolfe, Freida K. Cormack, Lynn DeLisi; *Psychiatric Genetics* (2015)

Variants of the CNTNAP2 5' promoter as risk factors for autism spectrum disorders: a genetic and functional approach. Andreas G. Chiocchetti, Marnie Kopp, Regina Waltes, Denise Haslinger, Eftikia Duketis, Tomasz A. Jarczok, Fritz Poustka, Anette Voran, Ulrike Graab, Jobst Meyer, Sabine M. Klauck, Simone Fulda, Christine M. Freitag; *Mol Psychiatry* (2015)

Common EIF4E variants modulate risk for autism spectrum disorders in the high-functioning range. Regina Waltes, Johannes Gfesser, Denise Haslinger, Katja Schneider-Momm, Monica Biscaldi, Anette Voran, Christine M. Freitag, Andreas G. Chiocchetti; *J Neural Transmission* (2014)

Protein signatures of oxidative stress response in a patient specific cell line model for autism. Andreas G Chiocchetti*, Denise Haslinger*, Maximilian Boesch, Thomas Karl, Stefan Wiemann, Christine M. Freitag, Fritz Poustka, Burghardt Scheibe, Johann W. Bauer, Helmut Hintner, Michael Breitenbach, Josef Kellermann, Friedrich Lottspeich, Sabine M. Klauck, Lore Breitenbach-Koller; *Molecular Autism* (2014)
* shared first authorship